The Thesis Committee for Jaime F. Hernandez
Certifies that this is the approved version of the following thesis:

Quasi-Static Testing of Cantilever Masonry Shear Wall Segments

APPROVED BY
SUPERVISING COMMITTEE:

Supervisor:

Richard E. Klingner

James O. Jirsa

Quasi-Static Testing of Cantilever Masonry Shear Wall Segments

by

Jaime F. Hernandez, B.S.

Thesis

Presented to the Faculty of the Graduate School of

The University of Texas at Austin

in Partial Fulfillment

of the Requirements

for the Degree of

Master of Science in Engineering

The University of Texas at Austin

May 2012

Dedication

To my parents, for their infinite love and support.

Acknowledgements

I am pleased to acknowledge the financial support provided by the National Institute of Standards and Technology (NIST). I would like to express my deep gratitude to Dr. Richard Klingner for the opportunity of participate in this project. His support, guidance, and patience have been an invaluable factor in the attainment of my Master's degree. I am very thankful to Dr. James Jirsa for serving as a committee member.

Many thanks are due to Dr. Benson Shing, Dr. David McLean, and the other project members for their valuable assistance and guidance. I want to express my special gratitude to Farhad Ahmadi for his hard work, which made it possible to carry out our test program successfully.

My sincere thanks go to the staff of the Ferguson Structural Engineering Laboratory for their help and guidance in the construction and testing of the walls. I wish also to extend my gratitude to Juan Diego Rodriguez, Steven Blair, Nick David, Geoff Scheid, Saleh Alogla, Whitney Lee, and other fellow students who participated in different stages of the construction of the walls.

My heartfelt gratitude goes to my friends in Austin, who made me feel at home in these two years; their support was been invaluable. Finally, I would like to acknowledge my beautiful family for their support, encouragement, and love. I cannot imagine my life without them. Lastly, I want to thank God for this fascinating experience of studying abroad; it has changed my life.

Jaime Hernandez

May 2012

Abstract

Quasi-Static Testing of Cantilever Masonry Shear Wall Segments

Jaime Hernandez, MSE

The University of Texas at Austin, 2012

Supervisor: Richard E. Klingner

The primary objective of this thesis was to study how the behavior of flexure-dominated masonry shear-wall segments is affected by changes in the normalized axial load and the percentage of vertical reinforcement. Six reinforced masonry shear-wall segment were constructed and tested at the Ferguson Structural Engineering Laboratory of the University of Texas at Austin. Specimens were 96-in. wide and 96-in. high (aspect ratio equal to 1.0) and were tested with different combinations of axial load ratio (zero and 0.10) and vertical reinforcement ratios (0.33% and 0.16%). Specimens met the 2011 MSJC Code requirements for special reinforced masonry shear walls, and were tested under quasi-static in-plane reversed cyclic loads. The specimens exhibited predominantly flexural behavior, as expected. Specimens exhibited high displacement ductility (5.6 to 16.7), as expected for flexure-dominated specimens. Specimens constructed with "green" units behaved essentially like otherwise identical specimens constructed with conventional ("gray") units.

Table of Contents

List of Tables

List of Figures

Chapter 1 : Quasi-Static Testing of Cantilever Masonry Shear Wall Segments

1.1. INTRODUCTION

In the United States, the structural design of reinforced masonry shear walls is governed by the provisions of legally adopted model codes such as the *International Building Code* (IBC 2012), which reference the general design provisions of ASCE 7 (ASCE7-10) and the material design provisions of the MSJC *Code and Specification* (MSJC 2011a,b). For seismic design, ASCE7-10 assigns Seismic Design Categories (SDC) to structures based on mapped accelerations, site characteristics and occupancy. Each SDC corresponds to a list of designated seismic force-resisting systems. Each designated seismic force-resisting system has prescribed seismic design factors, and prescribed design and detailing requirements that are intended to be consistent with the overall and local ductility implied by those factors.

The available ductility of a masonry shear wall depends on many factors, including the wall's aspect ratio (ratio of height to plan length), axial force, and longitudinal reinforcement ratio. One objective of the research described here is to permit the refinement of current MSJC design provisions for masonry shear walls. Another objective, discussed further in the chapter on background, is to provide additional information on the inelastic deformation capacity of masonry shear walls, which could be used to develop displacement-based approaches for the seismic design of masonry structures.

1.2. OBJECTIVES

This thesis describes work carried out as part of a project on "Performance-Based Seismic Design Methods and Tools for Reinforced Masonry Shear-Wall Structures," sponsored by the National Institute for Standards and Technology (NIST), and carried out jointly by researchers from the University of Texas at Austin (UT Austin), the University of California at San Diego (UCSD), and Washington State University (WSU). The overall objectives of the project are to produce much-needed experimental data to better understand the seismic performance of reinforced masonry shear-wall structures, and to develop improved design methodologies, detailing requirements, and analytical methods for the design and performance assessment of these structures.

The focus of this thesis is the quasi-static testing, under reversed cyclic loads, of cantilever segments of reinforced masonry shear walls with a range of aspect ratios, axial loads, and reinforcement patterns. Results from these tests are compared with predicted behavior, and are used to refine the design of similar wall segments in full-scale shaking-table tests of reinforced masonry building specimens, conducted at UCSD.

1.3. SCOPE

The overall project on "Performance-Based Seismic Design Methods and Tools for Reinforced Masonry Shear-Wall Structures" comprises four major tasks:

1. Develop a displacement-based design method for reinforced masonry shear walls.

2. Conduct an extensive series of quasi-static, reversed cyclic tests on wall segments with different design parameters and loading conditions

3. Improve analytical models for the performance assessment of reinforcement masonry shear walls; and

4. Conduct full-scale shaking-table tests to investigate the performance of shear-wall systems and to validate the new design method and analytical tools at the system level.

This thesis focuses on the quasi-static testing of cantilever wall segments of reinforced masonry, with a range of aspect ratios, axial load, and reinforcement patterns. These segments are designed for flexure-dominated behavior.

Analytical work in this thesis focuses on development and refinement of parameters for describing the nonlinear behavior of masonry wall segments.

Chapter 2 : Background

2.1. INTRODUCTION

The research described here is part of a multi-university research project, sponsored by the US National Institute for Standards and Technology (NIST). The overall goal of that research is to provide data to improve the seismic design of masonry shear-wall structures. In this thesis, consistent with that overall goal, the seismic design provisions currently used for masonry in the United States are first described. The limitations of those provisions are then pointed out, and are related to the goals of this thesis. After that, relevant research work on masonry shear walls is reviewed and evaluated. Finally, work that has recently been completed or is still in progress in this NIST research project is briefly reviewed.

2.2. CURRENT SEISMIC DESIGN PROVISIONS FOR MASONRY IN THE UNITED STATES

In the United States, masonry buildings must meet the seismic design requirements of ASCE 7-10 (ASCE7-10) and the 2011 MSJC *Code and Specification* (MSJC 2011a,b).

- First, the structure is assigned to a Seismic Design Category (SDC) according to its seismic zone, its function, and the properties of the underlying soil. Each SDC has a corresponding set of permissible seismic force-resisting systems, and corresponding set of permissible design methods. For moderate SDCs, those systems can consist of ordinary reinforced, intermediate reinforced, or special reinforced masonry shear walls; intermediate SDCs require intermediate reinforced or special reinforced masonry shear walls; and the highest SDCs require special reinforced masonry shear walls. Ordinary, intermediate, and

special walls have successively higher levels of prescriptive detailing, and more severe restrictions on maximum longitudinal reinforcement.

- ASCE 7-10 assigns each to system a set of seismic design factors, including the Response Modification Coefficient (*R*), which represents the combined effects of overall structural ductility and probable overstrength. The value of *R* is intended to be consistent with the available element ductility resulting from the required maximum reinforcement and prescriptive detailing. Because this is a force-based approach, the elastic lateral forces, reduced by *R*, are distributed among wall segments according to their relative stiffness. Each element is designed to resist flexural, axial and shear forces. For special reinforced masonry shear walls, capacity design for shear is required. (Masonry Designer's Guide, 2010)

2.3. LIMITATIONS OF CURRENT US SEISMIC DESIGN PROVISIONS FOR MASONRY

Current US seismic design provisions for masonry have inconsistencies and limitations. They are intended to result in elements (walls or wall segments) with available ductility consistent with the overall structural ductility demand assumed in design. This design objective cannot be satisfied solely by controlling prescriptive reinforcement and maximum reinforcement. It is also necessary to control the interaction of the segments comprising a perforated shear wall, and the performance of each wall segment. The performance of each wall segment is also influenced by its aspect ratio, which is not addressed by current US seismic design provisions.

To address these inconsistencies, research on the nonlinear behavior of walls with different combination of aspect ratios, vertical reinforcement, and level of axial load is needed. Information on inelastic parameters such as available displacement ductility, available curvature ductility, plastic hinge length, and equivalent hysteretic damping will

permit the designer to apply a variety of innovative design approaches (performance-, displacement-, or limit-based design) which may permit more cost-effective designs and more realistic predictions of structural performance.

2.4. PREVIOUS STUDIES ON REINFORCED MASONRY SHEAR WALLS

Several studies on reinforced masonry shear walls were conducted from the mid-1980s to the early 1990s. They focused on predicting flexural and shear capacities, and on ways of ensuring ductility in the wall segments. That information was essential for the application of force-based design.

Priestley (1986) studied the strength and ductility of masonry shear walls. He recommended the use of reinforced concrete equations for ultimate strength in flexural design with an ultimate compression strain of 0.0025 and a strength reduction factor of 0.05 less than the one used in reinforced concrete. He suggested the use of capacity design for shear to ensure ductile flexural behavior, and provided several detailing approaches intended to ensure ductility capacity.

Shing *et al.* (1989) explored the influences of axial stresses and amount of vertical reinforcement on the flexural and shear capacity of 16 story-height reinforced masonry shear walls as part of the US-Japan Coordinate Program for Masonry Building Research (Noland 1987). They concluded that the flexural and shear capacity of wall segments increased with the amount of vertical reinforcement and the axial stress applied, but the influence of axial load was higher on flexural strength than on shear strength. They also found that the amount of vertical and horizontal reinforcement increased the ductility and

energy dissipation of a shear-dominated wall, and could change the failure mode from a brittle to ductile. They also identified the influence of the wall aspect ratio on the inelastic performance of the wall and recommended more experimental studies of this.

The flexural and shear capacities of 22 masonry shear wall specimens were studied by Shing *et al.* (1990), who found that flexural capacity could be predicted from flexural theory assuming plane sections, and that such calculated flexural capacity would be conservative if it neglected strain hardening. They found that reductions in ductility due to increase in axial load could be overcome with proper toe confinement. This study also evaluated the shear-strength provisions of the *Uniform Building Code* (Uniform Building Code 1988), and concluded that while those provisions were conservative, they overestimated the contribution of horizontal reinforcement and ignored the effects of axial load. Shing *et al.* (1990) proposed a new shear-strength formula which was consistent with their experimental results.

Eikanas (2003) studied the effects of the aspect ratio and vertical reinforcement on failure modes and drift capacity. He compared the observed values of plastic hinge length with those proposed by Paulay and Priestley (1992), ACI (2002), and IBC (2000). He found that a decrease in aspect ratio would decrease the drift capacity and increase the shear contribution to the deflection. He also found that the 2000 IBC formula for plastic hinge length gave values greater than those observed in tests.

Voon and Ingham (2006) conducted an extensive evaluation of shear capacity in reinforced masonry shear walls. Although their work focused on comparison of test results with the New Zealand design code (NZS 4230:1990), they also obtained important

information about the influence of aspect ratio, vertical reinforcement, and axial load ratio on the shear capacity. They concluded that shear capacity increased with the level of axial load and vertical reinforcement, but decreased with increasing of wall aspect ratio. This last observation was attributed by the authors to variations in net area and masonry compression strength. They also observed an improvement in the behavior with uniform distribution of horizontal shear reinforcement.

Shedid *et al.* (2008) studied the influence of the distribution and amount of vertical reinforcement and the level of axial load in masonry shear walls dominated by flexure. Inelastic parameters such as height of plasticity, displacement ductility, and plastic hinge length were explored. They found that the extreme vertical reinforcement yielded over about 50% of the height of the cantilever wall specimens. Yield displacement was found to increase with increasing vertical reinforcement, but the ultimate displacements were approximately equal in all the tests (0.83%) regardless of the design parameters (axial load and vertical reinforcement ratio). As a result, displacement ductility increased with increasing vertical reinforcement. However, seven options for calculating displacement ductility were presented in this work, which explains the variability of results among earlier studies. Limitations in the calculation of displacement ductility for shear walls were also identified, including the layout of vertical bars and shear deformations that are not taken into account. Limitations in the calculation of plastic hinge length are mentioned, but no experimental results are provided.

Davis (2008) compared the results of 56 in-plane shear tests on reinforced masonry shear-wall specimens failing in shear, with the shear-wall design provisions (allowable-stress design and strength design) of the 2008 MSJC *Code* (MSJC 2008a), the

2004 New Zealand masonry design standard (NZS 4230:2004), the Canadian masonry standard (CSA S304.1-04), the 1997 *Uniform Building Code* (UBC 1997), the equations developed by Shing *et al.* (1990), and the equations developed by Anderson and Priestley (1992). Variables studied included masonry compressive strengths, reinforcement ratios, axial loads, displacement ductility, and wall aspect ratios. Davis found that the strength design provisions of the 2008 MSJC *Code* provided the best predictions. He also proposed some improvements to the 2008 MSJC *Code* shear provisions. The most relevant proposed change was the inclusion of an α factor to account for strength degradation in the plastic hinging region as suggested by Anderson and Priestley (1992).

Vaughn (2010) studied the effects of different combinations of aspect ratio, axial load ratio, and vertical reinforcement on ductility and drift capacity. This study concluded that ductility decreased with increasing of aspect ratio and vertical reinforcement, and increased with the percentage of horizontal reinforcement and level of axial load. The latter observation contradicts other studies, but was likely caused by the low values of the axial load applied in these tests. Drift capacity increased with increasing aspect ratio, decreased with increasing compressive axial load, and was not affected by increases in vertical reinforcement.

Shedid *et al.* (2010) continued the work of Shedid et al. (2008). Values of displacement ductility, average masonry compressive strain, curvature ductility, extent of plasticity, equivalent plastic hinge length, reduction factor, stiffness degradation, etc for the six walls with aspect ratio equal to 2 were obtained. The main recommendation given in this work was to consider the plastic hinge length and reduction factors dependent not only on the wall dimensions but also on the vertical reinforcement and axial load levels.

2.5. CURRENT RESEARCH OF NIST PROJECT

To improve current design procedures and provide more experimental data on the nonlinear behavior of wall segments, research on "Performance-Based Seismic Design Methods and Tools for Reinforced Masonry Shear-Wall Structures," is being conducted jointly by three universities: The University of Texas at Austin (UT Austin); the University of California at San Diego (UCSD); and Washington State University (WSU), under the sponsorship of the National Institute of Standards and Technology (NIST) and the National Science Foundation's Network for Earthquake Engineering Simulation (NEES) . This project is intended to provide the technical basis for displacement-based design of masonry structures.

To accomplish this objective, experimental studies on wall segments with different combinations of design parameters and configurations have been conducted to obtain information about their inelastic performance. The nonlinear parameters obtained in the tests were used to calibrate computational models which predict the performance of reinforced masonry structures more accurately. Finally, computational models will be compared and validated with large-scale shaking-table tests.

Some results from the experimental part of this project have already been published. Sherman (2011) tested 8 cantilever shear walls to evaluate different combinations of design parameters and the effects of splicing of longitudinal reinforcement. Sherman showed how axial load, vertical reinforcement ratio, and aspect ratios affected the wall stiffness, shearing and sliding deformations, yield and ultimate displacements, displacement ductility, plastic hinge length, and energy dissipation. He found that walls with lap splices were stiffer than walls with no splices; as a result, walls

with no splices developed larger displacements at failure and higher displacement ductilities. The most significant effect of splices was found in the curvature at the base of the wall. The concentration of the damage at the base for walls with lap splices reduced the wall curvatures and, therefore reduced the height of plasticity and the plastic hinge ratio, as well. Specimens with splices dissipated 67% and 43% of the energy dissipated by otherwise identical specimens without splices.

Kapoi (2012) tested 8 specimens to study the effects of concentrated reinforcement at the ends of the wall segments. Kapoi found that the drift ratio at failure, yielding displacement, ductility displacement, height of plasticity, and hysteretic damping values were about the same for specimens with jamb reinforcement and with uniformly distributed reinforcement. The average equivalent plastic hinge length increased in specimen with uniformly distributed vertical reinforcement, while the energy dissipation increased in specimen with jamb reinforcement. In Kapoi's tests, a specimen with large-diameter vertical reinforcement and lap splices at the base failed abruptly.

Other current research in the NIST study includes experimental studies by Cyrier (Washington State University) on the behavior of boundary elements in shear-wall segments, and studies on a set of 14 cantilever and 6 fixed-fixed wall specimens by Ahmadi (UT Austin). That work is still in progress.

Chapter 3 : Cantilever Shear-Wall Specimens

3.1. OVERVIEW OF SPECIMENS

Six cantilever reinforced masonry specimens representing shear-wall segments were tested under axial load and quasi-static in-plane cyclic lateral load at the Ferguson Structural Engineering Laboratory of the University of Texas at Austin. As shown in Figure 3-1, the specimens were 96-in. wide and 96-in. high (aspect ratio equal to 1.0). Specimen details are summarized in Table 3-1.

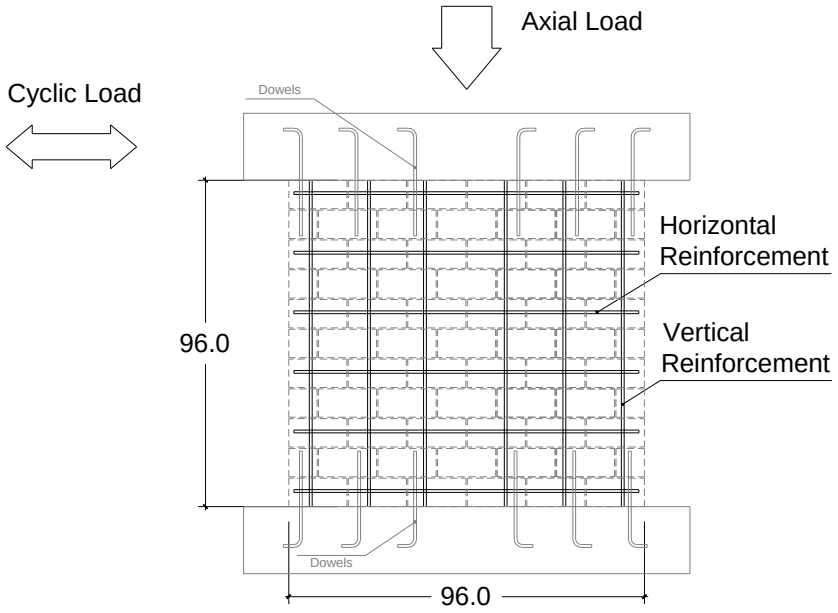

Figure 3-1 Details of cantilever shear-wall specimens

Table 3-1 Overview of cantilever shear-wall specimens

Wall Specimen	**Nominal Length, in**	**Nominal Height, in**	**Aspect Ratio**	$P / (f'_m A_g)$	**Vertical Reinforcement (Percentage, %)**	**Horizontal Reinforcement (Percentage, %)**
"Gray Blocks"						
PBS-3	96	96	1	0	#4 every 8 in. (0.33)	#4 every 8 in. (0.33)
PBS-4	96	96	1	0	#4 every 16 in. (0.16)	#4 every 16 in. (0.16)
PBS-11	96	96	1	0.10	#4 every 8 in. (0.33)	#4 every 8 in. (0.33)
PBS-12	96	96	1	0.10	#4 every 16 in. (0.16)	#4 every 16 in. (0.16)
"Green Blocks"						
PBS-4G	96	96	1	0	#4 every 16 in. (0.16)	#4 every 16 in. (0.16)
PBS-12G	96	96	1	0.10	#4 every 16 in. (0.16)	#4 every 16 in. (0.16)

Four specimens (PBS-3, PBS-4, PBS-11, and PBS-12) were constructed with conventional hollow concrete masonry units, referred to here as "gray blocks." The remaining two specimens (PBS-4G and PBS-12G) were constructed with hollow concrete

masonry units containing recycled material, referred to here as "green blocks." Those two specimens were otherwise identical to PBS-4 and PBS-12.

Each specimen was constructed with isotropic reinforcement (equal percentages of reinforcement in each direction). This layout of reinforcement differs from the traditional way of designing wall segments in accordance with the prescriptive requirements of the 2011 MSJC *Code* (MSJC 2011a). Isotropic reinforcement was proposed as a way of satisfying the reinforcement requirements of the Limit Design provisions of the draft 2013 MSJC *Code*. In accordance with 2011 MSJC *Code* requirements for Seismic Design Category (SDC) D and above, transverse (horizontal) reinforcement was hooked around extreme longitudinal (vertical) reinforcement with a 180-degree hook in the plane of the bed joint. Minimum diameter of bend for the 180-degree horizontal bar hooks restricted the bar diameter to a maximum of #4. Two bar spacings were used: 8 in. for PBS-3 and PBS-11, and 16 in. for PBS-4, PBS-4G, PBS-12, and PBS-12G. Two axial load levels were considered in this study: zero axial load (PBS-3, PBS-4, and PBS-4G), and a normalized axial load ratio $P / (f_m' A_g)$ of 0.10 (PBS-11, PBS-12, and PBS-12G).

3.2. Design of Cantilever Shear-wall Segments

Cantilever shear-wall segment designs proposed in Table 3-1 follow the 2011 MSJC Code requirements, including maximum reinforcement and capacity design for shear. Formulas are referred to the 2011 MSJC *Code* to facilitate their location within the text.

Wall Specimen PBS-3

Wall Specimen PBS-3 was 96-in. wide, 96-in. high, and 7.625-in. thick with #4 bars every 8 in. vertically and horizontally and an axial load equal to zero.

Prescriptive Reinforcement Requirement of Specimen PBS-3

Section 1.18.3.2.6 of the 2011 MSJC *Code* (MSJC 2011a) requires, for special reinforced masonry shear walls, that the minimum reinforcement ratio for each direction be at least 0.0007, and that the sum of the reinforcement ratios in each direction be at least 0.002.

$$\rho_v = \frac{A_{sv}}{b\ d} = \frac{0.20\ in.^2}{(7.625\ in.)\ (8\ in.)} = 0.0033 > 0.0007 \quad OK.$$

$$\rho_h = \frac{A_{sh}}{b\ d} = \frac{0.20\ in.^2}{(7.625\ in.)\ \ (8\ in.)} = 0.0033 > 0.0007 \quad OK.$$

$$\rho_h + \rho_v = 0.0033 + 0.0033 = 0.0066 > 0.002 \quad OK.$$

The maximum reinforcement ratio was calculated from Section 3.3.3.5 of 2011 MSJC *Code* (MSJC 2011a) where α was taken as 4 for special reinforced masonry shear walls.

$$\rho_{max} = \frac{0.64\ f'_m \left(\frac{\varepsilon_{mu}}{\varepsilon_{mu} + \alpha\ \varepsilon_y}\right) - \frac{P_n}{b\ d_v}}{f_y \left(\frac{\alpha\ \varepsilon_y - \varepsilon_{mu}}{\varepsilon_{mu} + \alpha\ \varepsilon_y}\right)}$$

$$\rho_{max} = \frac{0.64\ (2500\ psi)\ \left[\frac{0.0025}{0.0025 + (4)(0.00207)}\right] - \frac{0\ kips}{(7.625\ in.)(96\ in.)}}{60000\ psi\ \left[\frac{(4)(0.00207) - 0.0025}{0.0025 + (4)(0.00207)}\right]}$$

$$\rho_{max} = 0.01153 > 0.0033 \quad OK.$$

Flexural Capacity of Specimen PBS-3

The moment capacity of Specimen PBS-3 was calculated according to the design assumptions of the 2011 MSJC *Code* (MSJC 2011a), Section 3.3.2. The specified compressive strength of masonry, f_m', was taken as 2500 psi and the specified yield strength of reinforcement, f_y, was taken as 60 ksi. As shown in the nominal moment-axial force interaction diagram of Figure 3-2 for axial load equal to zero, the nominal moment capacity of Specimen PBS-3 is 526 ft-kips.

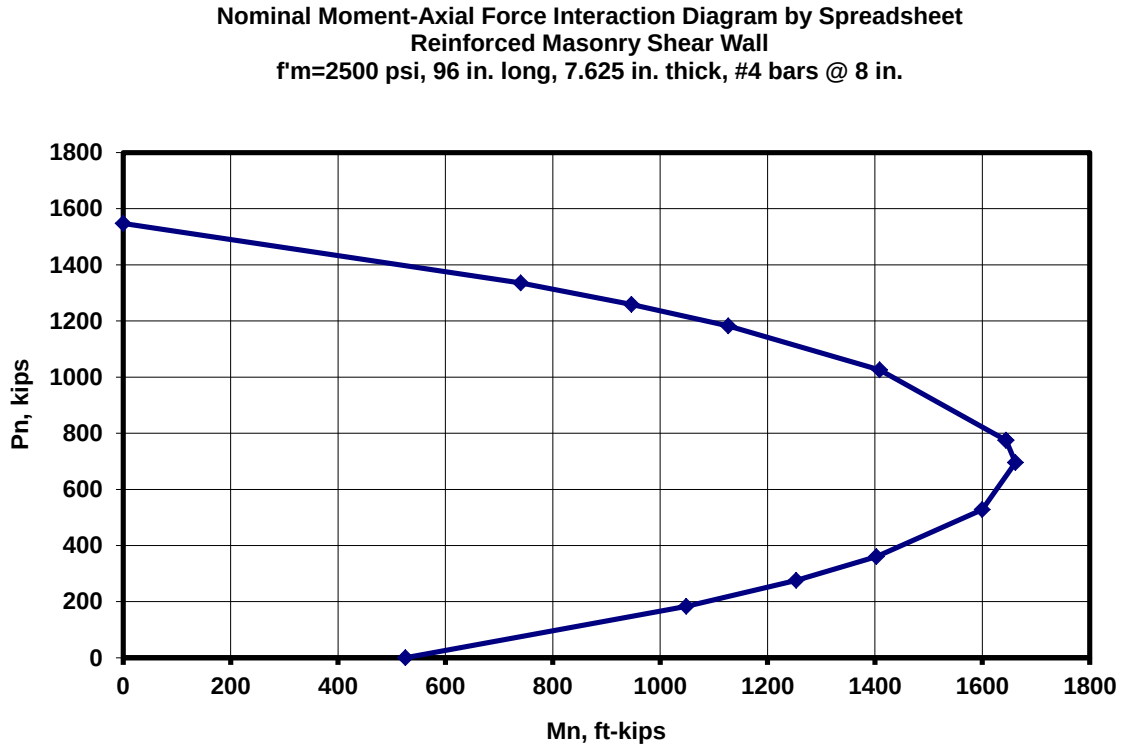

Figure 3-2 Moment-axial Force interaction diagram for Specimen PBS-3

The shear corresponding to the development of flexural capacity for Specimen PBS-3 would be

$$V_u(M_n) = \frac{M_n}{H} = \frac{526\ ft - kips}{8.75\ ft} = 60.11 \text{ kips}$$

where *H* is the distance from the base of the shear-wall segment to the mid-height of the loading beam (the line of action of the applied load).

Shear Capacity of Specimen PBS-3

The nominal masonry shear strength of Specimen PBS-3, V_{nm}, was calculated according to Section 3.3.4.1.2.1 of the 2011 MSJC *Code* (MSJC 2011a).

$$V_{nm} = \left[4.0 - 1.75\left(\frac{M_u}{V_u\ d_v}\right)\right] A_n\ \sqrt{f'_m} + 0.25\ P_n$$

For cantilever walls $M_u = V_u\ H$, so the term in parenthesis becomes the aspect ratio of the wall segment, which in this case equals 1.0.

$$V_{nm} = [4.0 - 1.75\ (1)]\ (7.625\ in.)\ (96\ in.)\ \sqrt{2500} + 0.25\ (0)$$

$$V_{nm} = 82.35\ kips$$

The nominal masonry shear strength, V_{nm}, is higher than the maximum shear corresponding to the flexural capacity, 60.11 kips; as a result, it is not necessary to have shear reinforcement to ensure a flexural failure.

The nominal shear strength provided by reinforcement, V_{ns}, was calculated according to Section 3.3.4.1.2.2 of 2011 MSJC *Code* (MSJC 2011a).

$$V_{ns} = 0.5\left(\frac{A_v}{s}\right) f_y\ d_v$$

$$V_{ns} = 0.5\left(\frac{0.20\ in.^2}{8\ in.}\right)(60000\ psi)\ (96\ in.)$$

$$V_{ns} = 72.0\ kips$$

The shear capacity design provisions of the 2011 MSJC *Code* (MSJC 2011a), Section 1.18.3.2.6.1, require that the design shear strength, ϕV_n, equal or exceed 1.25 times the shear corresponding to the flexural capacity.

$$V_n = V_{nm} + V_{ns}$$
$$V_n = 82.35\ kips + 72.0\ kips$$
$$V_n = 154.35\ kips$$

$$\emptyset\ V_n = (0.80)154.35\ kips > 1.25\ (60.11\ kips)$$
$$123.48\ kips > 75.14\ kips \qquad OK.$$

Sliding-shear Capacity of Specimen PBS-3

Sliding failure can occur in wall segments with low levels of axial load. Because the 2011 MSJC *Code* does not have general shear-friction provisions, the sliding-shear capacity of Specimen PBS-3 was estimated using the shear-friction provisions of Section 11.6.4 of ACI 318-08 (ACI 318-2008). The coefficient of friction, μ, was taken as 1.0.

$$V_s = \mu\ (A_v\ f_y)$$
$$V_s = (12)\ (0.20\ in.^2)\ (60000\ psi)$$
$$V_s = 144\ kips$$

Detailing of Specimen PBS-3

As shown in Figure 3-3, Specimen PBS-3 was 96-in. wide, 96-in. high, and 7.625-in. thick with #4 bars every 8 in. vertically and horizontally. This detailing meets the requirements of the 2011 MSCJ *Code*.

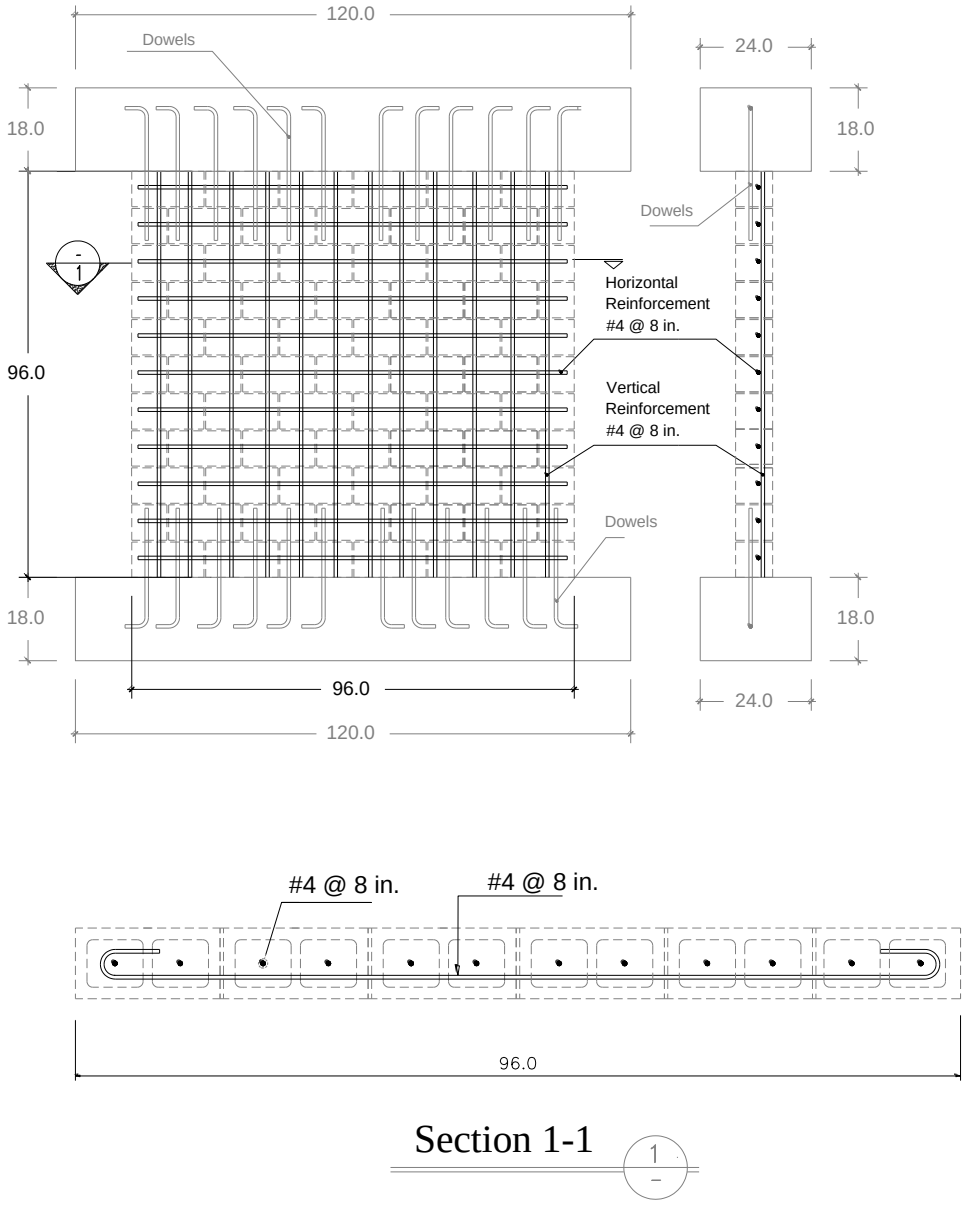

Figure 3-3 Detailing of Specimen PBS-3

Wall Specimens PBS-4 and PBS-4G

Wall Specimens PBS-4 and PBS-4G were 96-in. wide, 96-in. high, and 7.625-in. thick with #4 bars every 16 in. vertically and horizontally and axial load equal to zero.

Prescriptive Reinforcement Requirement of Specimen PBS-4 and PBS-4G

Section 1.18.3.2.6 of the 2011 MSJC *Code* (MSJC 2011a) requires, for special reinforced masonry shear walls, that the minimum reinforcement ratio for each direction be at least 0.0007, and that the sum of the reinforcement ratios in each direction be at least 0.002.

$$\rho_v = \frac{A_{sv}}{b\ d} = \frac{0.20\ in.^2}{(7.625\ in.)\ (16\ in.)} = 0.0016 > 0.0007 \quad OK.$$

$$\rho_h = \frac{A_{sh}}{b\ d} = \frac{0.20\ in.^2}{(7.625\ in.)\ (16\ in.)} = 0.0016 > 0.0007 \quad OK.$$

$$\rho_h + \rho_v = 0.0016 + 0.0016 = 0.0032 > 0.002 \quad OK.$$

The maximum reinforcement ratio was calculated from Section 3.3.3.5 of 2011 MSJC *Code* (MSJC 2011a) where α was taken as 4 for special reinforced masonry shear walls.

$$\rho_{max} = \frac{0.64\ f'_m \left(\frac{\varepsilon_{mu}}{\varepsilon_{mu} + \alpha\ \varepsilon_y}\right) - \frac{P_n}{b\ d_v}}{f_y \left(\frac{\alpha\ \varepsilon_y - \varepsilon_{mu}}{\varepsilon_{mu} + \alpha\ \varepsilon_y}\right)}$$

$$\rho_{max} = \frac{0.64\,(2500\,psi)\left[\frac{0.0025}{0.0025+(4)(0.00207)}\right] - \frac{0\,kips}{(7.625\,in.)(96\,in.)}}{60000\,psi\left[\frac{(4)(0.00207)-0.0025}{0.0025+(4)(0.00207)}\right]}$$

$$\rho_{max} = 0.01153 > 0.0016 \quad OK.$$

Flexural Capacity of Specimens PBS-4 and PBS-4G

The moment capacity of Specimens PBS-4 and PBS-4G was calculated according to the design assumptions of the 2011 MSJC *Code* (MSJC 2011a), Section 3.3.2. The specified compressive strength of masonry, f_m', was taken as 2500 psi and the specified yield strength of reinforcement, f_y, was taken as 60 ksi. As shown in the nominal moment-axial force interaction diagram of Figure 3-4 for axial load equal to zero, the nominal moment capacity of Specimens PBS-4 and PBS-4G is 275 ft-kips.

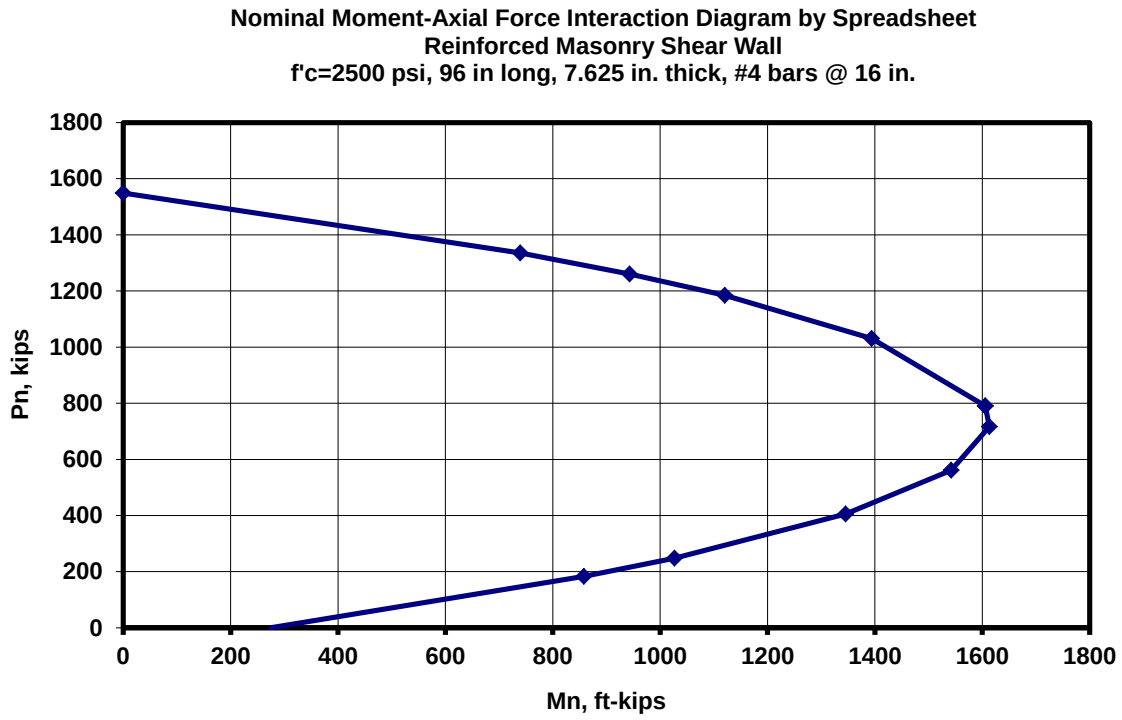

Figure 3-4 Moment-axial force interaction diagram for Specimens PBS-4 and PBS-4G

The shear corresponding to the development of flexural capacity for Specimens PBS-4 and PBS-4G would be

$$V_u(M_n) = \frac{M_n}{H} = \frac{275\ ft - kips}{8.75\ ft} = 31.43 \text{ kips}$$

where *H* is the distance from the base of the shear-wall segment to the mid-height of the loading beam (line of action of the applied load).

Shear Capacity of Specimens PBS-4 and PBS-4G

The nominal masonry shear strength of Specimens PBS-4 and PBS-4G, V_{nm}, was calculated according to Section 3.3.4.1.2.1 of the 2011 MSJC *Code* (MSJC 2011a).

$$V_{nm} = \left[4.0 - 1.75\left(\frac{M_u}{V_u\ d_v}\right)\right] A_n\ \sqrt{f'_m} + 0.25\ P_n$$

For cantilever walls $M_u = V_u\ H$, so the term in parenthesis becomes the aspect ratio of the wall segment, which in this case equals 1.0.

$$V_{nm} = [4.0 - 1.75\ (1)]\ (7.625\ in.)\ (96\ in.)\ \sqrt{2500} + 0.25\ (0)$$

$$V_{nm} = 82.35\ kips$$

The nominal masonry shear strength, V_{nm}, is higher than the maximum shear corresponding to the flexural capacity, 31.43 kips; as a result, it is not necessary to have shear reinforcement to ensure a flexural failure.

The nominal shear strength provided by reinforcement, V_{ns}, was calculated according to Section 3.3.4.1.2.2 of 2011 MSJC *Code* (MSJC 2011a).

$$V_{ns} = 0.5\left(\frac{A_v}{s}\right) f_y\ d_v$$

$$V_{ns} = 0.5\left(\frac{0.20\ in.^2}{16\ in.}\right)(60000\ psi)\ (96\ in.)$$

$$V_{ns} = 36.0\ kips$$

The shear capacity design provisions of the 2011 MSJC *Code* (MSJC 2011a), Section 1.18.3.2.6.1, require that the design shear strength, ϕV_n , equal or exceed 1.25 times the shear corresponding to the flexural capacity.

$$V_n = V_{nm} + V_{ns}$$

$$V_n = 82.35\ kips + 36.0\ kips$$

$$V_n = 118.35\ kips$$

$$\emptyset\ V_n = (0.80)118.35\ kips > 1.25\ (31.43)\ kips)$$

$$94.68\ kips > 39.29\ kips \qquad OK.$$

Sliding-shear Capacity of Specimen PBS-4 and PBS-4G

Sliding failure can occur in wall segments with low levels of axial load. Because the 2011 MSJC *Code* does not have general shear-friction provisions, the sliding-shear capacity of Specimens PBS-4 and PBS-4G was estimated using the shear-friction provisions of Section 11.6.4 of ACI 318-08 (ACI 318-2008). The coefficient of friction, μ, was taken as 1.0.

$$V_s = \mu\ (A_v\ f_y)$$

$$V_s = (6)\ (0.20\ in.^2)\ (60000\ psi)$$

$$V_s = 72\ kips$$

Detailing of Specimens PBS-4 and PBS-4G

As shown in Figure 3-5, Specimens PBS-4 and PBS-4G were 96-in. wide, 96-in. high, and 7.625-in. thick with #4 bars every 16 in. vertically and horizontally. This detailing meets the requirements of the 2011 MSCJ *Code*.

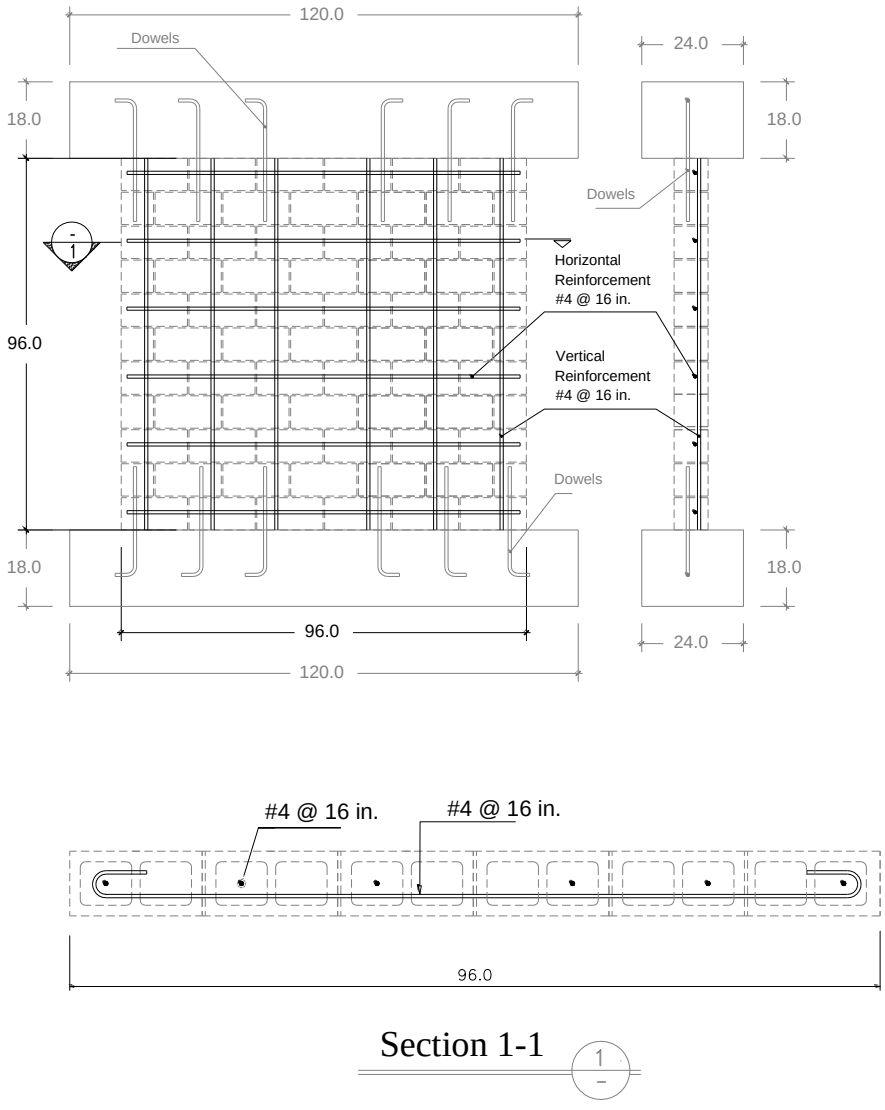

Figure 3-5 Detailing of Specimens PBS-4 and PBS-4G

Wall Specimen PBS-11

Wall Specimen PBS-11 was 96-in. wide, 96-in. high, and 7.625-in. thick with #4 bars every 8 in. vertically and horizontally and axial load ratio, $P / (f_m' A_g)$, equal to 0.10.

Prescriptive Reinforcement Requirement of Specimen PBS-11

Section 1.18.3.2.6 of the 2011 MSJC *Code* (MSJC 2011a) requires, for special reinforced masonry shear walls, that the minimum reinforcement ratio for each direction be at least 0.0007, and that the sum of the reinforcement ratios in each direction be at least 0.002.

$$\rho_v = \frac{A_{sv}}{b\ d} = \frac{0.20\ in.^2}{(7.625\ in.)\ (8\ in.)} = 0.0033 > 0.0007 \quad OK.$$

$$\rho_h = \frac{A_{sh}}{b\ d} = \frac{0.20\ in.^2}{(7.625\ in.)\ \ (8\ in.)} = 0.0033 > 0.0007 \quad OK.$$

$$\rho_h + \rho_v = 0.0033 + 0.0033 = 0.0066 > 0.002 \quad OK.$$

The maximum reinforcement ratio was calculated from Section 3.3.3.5 of 2011 MSJC *Code* (MSJC 2011a) where α was taken as 4 for special reinforced masonry shear walls.

$$\rho_{max} = \frac{0.64\ f'_m \left(\frac{\varepsilon_{mu}}{\varepsilon_{mu} + \alpha\ \varepsilon_y}\right) - \frac{P_n}{b\ d_v}}{f_y \left(\frac{\alpha\ \varepsilon_y - \varepsilon_{mu}}{\varepsilon_{mu} + \alpha\ \varepsilon_y}\right)}$$

Where,

$$P_n = 0.10\, f'_m\, A_g$$

$$P_n = 0.10\,(2500\ psi)(96\ in.)(7.625\ in.)$$

$$P_n = 183\ kips$$

$$\rho_{max} = \frac{0.64\,(2500\ psi)\left[\frac{0.0025}{0.0025 + (4)(0.00207)}\right] - \frac{183000\ lb}{(7.625\ in.)(96\ in.)}}{60000\ psi\left[\frac{(4)(0.00207) - 0.0025}{0.0025 + (4)(0.00207)}\right]}$$

$$\rho_{max} = 0.00376 > 0.0033 \quad OK.$$

Flexural Capacity of Specimen PBS-11

The moment capacity of Specimen PBS-11 was calculated according to the design assumptions of the 2011 MSJC *Code* (MSJC 2011a), Section 3.3.2. The specified compressive strength of masonry, f_m', was taken as 2500 psi and the specified yield strength of reinforcement, f_y, was taken as 60 ksi. As shown in the nominal moment-axial force interaction diagram of Figure 3-6 for axial load ratio, P / ($f_m' A_g$), equal to 0.10 the nominal moment capacity of Specimen PBS-11 is 1049 ft-kips.

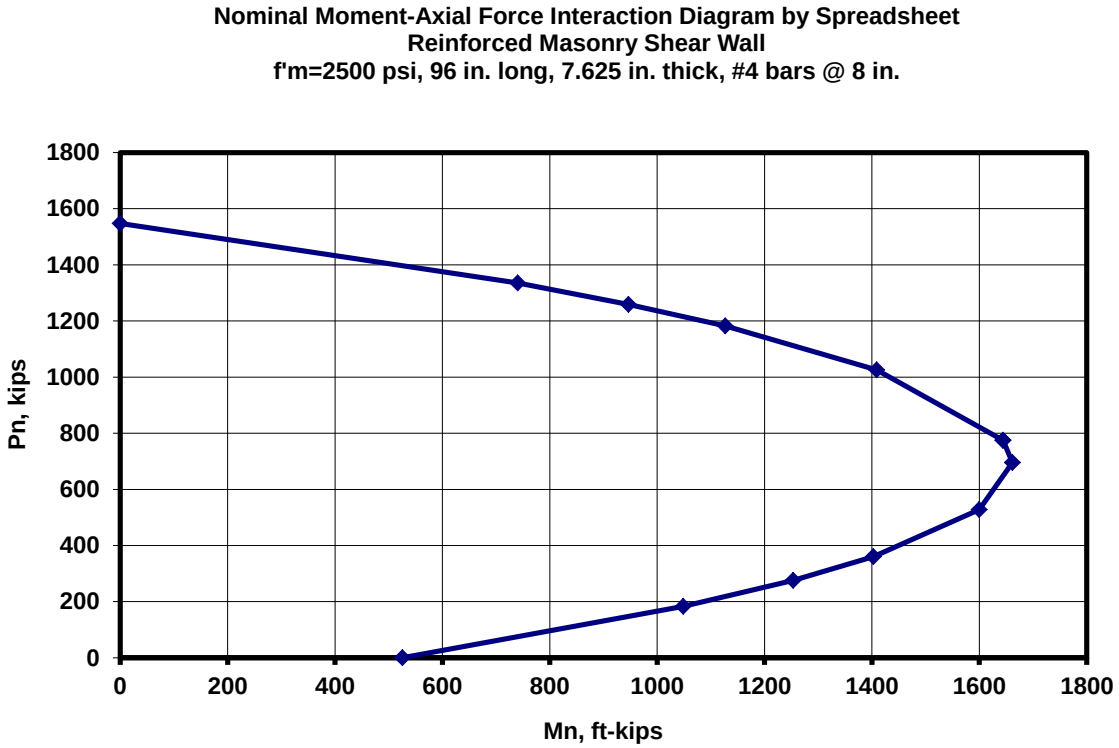

Figure 3-6 Moment-axial force interaction diagram for Specimen PBS-11

The shear corresponding to the development of flexural capacity for Specimen PBS-11 would be

$$V_u(M_n) = \frac{M_n}{H} = \frac{1049 ft - kips}{8.75\ ft} = 119.89 \text{ kips}$$

where *H* is the distance from the base of the shear-wall segment to the mid-height of the loading beam (line of action of the applied load).

Shear Capacity of Specimen PBS-11

The nominal masonry shear strength of Specimen PBS-11, V_{nm}, was calculated according to Section 3.3.4.1.2.1 of the 2011 MSJC *Code* (MSJC 2011a).

$$V_{nm} = \left[4.0 - 1.75\left(\frac{M_u}{V_u\ d_v}\right)\right] A_n\ \sqrt{f'_m} + 0.25\ P_n$$

For cantilever walls $M_u = V_u\ H$, so the term in parenthesis becomes the aspect ratio of the wall segment, which in this case equals 1.0.

$$V_{nm} = [4.0 - 1.75\ (1)]\ (7.625\ in.)\ (96\ in.)\ \sqrt{2500} + 0.25\ (183000\ lb)$$

$$V_{nm} = 128.10\ kips$$

The nominal masonry shear strength, V_{nm}, is higher than the maximum shear corresponding to the flexural capacity, 119.89 kips; as a result, it is not necessary to have shear reinforcement to ensure a flexural failure.

The nominal shear strength provided by reinforcement, V_{ns}, was calculated according to Section 3.3.4.1.2.2 of 2011 MSJC *Code* (MSJC 2011a).

$$V_{ns} = 0.5\left(\frac{A_v}{s}\right) f_y\ d_v$$

$$V_{ns} = 0.5\left(\frac{0.20\ in.^2}{8\ in.}\right)(60000\ psi)\ (96\ in.)$$

$$V_{ns} = 72.0\ kips$$

The shear capacity design provisions of the 2011 MSJC *Code* (MSJC 2011a), Section 1.18.3.2.6.1, require that the design shear strength, ϕV_n, equal or exceed 1.25 times the shear corresponding to the flexural capacity.

$$V_n = V_{nm} + V_{ns}$$
$$V_n = 128.10\ kips + 72.0\ kips$$
$$V_n = 200.10\ kips$$

$$\emptyset\ V_n = (0.80)\ 200.10\ kips \quad > \quad 1.25\ (119.89\ kips)$$
$$160.08\ kips > 149.86\ kips \quad Ok.$$

Sliding-shear Capacity of Specimen PBS-11

Sliding failure can occur in wall segments with low levels of axial load. Because the 2011 MSJC *Code* does not have general shear-friction provisions, the sliding-shear capacity of Specimen PBS-11 was estimated using the shear-friction provisions of Section 11.6.4 of ACI 318-08 (ACI 318-2008). The coefficient of friction, μ, was taken as 1.0.

$$V_s = \mu\ (A_v\ f_y + P_n)$$
$$V_s = (12)\ (0.20\ in.^2)(60000\ psi) + 183000\ lb$$
$$V_s = 327\ kips$$

Detailing of Specimen PBS-11

As shown in Figure 3-7, Specimen PBS-11 was 96-in. wide, 96-in. high, and 7.625-in. thick with #4 bars every 8 in. vertically and horizontally. This detailing meets the requirements of the 2011 MSCJ *Code*.

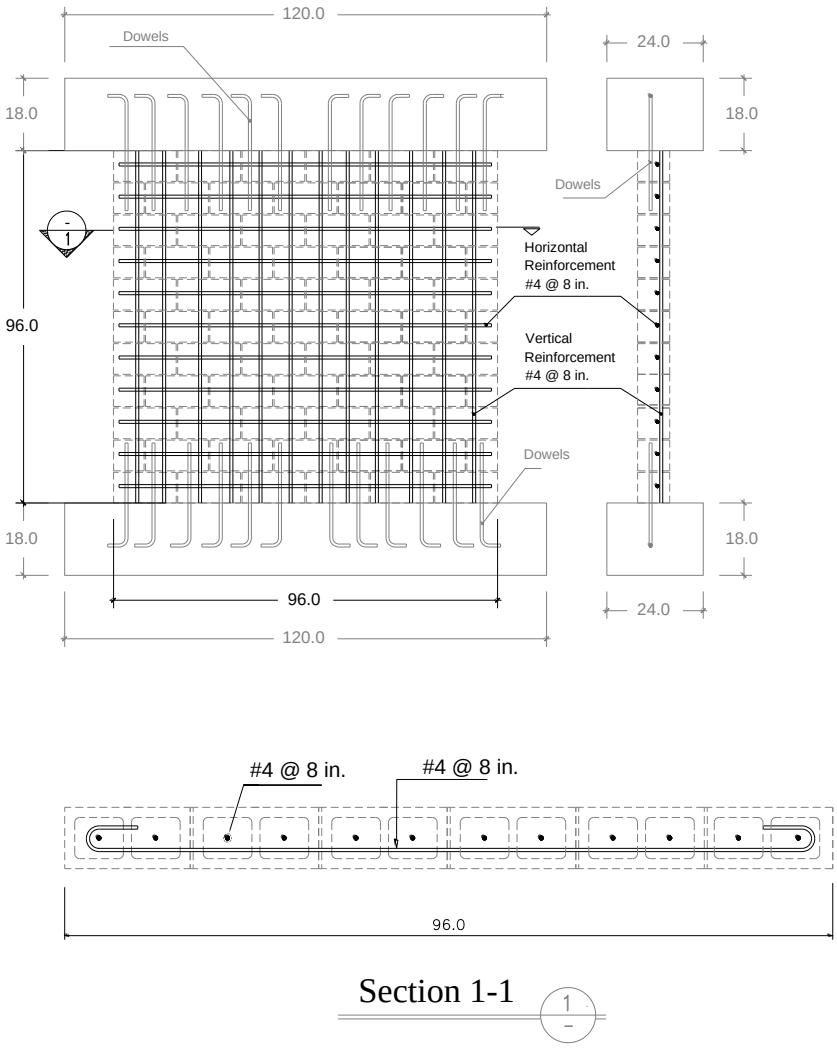

Figure 3-7 Detailing of Specimen PBS-11

Wall Specimens PBS-12 and PBS-12G

Wall specimen PBS-12 and PBS-12G were 96-in. wide, 96-in. high, and 7.625-in. thick with #4 bars every 16 in. vertically and horizontally and axial load ratio, $P / (f_m' A_g)$, equal to 0.10.

Prescriptive Reinforcement Requirement of Specimen PBS-12 and PBS-12G

Section 1.18.3.2.6 of the 2011 MSJC *Code* (MSJC 2011a) requires, for special reinforced masonry shear walls, that the minimum reinforcement ratio for each direction be at least 0.0007, and that the sum of the reinforcement ratios in each direction be at least 0.002.

$$\rho_v = \frac{A_{sv}}{b\ d} = \frac{0.20\ in.^2}{(7.625\ in.)\ (16\ in.)} = 0.0016 > 0.0007 \quad OK.$$

$$\rho_h = \frac{A_{sh}}{b\ d} = \frac{0.20\ in.^2}{(7.625\ in.)\ (16\ in.)} = 0.0016 > 0.0007 \quad OK.$$

$$\rho_h + \rho_v = 0.0016 + 0.0016 = 0.0032 > 0.002 \quad OK.$$

The maximum reinforcement ratio was calculated from Section 3.3.3.5 of 2011 MSJC *Code* (MSJC 2011a) where α was taken as 4 for special reinforced masonry shear walls.

$$\rho_{max} = \frac{0.64\ f'_m \left(\frac{\varepsilon_{mu}}{\varepsilon_{mu} + \alpha\ \varepsilon_y}\right) - \frac{P_n}{b\ d_v}}{f_y \left(\frac{\alpha\ \varepsilon_y - \varepsilon_{mu}}{\varepsilon_{mu} + \alpha\ \varepsilon_y}\right)}$$

Where,

$$P_n = 0.10\, f'_m\, A_g$$

$$P_n = 0.10\,(2500\ psi)(96\ in.)(7.625\ in.)$$

$$P_n = 183\ kips$$

$$\rho_{max} = \frac{0.64\,(2500\ psi)\left[\frac{0.0025}{0.0025 + (4)(0.00207)}\right] - \frac{183000\ lb}{(7.625\ in.)(96\ in.)}}{60000\ psi\left[\frac{(4)(0.00207) - 0.0025}{0.0025 + (4)(0.00207)}\right]}$$

$$\rho_{max} = 0.00376 > 0.0033 \quad OK.$$

Flexural Capacity of Specimen PBS-12 and PBS-12G

The moment capacity of Specimens PBS-12 and PBS-12G was calculated according to the design assumptions of the 2011 MSJC *Code* (MSJC 2011a), Section 3.3.2. The specified compressive strength of masonry, f_m', was taken as 2500 psi and the specified yield strength of reinforcement, f_y, equal to 60 ksi. As shown in the nominal moment-axial force interaction diagram of Figure 3-8 for axial load ratio, P / ($f_m' A_g$), equal to 0.10 the nominal moment capacity of Specimens PBS-12 and PBS-12G is 858 ft-kips.

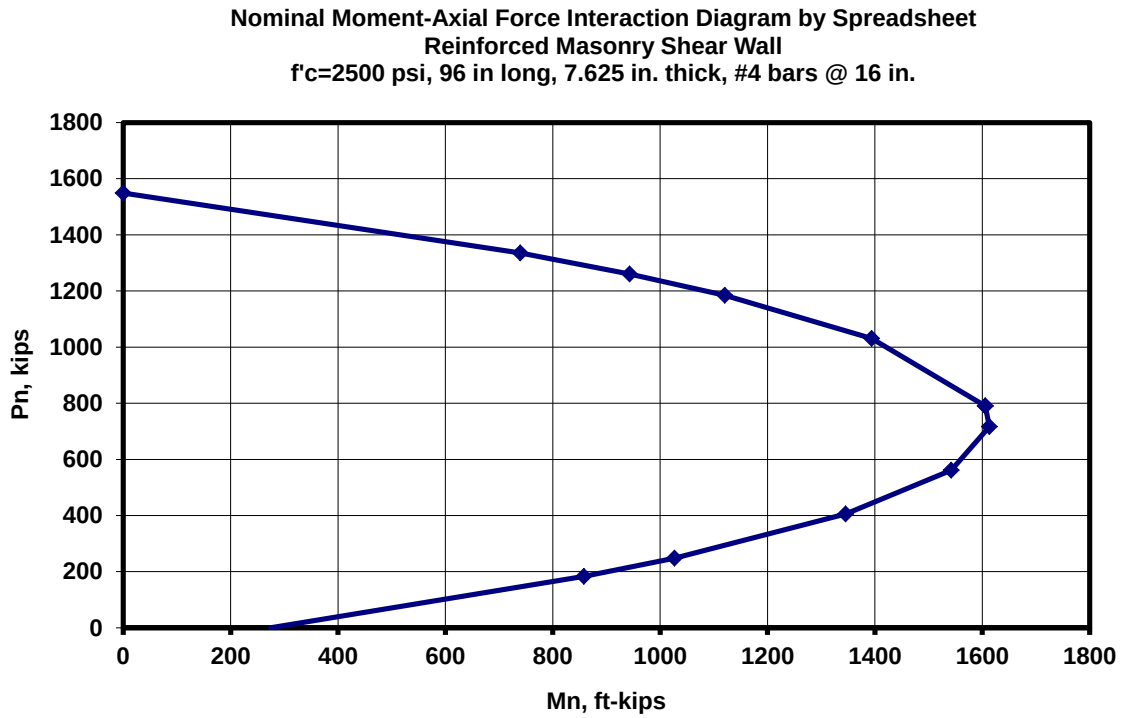

Figure 3-8 Moment-axial Force interaction diagram for Specimens PBS-12 and PBS-12G

The shear corresponding to the development of flexural capacity for Specimens PBS-12 and PBS-12G would be

$$V_u(M_n) = \frac{M_n}{H} = \frac{858ft - kips}{8.75\ ft} = 98.06 \text{ kips}$$

where *H* is the distance from the base of the shear-wall segment to the mid-height of the loading beam (line of action of the applied load).

Shear Capacity of Specimen PBS-12 and PBS-12G

The nominal masonry shear strength of Specimens PBS-12 and PBS-12G, V_{nm}, was calculated according to Section 3.3.4.1.2.1 of the 2011 MSJC *Code* (MSJC 2011a).

$$V_{nm} = \left[4.0 - 1.75\left(\frac{M_u}{V_u\ d_v}\right)\right] A_n\ \sqrt{f'_m} + 0.25\ P_n$$

For cantilever walls $M_u = V_u\ H$, so the term in parenthesis becomes the aspect ratio of the wall segment, which in this case equals 1.0.

$$V_{nm} = [4.0 - 1.75\ (1)]\ (7.625\ in.)(96\ in.)\ \sqrt{2500} + 0.25\ (183000\ lb)$$

$$V_{nm} = 128.10\ kips$$

The nominal masonry shear strength, V_{nm}, is higher than the maximum shear corresponding to the flexural capacity, 98.06 kips; as a result, it is not necessary to have shear reinforcement to ensure a flexural failure.

The nominal shear strength provided by reinforcement, V_{ns}, was calculated according to Section 3.3.4.1.2.2 of 2011 MSJC *Code* (MSJC 2011a).

$$V_{ns} = 0.5\left(\frac{A_v}{s}\right) f_y\ d_v$$

$$V_{ns} = 0.5\left(\frac{0.20\ in.^2}{16\ in.}\right)(60000\ psi)\ (96\ in.)$$

$$V_{ns} = 36.0\ kips$$

The shear capacity design provisions of the 2011 MSJC *Code* (MSJC 2011a), Section 1.18.3.2.6.1, require that the design shear strength, ϕV_n, equal or exceed 1.25 times the shear corresponding to the flexural capacity.

$$V_n = V_{nm} + V_{ns}$$

$$V_n = 128.10\ kips + 36.0\ kips$$

$$V_n = 164.10\ kips$$

$$\emptyset\ V_n = (0.80)\ 164.10\ kips \quad > \quad 1.25\ (98.06)\ kips)$$

$$131.28\ kips\ >\ 122.57\ kips \quad Ok$$

Sliding-shear Capacity of Specimens PBS-12 and PBS-12G

Sliding failure can occur in wall segments with low levels of axial load. Because the 2011 MSJC *Code* does not have general shear-friction provisions, the sliding-shear capacity of Specimens PBS-12 and PBS-12G was estimated using the shear-friction provisions of Section 11.6.4 of ACI 318-08 (ACI 318-2008). The coefficient of friction, μ, was taken as 1.0.

$$V_s = \mu\ (A_v\ f_y + P_n)$$

$$V_s = (6)\ (0.20\ in.^2)(60000\ psi) + 183000\ lb$$

$$V_s = 255\ kips$$

Detailing of Specimen PBS-12 and PBS-12G

As shown in Figure 3-9, Specimens PBS-12 and PBS-12G were 96-in. wide, 96-in. high, and 7.625-in. thick with #4 bars every 16 in. vertically and horizontally. This detailing meets the requirements of the 2011 MSCJ *Code*.

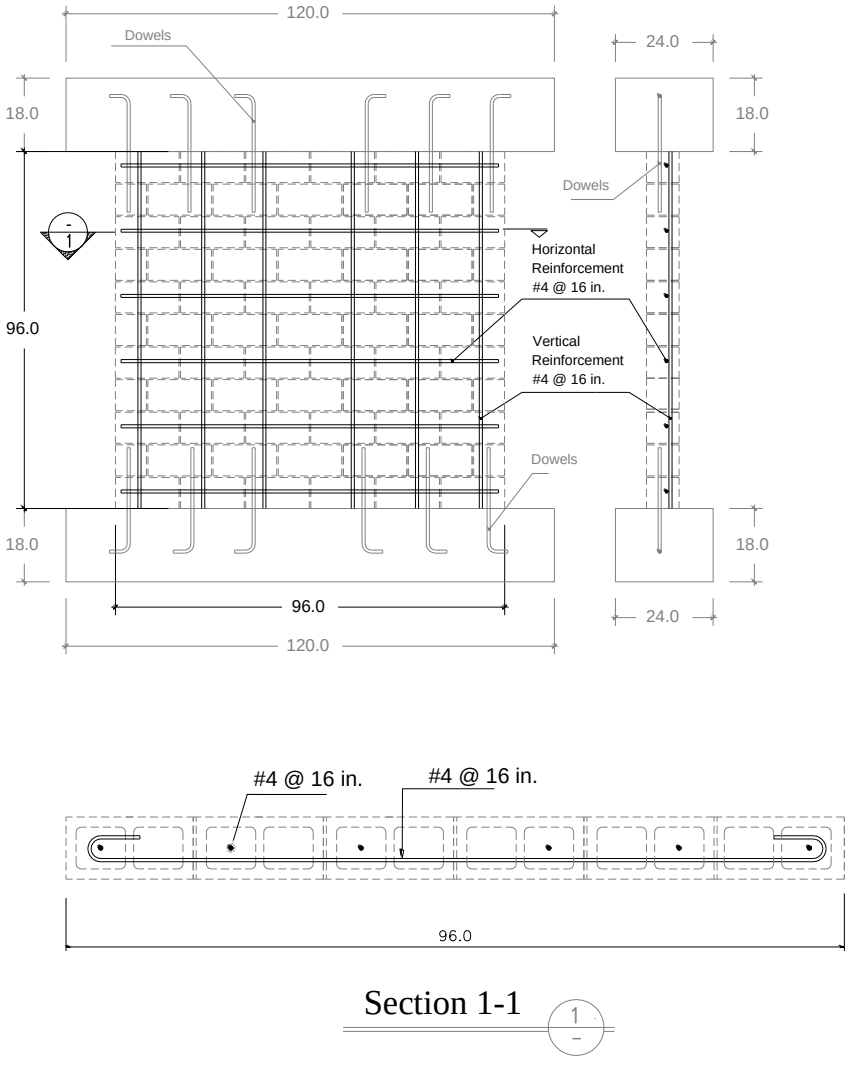

Figure 3-9 Detailing of Specimen PBS-12 and PBS-12G

3.3. DESIGN SUMMARY

Table 3-2 presents the maximum nominal capacities of each wall specimen as governed by flexure, shear, and sliding. Flexure governs for all specimens.

Table 3-2 Nominal capacities of each wall specimen

Wall Specimen	**Aspect Ratio**	**P / (f'm Ag)**	**Vertical Reinforcement (Percentage, %)**	**Horizontal Reinforcement (Percentage, %)**	**Nominal Flexural Capacity kips**	**Nominal Shear Capacity kips**	**Nominal Sliding Capacity kips**
"Gray Blocks"							
PBS – 3	1.0	0	#4 @ 8 in. (0.33)	#4 @ 8 in. (0.33)	60.11	154.35	144.00
PBS – 4	1.0	0	#4 @ 16 in. (0.16)	#4 @ 16 in. (0.16)	31.43	118.35	72.00
PBS – 11	1.0	0.10	#4 @ 8 in. (0.33)	#4 @ 8 in. (0.33)	119.89	200.10	327.00
PBS – 12	1.0	0.10	#4 @ 16 in. (0.16)	#4 @ 16 in. (0.16)	98.06	164.10	255.00
"Green Blocks"							
PBS – 4G	1.0	0	#4 @ 16 in. (0.16)	#4 @ 16 in. (0.16)	31.43	118.35	72.00
PBS – 12G	1.0	0.10	#4 @ 16 in. (0.16)	#4 @ 16 in. (0.16)	98.06	164.10	255.00

Chapter 4 : Test Setup for Cantilever Shear-Wall Segments

4.1. Overall Description of Test Setup

Six masonry shear-wall specimens, each representing a segment of a perforated shear wall, were constructed at the Ferguson Structural Engineering Laboratory of the University of Texas at Austin. Each of these specimens was 96-in. wide, 96-in. high and 7.625-in. thick, constructed of concrete masonry units (CMU), and fully grouted. Each specimen was supported on a reinforced-concrete base beam, which was anchored to the laboratory floor through two foundation beam (one on each side of the base beam) to prevent sliding or rocking during tests. Each specimen was loaded vertical and laterally in-plane through a reinforced-concrete loading beam. The components comprising each cantilever wall specimen are shown in Figure 4-1.

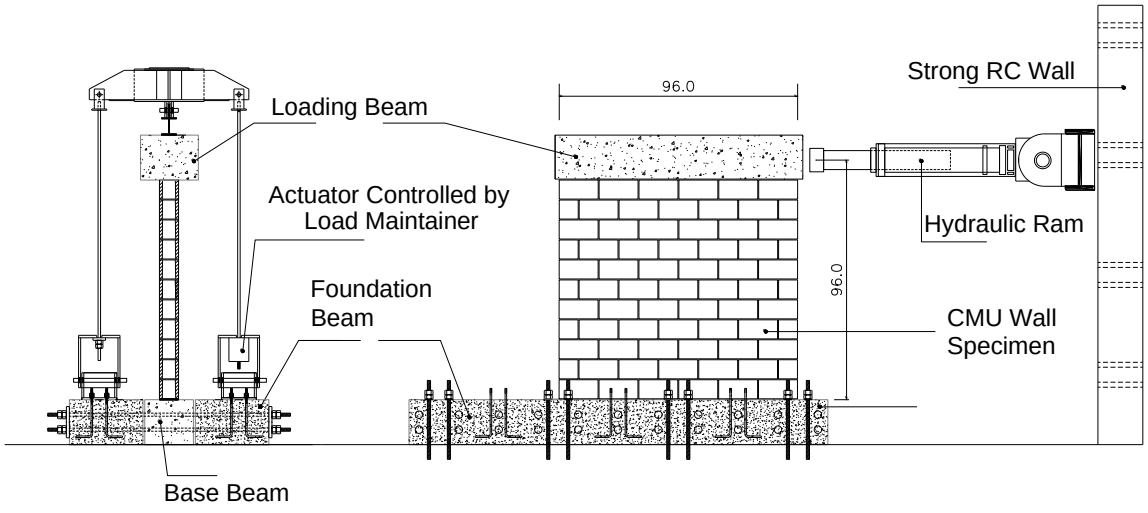

Figure 4-1 Components comprising each cantilever wall specimen

4.1.1 Wall Segment

In this study, wall segments were reinforced and fully grouted concrete masonry walls 96-in. high, 96-in. long, and 7.625-in. thick. Vertical and horizontal reinforcement consisted of #4 bars, whose spacing for each specimen was developed as explained in Section 3.1.

4.1.2 Reinforced-concrete Loading Beam

The reinforced-concrete loading beam was designed to permit the application of lateral and axial load to the wall segment, independent of the design of the segment itself. One loading beam was constructed for each specimen. Each loading beam was 120-in. long, 24-in. wide and 18-in. high. Two horizontal PVC tubes were placed inside the beam to aid in moving it by crane in the lab. Six vertical PVC tubes were placed in the beam, four to attach the axial load system and two to facilitate the grouting process. As shown in Figure 4-2, dowels in the loading beam were spliced to vertical reinforcement in the wall segment and prevented sliding at the interface between the wall segment and the loading beam.

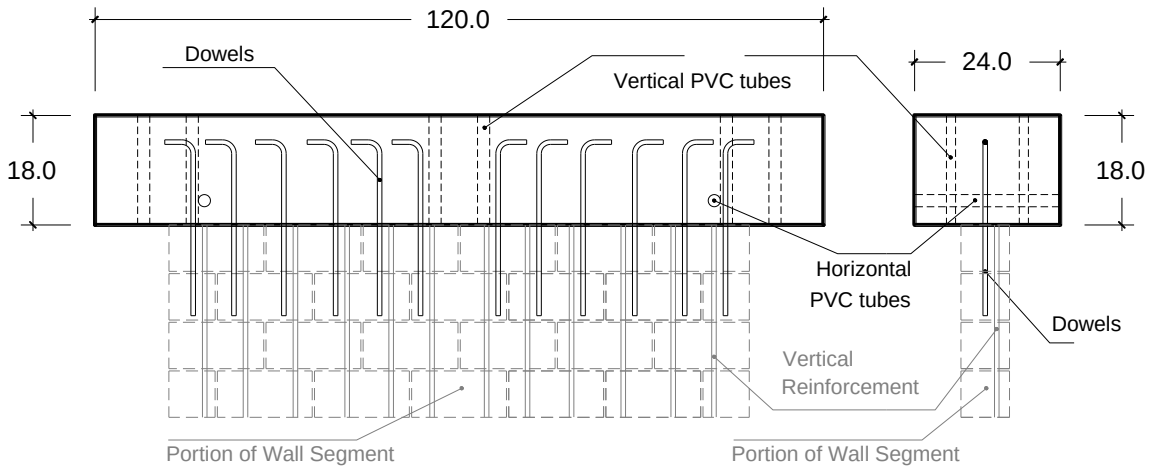

Figure 4-2 Details of loading beam

4.1.3 Reinforced-concrete Base Beam

A reinforced-concrete base beam was used to anchor wall segments to two foundation beams and transmit the load to the laboratory floor. Each base beam was 120-in. long, 24-in. wide and 18-in. high. Horizontal PVC tubes were placed inside each base beam to post-tension them to the foundation beams using threaded rods. As shown in Figure 4-3, dowels in the base beam were spliced to vertical reinforcement in the wall segment and prevented sliding at the interface between the wall segment and the base beam.

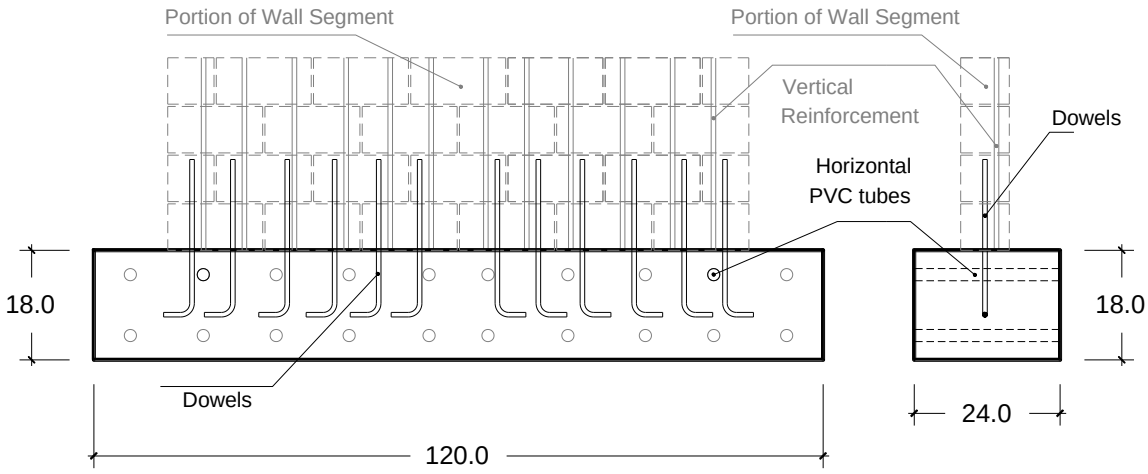

Figure 4-3 Details of base beam

4.1.4 Reinforced-concrete Foundation Beams

Foundation beams consisted in two reinforced-concrete beams which were post-tensioned horizontally to the specimen (through the base beam) and post-tensioned vertically to tie the specimen to the strong floor of the laboratory. A single set of two foundation beams was used for all tests.

As shown in Figure 4-4, each of the two foundation beams was 168-in. long, 28-in. wide and 18-in. high. Horizontal PVC tubes inside each foundation beam were used to guide the threaded rods that were used to post-tension the foundation beams to the base beam. Vertical PVC tubes inside each foundation beam, located to match the holes in the laboratory floor, were used to guide the threaded rods that were used to post-tension the foundation beams to the laboratory floor. Coil-rod inserts in the foundation beams were used to connect the axial load system, and also to move beams in the laboratory.

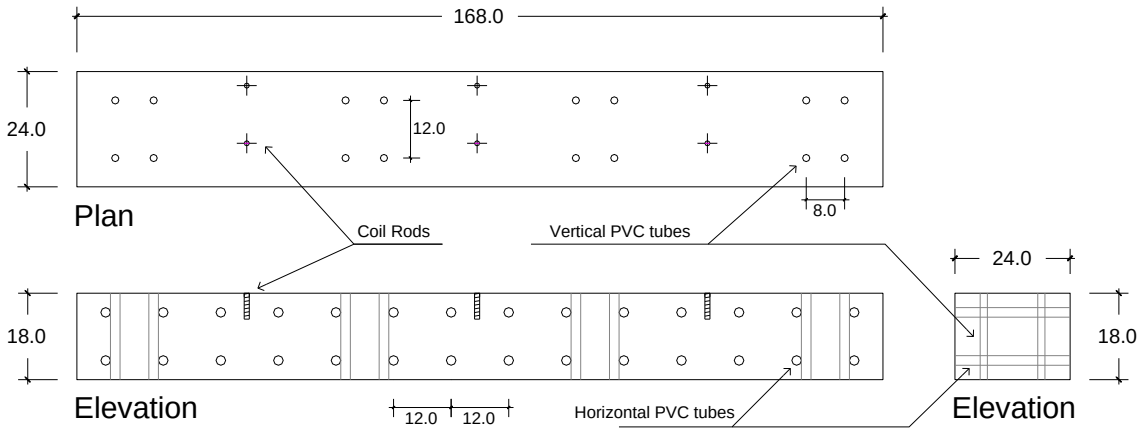

Figure 4-4 Details of foundation beams

4.2. DESIGN OF TEST SETUP

4.2.1 Design of Foundation Beams

The foundation beams were designed to resist the maximum overturning moment applied to each wall specimen, using the provisions of ACI 318-11. As shown in Figure 4-5, reinforcement consisted of 3 #8 bars at the top and 3 #8 bars at the bottom, with one tie and one supplementary #4 cross-tie every 6 in.

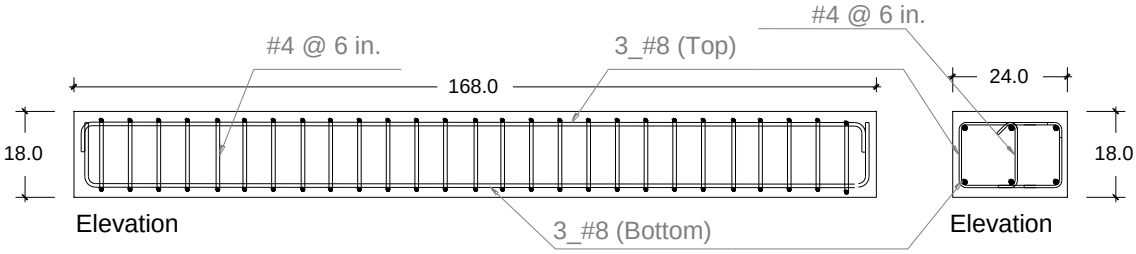

Figure 4-5 Details of foundation beams

4.2.2 Design of Base Beams

Base beams were designed to resist the maximum shear from the toe of wall segments. As shown in Figure 4-6, reinforcement consisted in 3 #8 bars at the top and 3 #8 bars at the bottom, with one #4 tie and one #4 supplementary cross-tie every 6 in. Dowels in the base beam were designed according to the 2011 MSJC Code (MSJC 2011a). Dowels had the same diameter as the vertical reinforcement of the corresponding wall segment.

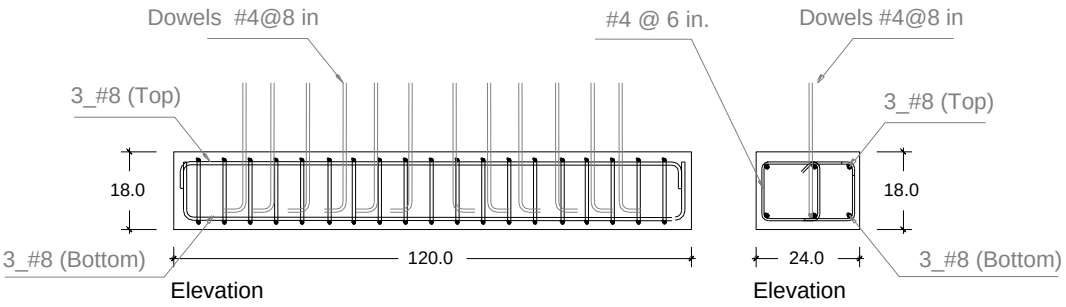

PBS-3 and PBS-11

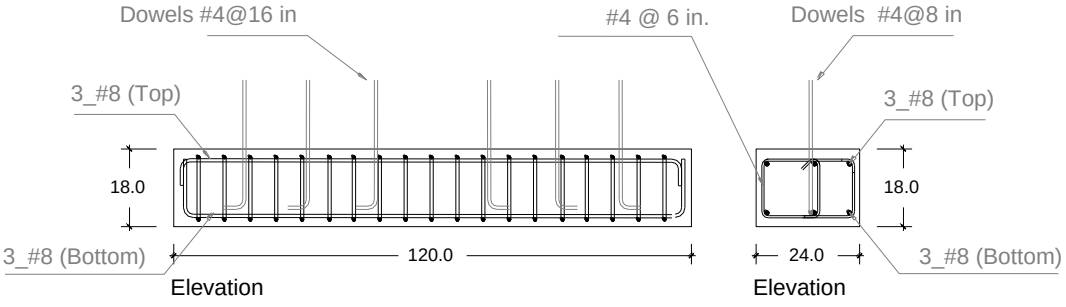

PBS-4, PBS-4G, PBS-12, and PBS-12G

Figure 4-6 Details of the base beams

4.2.3 Design of Loading Beam

No calculations were carried out for the design of the loading beam. The loading beam was required to resist the axial force from the lateral load applied by the hydraulic ram.

As shown in Figure 4-7, reinforcement consisted of 4 #8 bars at the top and 4 #8 bars at the bottom, with one #4 tie and two supplementary cross-ties every 6 in. Dowels in the loading beams were designed according to the 2011 MSJC Code (MSJC 2011a). Dowels had the same diameter as the vertical reinforcement of the corresponding wall segment.

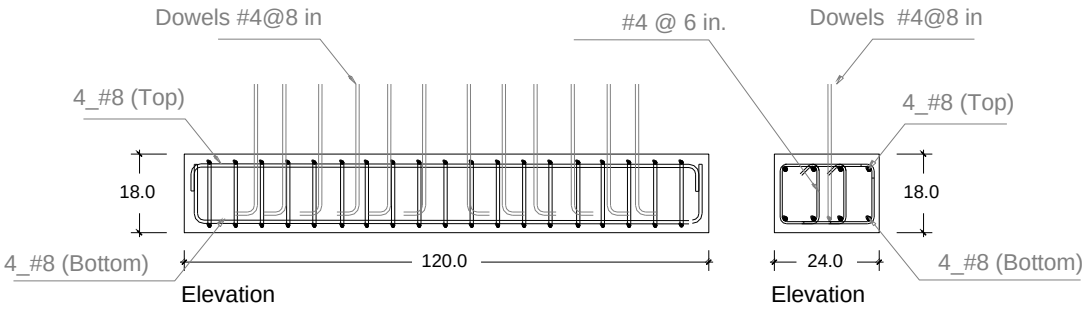

PBS-3 and PBS-11

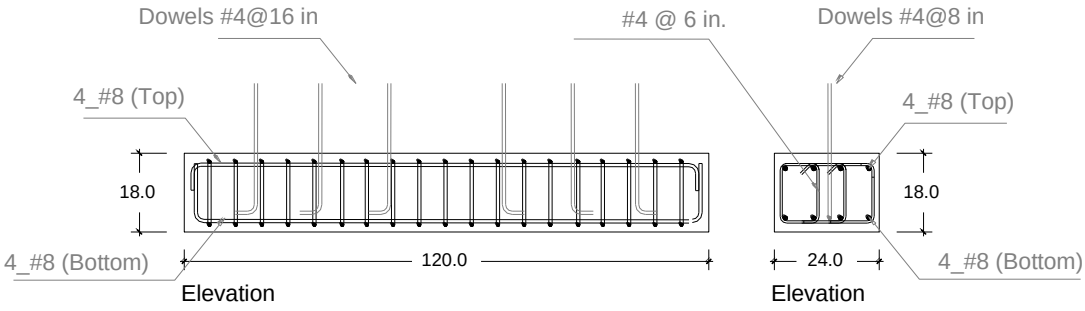

PBS-4, PBS-4G, PBS-12, and PBS-12G

Figure 4-7 Details of loading beams

4.3. CONSTRUCTION OF TEST SETUP

4.3.1 Construction of the Base Beam, Loading Beam and Foundation Beam

Most of the steps in the construction of each of the beams were the same. Small differences in the function of the beams were considered without changing the construction process. The general construction steps are explained below.

Construction of beams began with the construction of the formwork. Each side of wooden formwork consisted of a piece of plywood over a 2- x 4-in. frame with 2- by 4-in. bracing. As shown in Figure 4-8, holes were drilled in lateral form members where PVC tubes would be inserted later.

Figure 4-8 Construction of formwork for beams

When all formwork sides were ready, they were placed in the casting platform (wooden floor). The formwork sides were aligned, squared and screwed to the floor and to other perpendicular sides. Joints between the formwork sides and the platform were sealed to prevent leakage and consequent voids or segregation of concrete.

Parallel to the construction of the formwork, reinforcement cages were assembled as shown in Figure 4-9. Transverse reinforcement was tied to the longitudinal bars to prevent interference with horizontal and vertical PVC tube locations.

Figure 4-9 Assembling reinforcement cages for beams

Small circular disks of plywood (1.5-in. in diameter) were used to hold vertical PVC tubes straight; they were screwed to the platform inside the formwork before the cages were positioned in place. Cages were placed inside the formwork; PVC tubes were placed in holes and on the wooden disks; and gaps between the tubes and formwork were sealed. The tops of the vertical PVC tubes were covered and braced with wooden 2- by 4-in. pieces screwed to lateral formwork. Dowels were attached to the cage for the base beams and loading beams. For foundation beams, three pairs of coil rods were attached to the cage. Figure 4-10 shows typical beams before casting.

Figure 4-10 Typical beams before casting

Beams were cast with using concrete with a specified compressive strength of at least 4000 psi, and slumps between 8 and 9 in.

4.3.2 Construction of Masonry Wall Segments.

Masonry wall segments were constructed at the Ferguson Structural Engineering Laboratory at the University of Texas at Austin by professional masons. The first course of masonry units were placed on mortar bedding, creating a bond with the base beam, and with mortar joints between units. Cleanouts were cut into the masonry units in the lowest course, and the cut pieces were replaced in position before grouting. When necessary, webs were partially removed to permit the placement of horizontal reinforcement. As shown in Figure 4-11, special care was taken to locate the extreme vertical reinforcement inside of the 180-degree hook at each end of the horizontal bars.

Figure 4-11 Placement of horizontal reinforcement in cells of units

Additional courses were constructed using the same procedure. Masonry units were placed level, plumb, and true. When the wall segment was complete, the required vertical reinforcement was placed in the appropriate cells, and was checked using the weepholes, which were then sealed. The loading beam was lifted, inverted from its casting position so that the dowels would point down, and its alignment was checked by locating the loading beam temporarily on top of the wall segment. The loading beams were then lifted by crane, and the cells of the masonry wall segments were filled to the top with grout. The loading beam were again placed on the wall and aligned. Finally, grout was poured through vertical PVC tubes next to the dowels to fill empty spaces in cells.

4.4. MATERIAL PROPERTIES AND TESTING

Materials used to construct the masonry wall segments were tested to determine their strengths. Concrete masonry units, mortar, grout and prisms were tested at the Ferguson Structural Engineering Laboratory and Concrete Durability Center at the University of Texas at Austin

Concrete Masonry Units (CMU)

Wall segments described in part of this thesis were constructed with two different types of concrete masonry units: “Gray blocks” and “Green blocks” (made of recycled materials). Blocks were nominal 8- x 8-x 16-in. hollow CMU meeting ASTM C90. For the compressive strength test, three blocks of each type were saw-cut into 8-x 8- x 8-in. specimens. Compressive strengths were obtained according to ASTM C140 (Figure 4-12). Results are shown in Table 4-1.

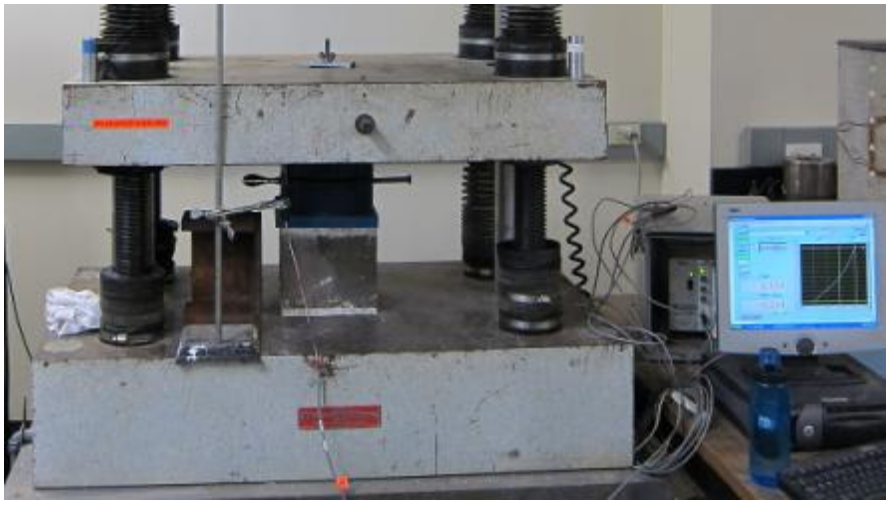

Figure 4-12 Compressive strength testing of concrete masonry units

Table 4-1 Dimensions and compressive strengths of concrete masonry units

CMU Specimen	Average Width (in.)	Average Height (in.)	Average Length (in.)	Average Thickness (in.)	Compressive Strength (ksi)	Average (ksi)
"Gray" #1	7.68	7.58	7.65	1.40	3.55	3.48
"Gray" #2					3.55	
"Gray" #3					3.35	
"Green" #1	7.65	7.62	7.64	1.38	2.80	2.85
"Green" #2					2.75	
"Green" #3					3.05	

Mortar

Mortar conformed to ASTM C270, cement-lime, Type S by proportion. Two-in. mortar cubes were tested according to ASTM C780. Two specimens from the sample "Gray 2" and one from sample "Green 1" had compressive strengths that differed more than 10% from the average of the corresponding sample; as a result, those specimens were not included in averages. All "Gray 2" sample results were discarded for having just one valid specimen. Results are shown in Table 4-2.

Table 4-2 Compressive strengths of mortar cubes

Set of mortar cubes	Compressive strengths of mortar cubes, ksi			
	"Gray" 1	"Gray" 2	"Green'' 1	"Green" 2
Set 1	2.144	-	-	1.864
Set 2	1.923	-	1.637	1.951
Set 3	2.242	-	1.702	1.950
Average	2.103		1.821	

Grout

Wall segments were filled with coarse grout specified by proportion conforming to ASTM C476. Grout specimens of 4- x 4-x 8-in. were tested according to ASTM C1019. Compressive strengths are presented in Table 4-3.

Table 4-3 Compressive strengths of grout specimens

Set of grout specimens	"Gray" Blocks	"Green" Blocks
Grout Specimen 1 (psi)	4635	5114
Grout Specimen 2 (psi)	4585	4379
Grout Specimen 3 (psi)	4321	4518
Average (psi)	**4513**	**4670**

Concrete Masonry Prisms

Six grouted concrete masonry prisms were tested according to ASTM C1314. Grouted prims were 8- x 8- x 16-in. Each prism was constructed using two concrete masonry half-units. Prisms were capped with hydrostone. The compressive strength of two of these prisms exceeded the capacity of the compression test machine, so they could not been tested completely and they were discarded. A higher-capacity compression machine was used to test the remaining specimens (Figure 4-13). Results are shown in Table 4-4.

Table 4-4 Compressive strengths of CMU prisms

Set of prism specimens	"Gray"	"Green"
Prism 1 (psi)	4798	3540
Prism 2 (psi)	3615	3505
Prism 3 (psi)	-	-
Average (psi)	**4206**	**3522**

Figure 4-13 Compressive strength testing of masonry prisms

Reinforcement

Vertical and horizontal reinforcement was Grade 60. Three #4 bars taken from the same heat as those used in the wall segments were tested to determine yield stress, f_y, and ultimate stress, f_u. Results are presented in Table 4-5.

Table 4-5 Tensile strengths of #4 reinforcing bars

Specimen Number	Yield Stress (ksi)	Ultimate Stress (ksi)
1	62.8	100.6
2	60.9	98.1
3	60.6	97.5
Average	**61.43**	**98.72**

Chapter 5 : Testing Procedures

5.1. LOADING SYSTEM

Specimens were tested at the Ferguson Structural Engineering Laboratory of The University of Texas at Austin. The loading system consisted of a lateral loading system, a gravity loading system, and an out-of-plane bracing system. The lateral loading system was composed of a hydraulic ram reacting against the laboratory strong wall. The gravity loading system included two small rams controlled by a load maintainer and connected to a swivel steel beam at the top of the specimen. The out-of-plane bracing system consisted of two steel channels bolted to W-shape steel columns. Figure 5-1 illustrates the test setup.

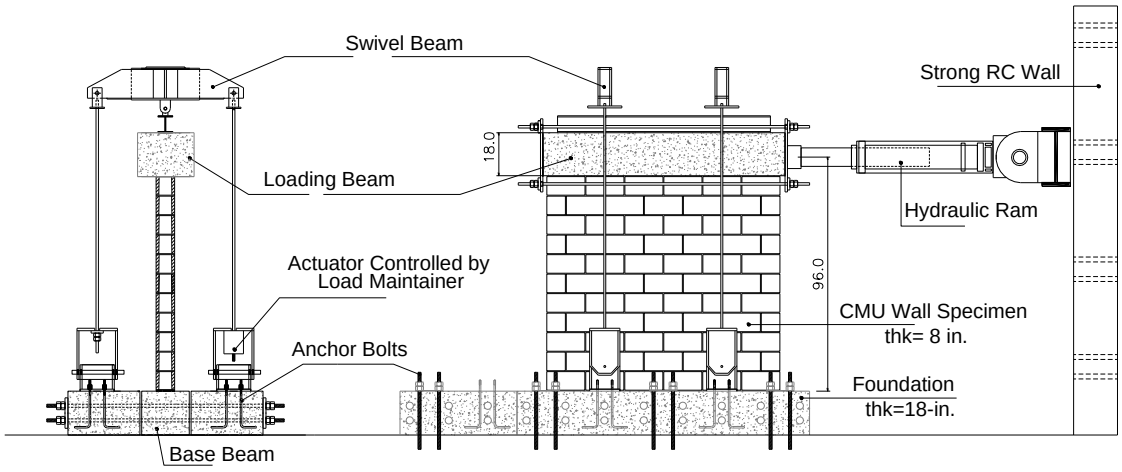

Figure 5-1 Test setup

Lateral Loading System

The lateral load system consisted of a Miller Cylinder hydraulic ram connected to the loading beam of the specimen and reacting against a strong wall (see Figure 5-2). The ram was connected to a hydraulic pump, which was controlled manually. The ram had a maximum capacity of 130 kips in tension and 192 kips in compression, and a total stroke of 18 in.

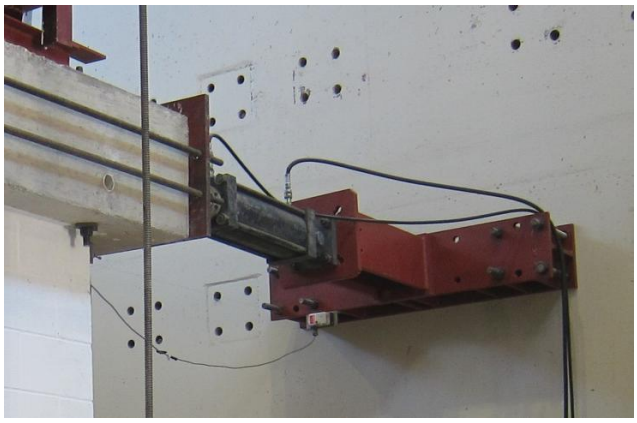

Figure 5-2 Hydraulic Ram

Axial Loading System

Axial loads in the wall segments due to gravity load were reproduced by applying a constant axial load to the specimen. The gravity loading system consisted of two swivel beam attached to the loading beam and connected to the foundation through four threaded rods. Each set of two threaded rods in front of and behind the specimen was placed in tension using a small ram installed over the foundation, as shown in Figure 5-3. The swivel beam could rotate freely, preventing out-of-plane moment in the wall. The pressure in the axial loading rams was kept constant with a load maintainer.

Figure 5-3 Axial loading system

Out-of-plane Bracing System

Specimens were braced laterally using two steel channels bolted to two strong columns and clamped to a steel beam on the loading beam. Sheets of tetrafluoroethylene (Teflon®) were placed in the surface of contact between channels and the steel beam to reduce friction. Out-of-plane bracing system is shown in Figure 5-4.

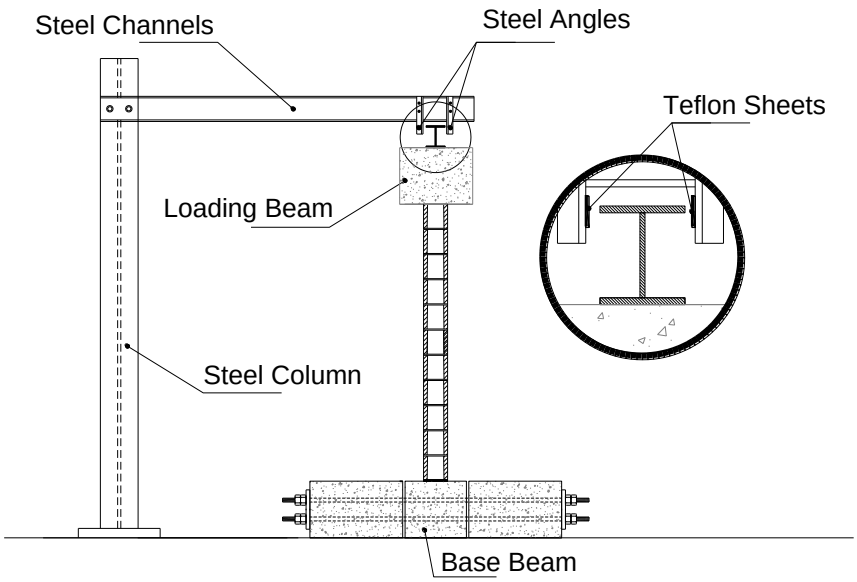

Figure 5-4 Out-of-plane bracing system

5.2. INSTRUMENTATION

Linear potentiometers, string potentiometers, strain gages, and load cells were used to measure the lateral displacement of each specimen, strains in reinforcing bars, strain in the concrete extreme fiber, base sliding, and applied lateral load.

Strain gages were attached to base beam dowels, vertical reinforcement and horizontal reinforcement (labeled as D, B and H respectively in Figure 5-5). Base beam dowels included: one strain gage at the base of the wall in every interior dowels, two strain gages at the base of the wall (north and south) and one strain gage 8-in from the base for exterior dowels. Strain gages in vertical reinforcement were attached only on extreme bars. For Specimens PBS-3 and PBS-11, strain gages in vertical reinforcement were located at 8, 16, 24, and 32 inches from the base of the wall. For Specimens PBS-4,

PBS-4G, PBS-12, and PBS-12G, strain gages in vertical reinforcement were located at 8, 16, 24, 32, and 40 inches from the base of the wall. In addition, four strain gages were attached to horizontal bars: one strain gage on each ends of the bar in the first course, and one strain gage each on the middle of the bars at the third and fifth courses.

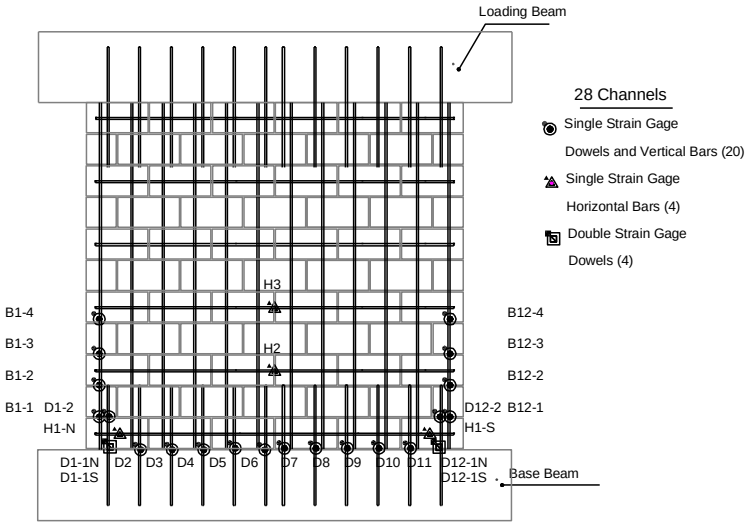

PBS-3 and PBS-11 Specimens

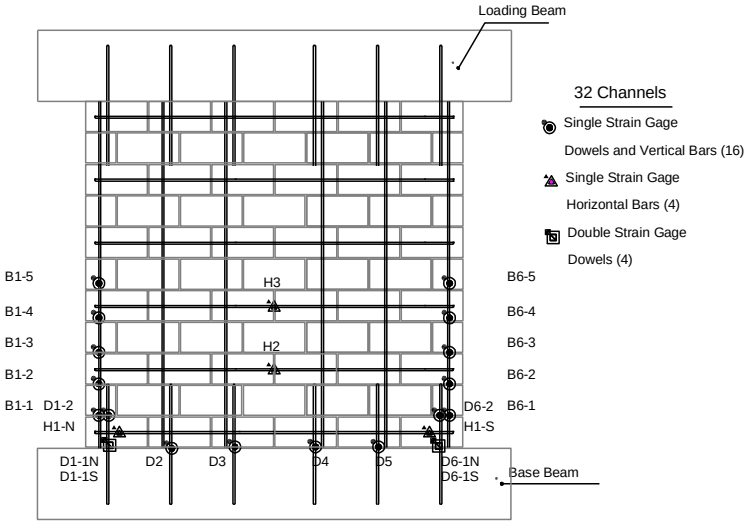

PBS-4, PBS-4G, PBS-12, and PBS-12G Specimens

Figure 5-5 Locations of strain gages in wall specimens

Eight linear potentiometers (LP-1 to LP-8) were used to measure strains in the extreme fiber of each specimen. Three more linear potentiometers were used to measure

sliding, two at the base (BS-N and BS-S) and one in the loading beam (top). Locations of linear potentiometers are shown in Figure 5-6.

Four string potentiometers were attached to the wall segment to measure shearing and flexural deformations (Shear-N, Shear-S, Dia-N, and Dia-S). One string potentiometers (Lat-Dis) was attached to the strong wall and connected to the loading beam to measure the wall lateral displacement. Figure 5-6 illustrates the location of the string potentiometers on the specimen.

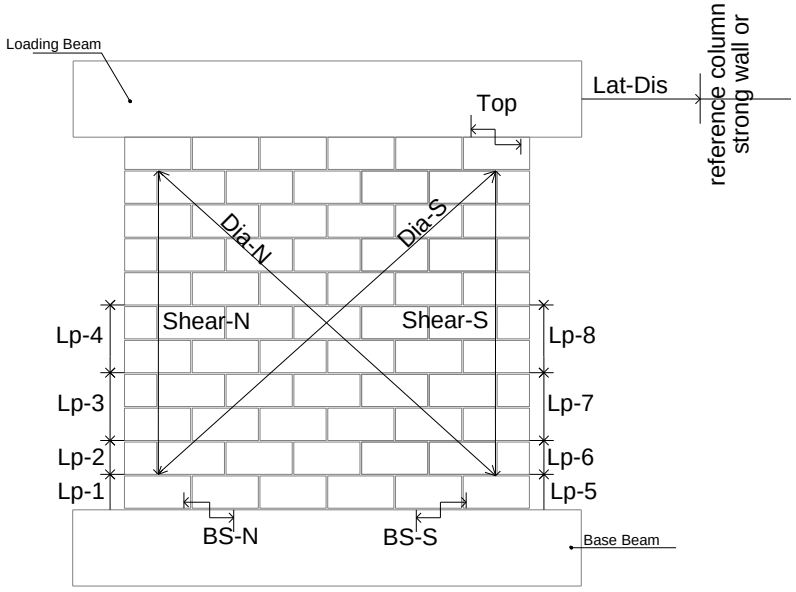

Figure 5-6 Locations of potentiometers on wall specimens

The applied lateral force was measured using a loading cell between the ram and clevis. The applied axial load was measured using a load cell in the rams of the axial load system. Figure 5-7 shows the loading cells in the test setup.

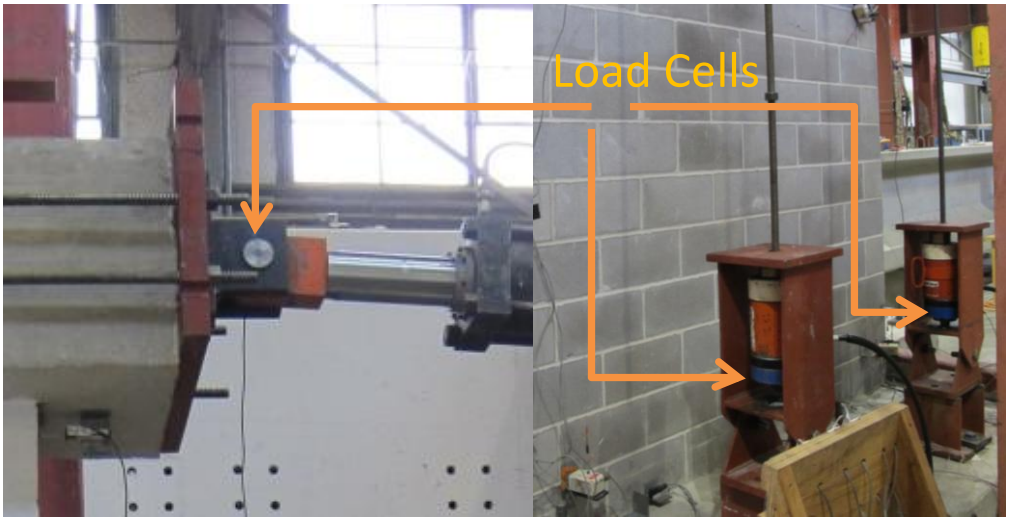

Figure 5-7 Load cells in lateral and axial loading systems

5.3. DATA ACQUISITION SYSTEM

The data acquisition system (DAQ) consisted of a power supply, a HP-3852 data acquisition unit, and a PC computer with custom data acquisition software written in National Instruments LabView® programming system.

The power supply provided an excitation voltage of 2V for strain gauges, and 10V for load cell and linear and string potentiometers. The HP-3852 data acquisition unit measured the analog signal (voltage) from the transducers. The transducers were connected in three different configurations. Strain gages used a quarter-bridge circuit. Load cells were full-bridge circuits. Linear and string potentiometers used a voltage divider circuit. An analog-to-digital converter, also included in the HP-3852, provided the digital data that was processed in the LabView® program.

5.4. TESTING PROTOCOL

A testing protocol was established not only for the six specimens pertaining to this thesis but also for other specimens which were part of the entire multi-university project.. The testing protocol for each specimen adhered to the following steps:

1. The expected maximum moment capacity of the specimen was calculated using expected values of f_y and f'_m as shown in Section 3.2.

2. Next, the horizontal load that produces the maximum moment predicted for the specimen was calculated.

3. A preliminary test which consisted of two reversed cycles at 25, 50 and 75% of the expected maximum load was conducted.

4. The value of the lateral displacements at +75% and -75% of the expected maximum load at the first cycle was averaged and considered equal to $\Delta_{75\%}$.

5. The lateral displacement for 100% the expected maximum load, $\Delta_{100\%}$, was then obtained by extrapolating from $\Delta_{75\%}$ ($\Delta_{100\%} = 4/3 * \Delta_{75\%}$). This value was considered as the yield displacement, Δ_y.

6. Two reversed cycles at 1, 2, 4, 6, 8, 10, 12, 14, 16 and 20Δ_y were defined as the steps in the testing protocol.

7. The test was ended when an 80% drop in the maximum load occurred.

Figure 5-8 to Figure 5-13 and Table 5-1 show the testing protocols for the specimens that are part of this thesis.

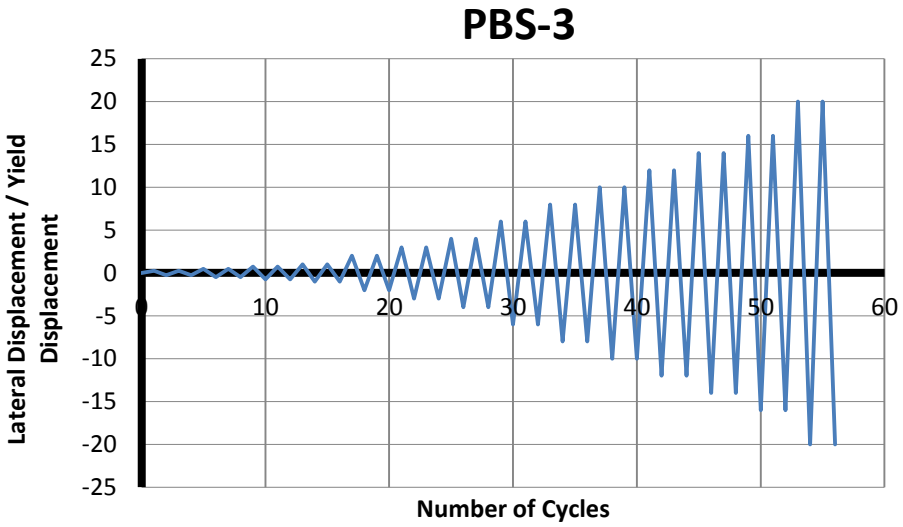

Figure 5-8 Testing protocol for specimen PBS-3

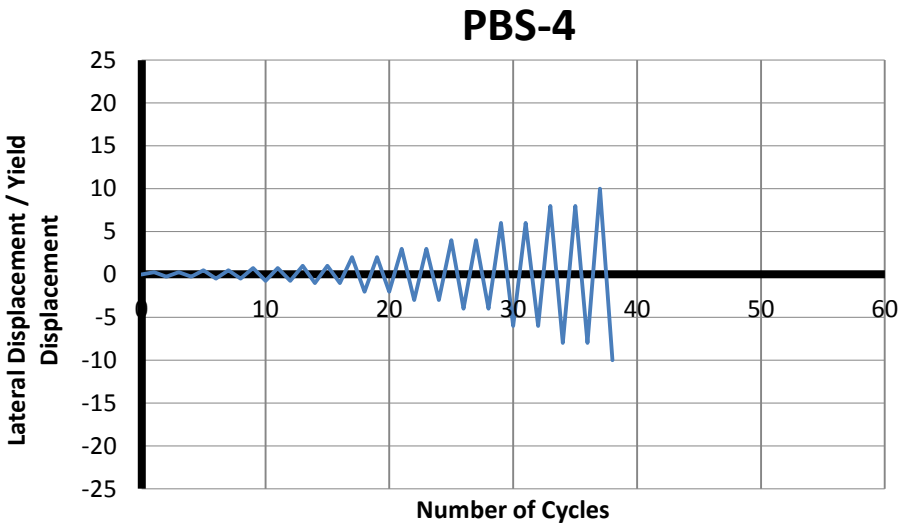

Figure 5-9 Testing protocol for specimen PBS-4

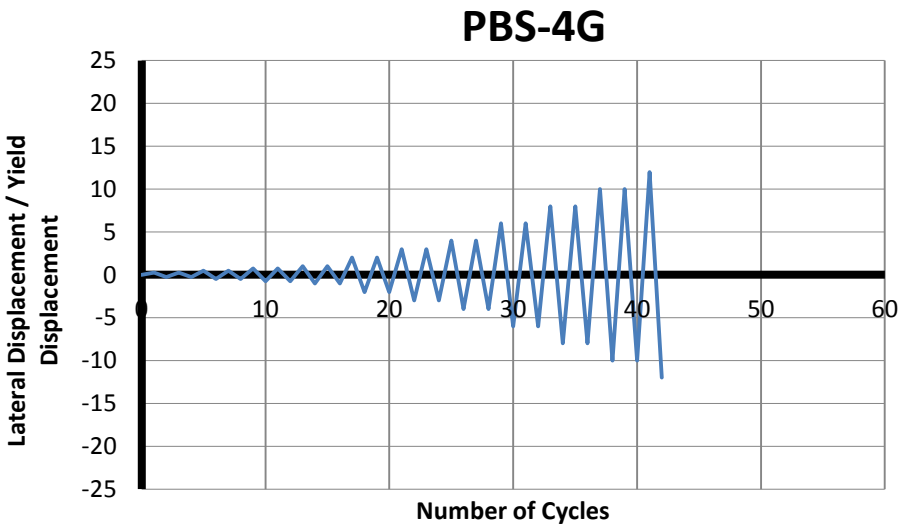

Figure 5-10 Testing protocol for specimen PBS-4G

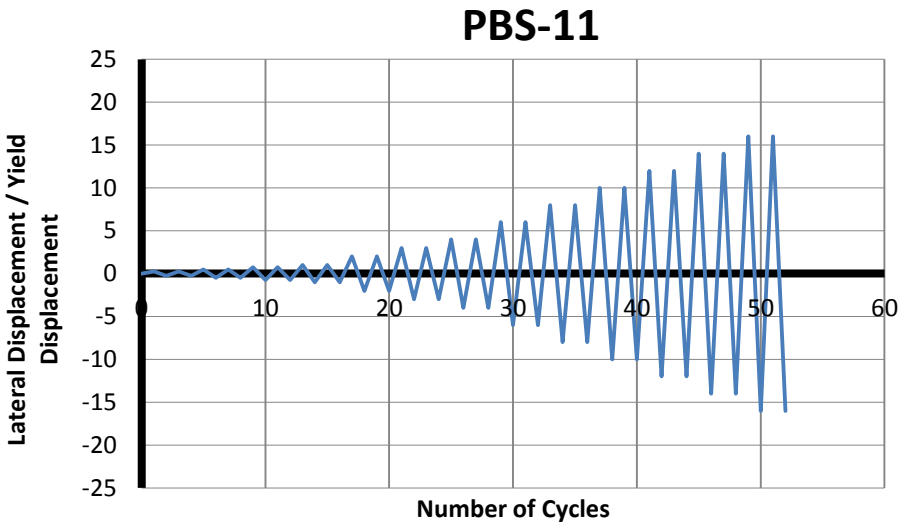

Figure 5-11 Testing protocol for specimen PBS-11

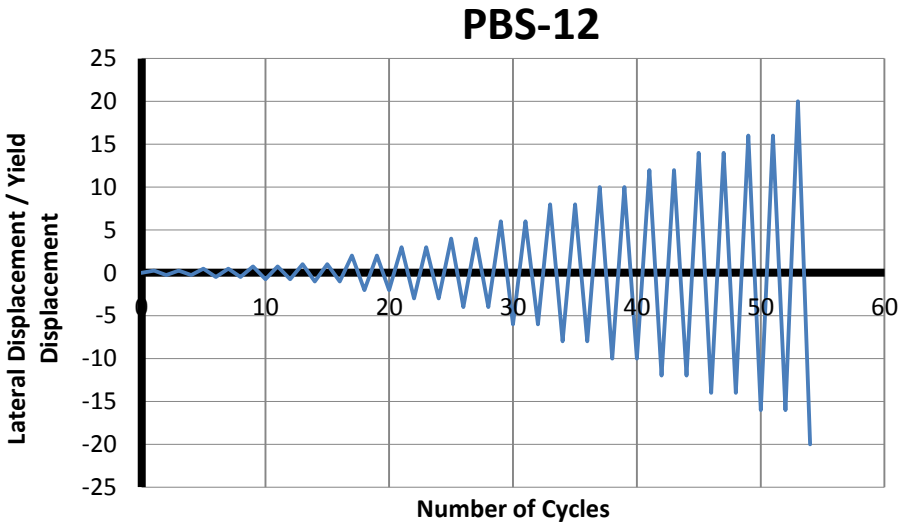

Figure 5-12 Testing protocol for specimen PBS-12

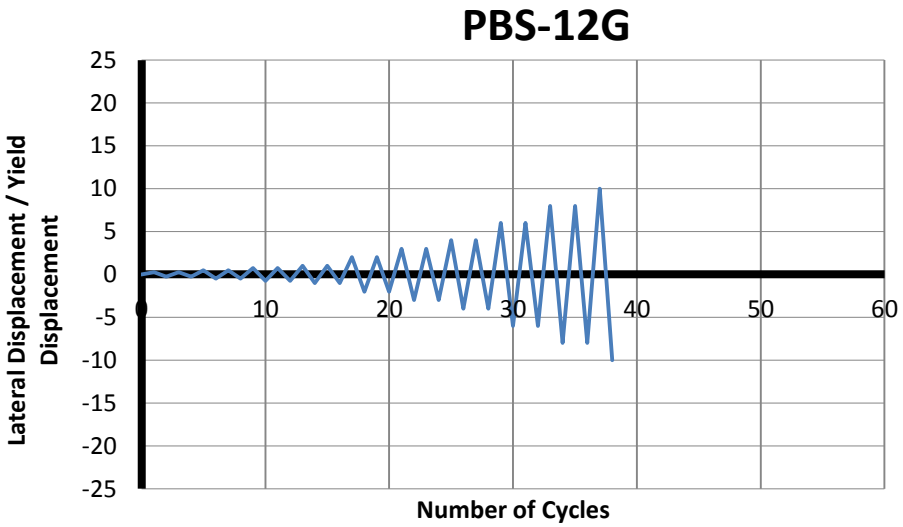

Figure 5-13 Testing protocol for specimen PBS-12G

Table 5-1 Testing protocol for all specimens

Specimen	PBS-3	PBS-4	PBS-4G	PBS-11	PBS-12	PBS-12G
Fraction of Predicted Maximum Load						
Preliminary Test	± 0.25	± 0.25	± 0.25	± 0.25	± 0.25	± 0.25
	± 0.25	± 0.25	± 0.25	± 0.25	± 0.25	± 0.25
	± 0.50	± 0.50	± 0.50	± 0.50	± 0.50	± 0.50
	± 0.50	± 0.50	± 0.50	± 0.50	± 0.50	± 0.50
	± 0.75	± 0.75	± 0.75	± 0.75	± 0.75	± 0.75
	± 0.75	± 0.75	± 0.75	± 0.75	± 0.75	± 0.75
Multiple of Calculated Yield Displacement (Δy)						
Loading Protocol	± 1	± 1	± 1	± 1	± 1	± 1
	± 1	± 1	± 1	± 1	± 1	± 1
	± 2	± 2	± 2	± 2	± 2	± 2
	± 2	± 2	± 2	± 2	± 2	± 2
	± 3	± 3	± 3	± 3	± 3	± 3
	± 3	± 3	± 3	± 3	± 3	± 3
	± 4	± 4	± 4	± 4	± 4	± 4
	± 4	± 4	± 4	± 4	± 4	± 4
	± 6	± 6	± 6	± 6	± 6	± 6
	± 6	± 6	± 6	± 6	± 6	± 6
	± 8	± 8	± 8	± 8	± 8	± 8
	± 8	± 8	± 8	± 8	± 8	± 8
	± 10	± 10	± 10	± 10	± 10	± 10
	± 10		± 10	± 10	± 10	
	± 12		± 12	± 12	± 12	
	± 12			± 12	± 12	
	± 14			± 14	± 14	
	± 14			± 14	± 14	
	± 16			± 16	± 16	
	± 16			± 16	± 16	
	± 20				± 20	
	± 20					

Chapter 6 : Results of Tests

6.1. INTRODUCTION

In this chapter, the behavior of the cantilever masonry shear-wall segments under reversed in-plane cyclic load is described. The progressive deterioration and failure modes of the specimens during the tests are presented. A load-displacement curve is plotted for each specimen, including the major events considered for this evaluation (maximum useful strain in masonry, vertical reinforcement yielding, toe crushing, maximum lateral load, and 20% decrease in load capacity).

6.2. SPECIMEN PBS-3

Specimen PBS-3 was 96-in. wide and 96-in. high (aspect ratio equal to 1.0) with #4 bars every 8 in. vertically and horizontally and an axial load equal to zero. The dowels were extended 16 in. (two courses) from the base of the wall segment. The expected moment capacity of Specimen PBS-3 was 526 ft-kips, equivalent to a lateral load of 60.11 kips as calculated in Section 3.2. Specimen PBS-3 before the test is shown in Figure 6-1.

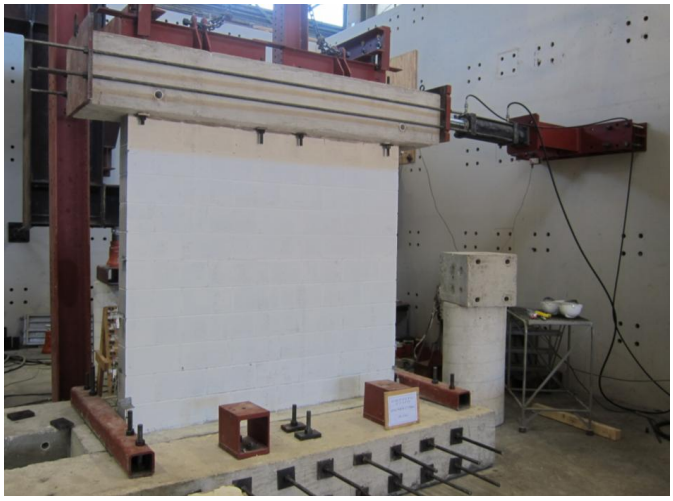

Figure 6-1 Specimen PBS-3 before testing

6.2.1. Test Observations, Specimen PBS-3

The behavior of Specimen PBS-3 was controlled by flexure. The value of Δ_y calculated in the preliminary phase of the test (the first cycles of the test, whose objective was to calculate the theoretical yielding displacement) was equal to 0.10 in., equivalent to a drift ratio of 0.10 %. Flexural cracks (horizontal cracks in the bed joints) started early in the test before $1\Delta_y$, followed by shear cracks (diagonal cracks) which propagated at $2\Delta_y$ (0.21% drift ratio) as shown in Figure 6-2a. A major concentration of shear cracks at mid-height of the wall segment was noticed at $6\Delta_y$ (0.63% drift ratio), coinciding with yield of the horizontal reinforcement in the fifth course (Figure 6-2b). Minor sliding at the base was observed at $8\Delta_y$ (0.83% drift ratio). Evidence of toe crushing was found first at the south end at $14\Delta_y$ (1.46% drift ratio) and then at the north end at $16\Delta_y$ (1.67% drift). Four vertical bars at the north end fractured: two at the first cycle to $16\Delta_y$ (1.67% drift ratio), one at the first cycle to $20\Delta_y$ (2.08% drift ratio), and one more at the second cycle to $20\Delta_y$ (2.08% drift ratio), when the test ended. There was no evidence of fracture of the

vertical bars at the south end. The specimen at the end of the test is shown in Figure 6-3 and Figure 6-4.

(a) Cycle 2Δy (b) Cycle 6Δy

Figure 6-2 Specimen PBS-3, flexural and shear cracking

Figure 6-3 Specimen PBS-3 at end of test

(a) North end

(b) South end

Figure 6-4 Toe crushing in Specimen PBS-3

6.2.2. Load-Displacement Curve, Specimen PBS-3

The load-displacement curve (hysteretic curve) for Specimen PBS-3 is shown in Figure 6-5. The plot references five major events during testing: first yield of the extreme vertical reinforcement (ε_s=0.0021); maximum useful strain in the masonry (ε_{mu}=0.0025); maximum capacity of the specimen; onset of toe crushing; and 20% decrease in the maximum load capacity. First yield of the extreme bars was determined based on the average of the strains in the strain gauges located in the dowels at the base of the wall segment. The value of the maximum useful strain in the masonry was calculated using the displacement of the first two linear potentiometers of each side of the specimen (LP-1 and LP-2 for the north and LP-5 and LP-6 for the south). The displacements from LP-1 and LP-5 were divided by 8.375 in. and those from LP-2 and

LP-6 by 8 in., to obtain the average strain at 4 and 12 in. above the base of the wall segment, respectively. The average strain at the base of the wall segment was obtained by extrapolating the average strains of the linear potentiometers mentioned above. The onset of toe crushing was determined visually during testing after each cycle, and the maximum capacity and 20% decrease in the maximum capacity were determined from the hysteretic curve.

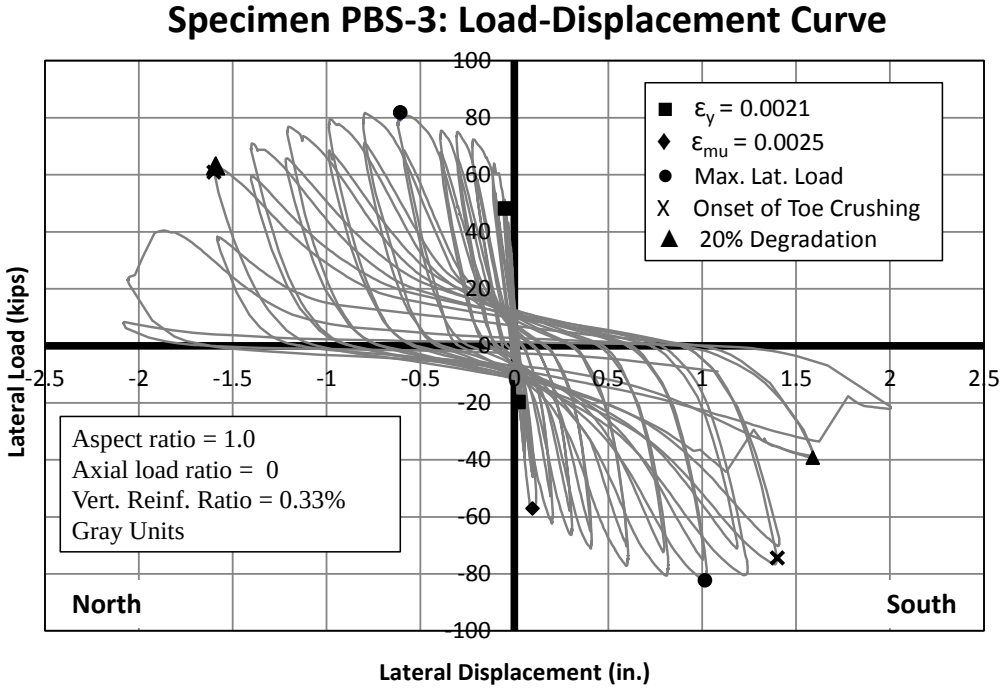

Figure 6-5 Load-displacement curve for Specimen PBS-3

The extreme vertical reinforcement in both ends yielded in the preliminary phase of the test. The maximum useful strain in the masonry at the south toe occurred before 1Δy (0.1% drift ratio); however, the maximum useful strain in the masonry at the north toe occurred at 6Δy (0.6% drift ratio). The maximum lateral load in the north direction was 81.85 kips at 6Δy (0.6% drift ratio) and 82.26 kips at 10Δy (1.0% drift ratio) in the south direction. Maximum useful strain and maximum load in the north direction

occurred almost simultaneously. Toe crushing began in the south direction at 14Δy (1.4% drift ratio) and in the north direction at 16Δy (1.6% drift ratio). The 20% degradation of the maximum load in both directions occurred at 16Δy (1.6% drift ratio) after the first bar fractured.

6.3. SPECIMEN PBS-4

Specimen PBS-4 was 96-in. wide and 96-in. high (aspect ratio equal to 1.0) with #4 bars every 16 in. vertically and horizontally and an axial load equal to zero. The dowels were extended 16 in. (two courses) from the base of the wall. The expected moment capacity of Specimen PBS-4 was 275 ft-kips, equivalent to a lateral load of 31.43 kips as shown in Section 3.2. Specimen PBS-4 before testing is shown in Figure 6-6.

Figure 6-6 Specimen PBS-4 before testing

6.3.1. Test Observations, Specimen PBS-4

The value of Δ_y calculated in the preliminary test was equal to 0.28 in., equivalent to a drift ratio of 0.29 %. Asymmetrical flexural and shear cracking started at $2\Delta_y$ (0.54% drift ratio) as shown in Figure 6-7. The asymmetry could have been produced by slip of the extreme vertical bar at the south end. At $3\Delta_y$ (0.81% drift ratio), widening of the 2nd bed joint from the base (extension of dowels) and sliding at the base were observed. Toe crushing at the north end was identified at $4\Delta_y$ (1.08% drift ratio). Spalling at ends, buckling and fracture occurred during the two cycles to $6\Delta_y$ (1.61% drift ratio), as shown in Figure 6-8. The test was ended at $10\Delta_y$ (2.69% drift ratio) when the lateral capacity dropped to 20%. Specimen PBS-4 at the end of the test is shown in Figure 6-9.

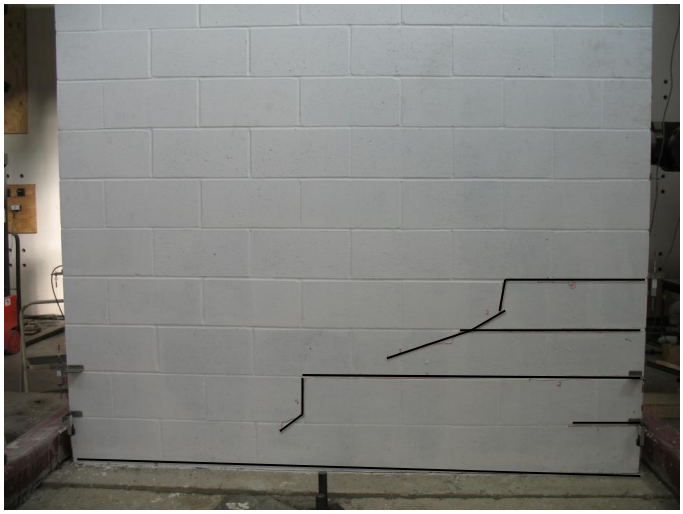

Figure 6-7 Specimen PBS-4 at 2∆y

(a) Spalling at north end

(b) Spalling at south end

(c) Fracture at north end

(d) Fracture at south end

Figure 6-8 Specimen PBS-4 at 6∆y

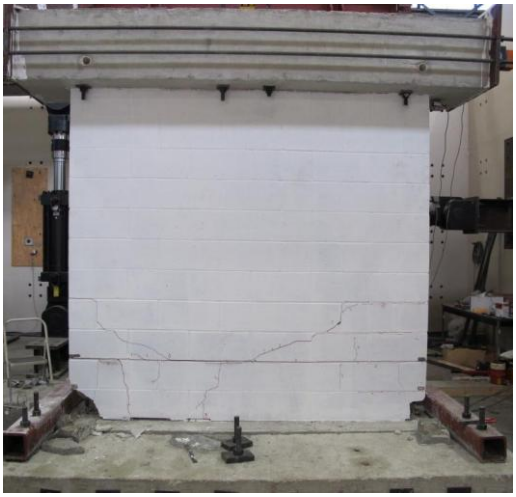

Figure 6-9 Specimen PBS-4 at end of test

6.3.2. Load-Displacement Curve, Specimen PBS-4

The load-displacement curve (hysteretic curve) for Specimen PBS-4 is shown in Figure 6-10.

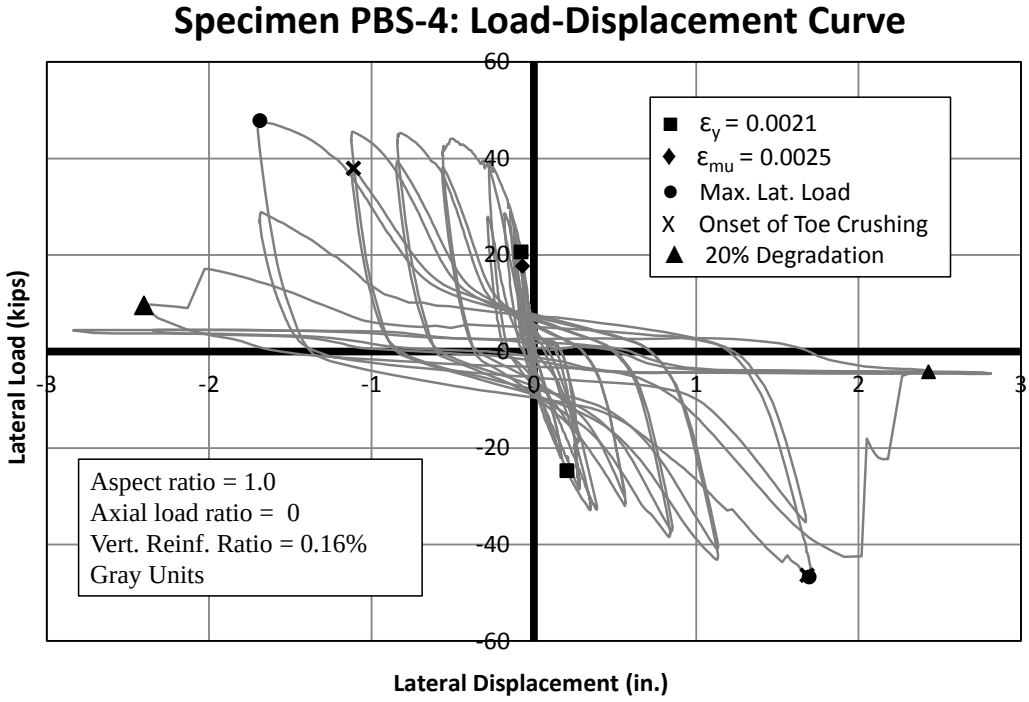

Figure 6-10 Load-displacement curve for Specimen PBS-4

The maximum useful strain in the masonry at the north end occurred before the yielding of the extreme bar at the south end, in the preliminary phase of the test. The extreme bar at the north end also yielded during the preliminary phase of the test. The maximum lateral load in both directions, 47.85 kips (pushing to the north) and 46.77 kips (pulling to the south), occurred at $6\Delta_y$ (1.61% drift ratio). The lateral capacity in both directions dropped suddenly to much lower values than 20% degradation at the cycle of $8\Delta_y$ (2.15% drift ratio), at which point the test was ended.

6.4. SPECIMEN PBS-4G

Specimen PBS-4G was 96-in. wide and 96-in. high (aspect ratio equal to 1.0) with #4 bars every 16 in. vertically and horizontally and an axial load equal to zero. The dowels were extended 16 in. (two courses) from the base of the wall. The expected moment capacity of Specimen PBS-4G was 275 ft-kips, equivalent to a lateral load of 31.43 kips as shown in Section 3.2. Specimen PBS-4G before testing is shown in Figure 6-11.

Figure 6-11 Specimen PBS-4G before testing

6.4.1. Test Observations, Specimen PBS-4G

The value of Δ_y calculated in the preliminary test was equal to 0.29 in., equivalent to a drift ratio of 0.30 %. A few flexural cracks (horizontal cracks) were observed at $1\Delta_y$ (0.30% drift ratio), followed rapidly for shear cracks (diagonal cracks) at $2\Delta_y$ (0.60% drift ratio). At $3\Delta_y$ (0.91% drift ratio), flexural and shear cracks concentrated at four

courses from the base and started to widen. During the next cycle, to $4\Delta_y$ (1.21% drift ratio), a 0.40-in. gap was measured at the base of the wall segment. Several new flexural and shear cracks appeared at higher courses, and toe crushing was observed at both ends of the wall at $6\Delta_y$ (1.81% drift ratio). A large gap opened at the north side along the 2nd bed joint from the bottom (Figure 6-12a), suggesting that splices slipped at $8\Delta_y$ (2.42% drift ratio). Similarly, a large gap opened at the south side at the base of the wall segment, suggesting fracture in the vertical reinforcement as shown in Figure 6-12b. After this point, the specimen degraded by fracture of the longitudinal bars and crushing of the toes. The test was ended when the lateral capacity dropped to 20% at the first cycle to $12\Delta_y$ (3.63% drift ratio). Figure 6-13 and Figure 6-14 show Specimen PBS-4G at the end of the test.

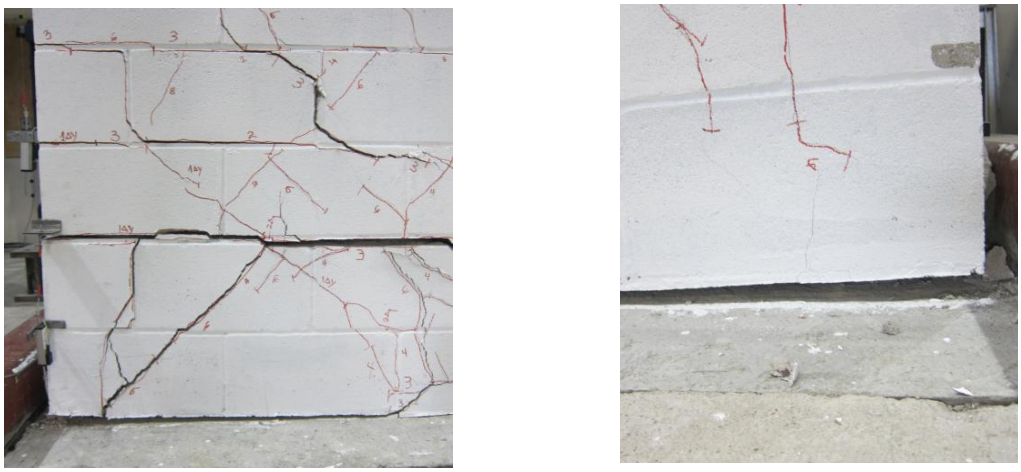

(a) North end (b) South end

Figure 6-12 Specimen PBS-4G at 8Δy

Figure 6-13 Specimen PBS-4G at end of test

(a) North end (b) South end

Figure 6-14 Toes of Specimen PBS-4G at end of test

6.4.2. Load-Displacement Curve, Specimen PBS-4G

A load-displacement curve (hysteretic curve) was obtained from the test of Specimen PBS-4G, as shown in Figure 6-15.

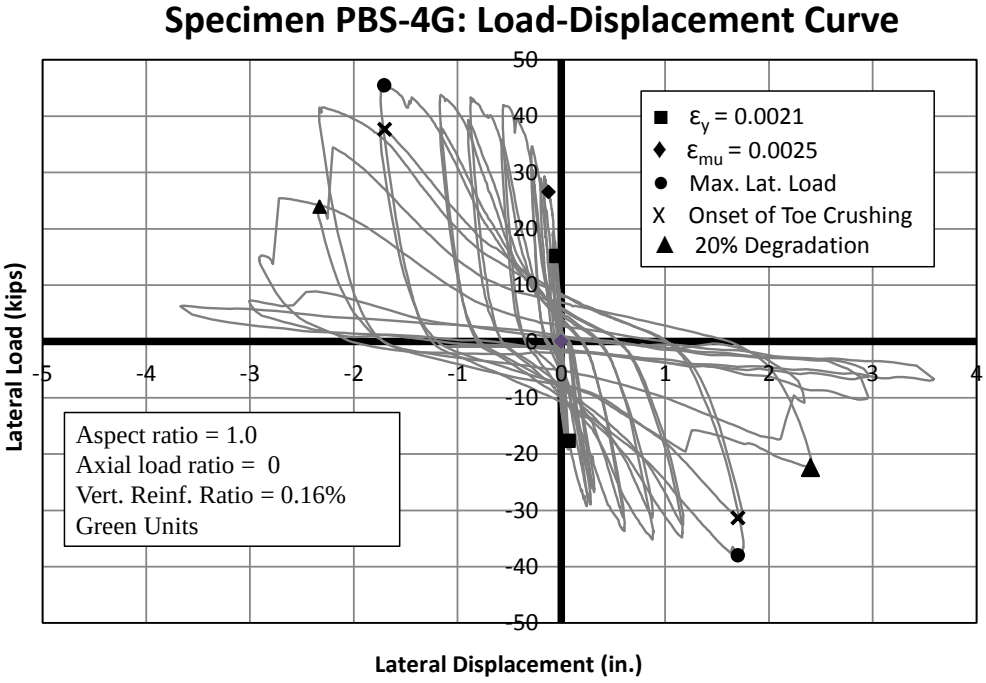

Figure 6-15 Load-displacement curve for Specimen PBS-4G

In the preliminary phase of the test, the extreme vertical reinforcement yielded at both ends and the masonry reached its maximum useful strain at the north end. The maximum lateral load occurred at $6\Delta_y$ (1.70% drift ratio): 45.47 kips in the north direction and 38.00 kips in the south direction. Toe crushing was observed at the second cycle in both directions at $6\Delta_y$ (1.70% drift ratio).The 20% degradation of the maximum load took place at the first cycle in the south direction to $8\Delta_y$ (2.32% drift ratio) and at the second cycle in the north direction to $8\Delta_y$ (2.32% drift ratio).

6.5. SPECIMEN PBS-11

Specimen PBS-11 was 96-in. wide and 96-in. high (aspect ratio equal to 1.0) with #4 bars every 8 in. vertically and horizontally and axial load ratio, $P / (f_m' A_g)$, equal to

0.10. The dowels were extended 16 in. (two courses) from the base of the wall segment. The expected moment capacity of Specimen PBS-11 was 1049 ft-kips, equivalent to a lateral load of 119.89 kips as shown in Section 3.2. Specimen PBS-11 before the test is shown in Figure 6-16.

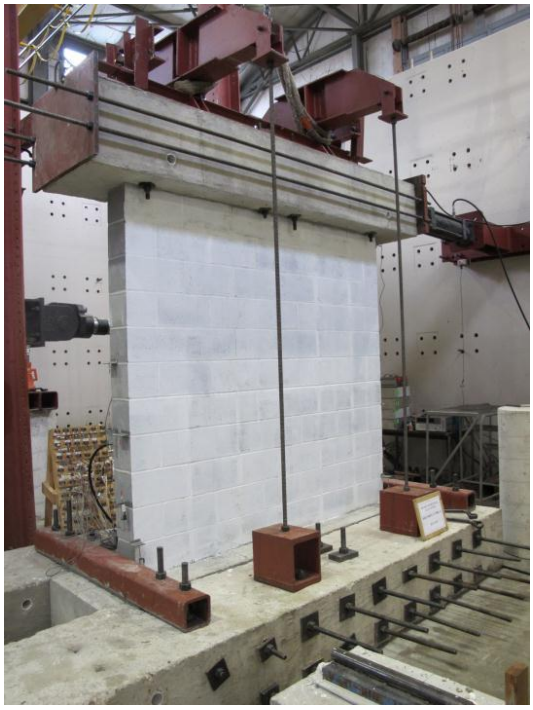

Figure 6-16 Specimen PBS-11 before testing

6.5.1. Test Observations, Specimen PBS-11

The value of Δ_y calculated in the preliminary phase of the test was equal to 0.12 in., equivalent to a drift ratio of 0.125 %, and no cracks were observed. Minor flexural and shear cracks were present at $2\Delta_y$ (0.25% drift ratio); a major flexural crack at the base of the wall segment was observed at the south end (Figure 6-17a), along with crushing at the north end. At $4\Delta y$ (0.50% drift ratio) flexural cracks reached the ninth course from

the base and shear cracks extended from that point to the north toe; toe crushing at the south end was identified (Figure 6-17b), and the crack at the base widened. From this point, significant shear degradation and spalling at toes were observed; the spalling showed that several vertical bars buckled (Figure 6-18) at the second cycle to $8\Delta_y$ (1.00% drift ratio). Crushing extended two courses high which permitted vertical bars to slide at $12\Delta_y$ (1.50% drift ratio). The test was ended when the lateral capacity dropped to 20% at the first cycles of $16\Delta_y$ (2.00% drift ratio). The specimen at the end of the test is shown in Figure 6-19 and Figure 6-20.

(a) North end ($2\Delta_y$)

(b) South end ($4\Delta_y$)

Figure 6-17 Toe crushing in Specimen PBS-11

Figure 6-18 Buckling of longitudinal bars at south end of Specimen PBS-11 (8Δy)

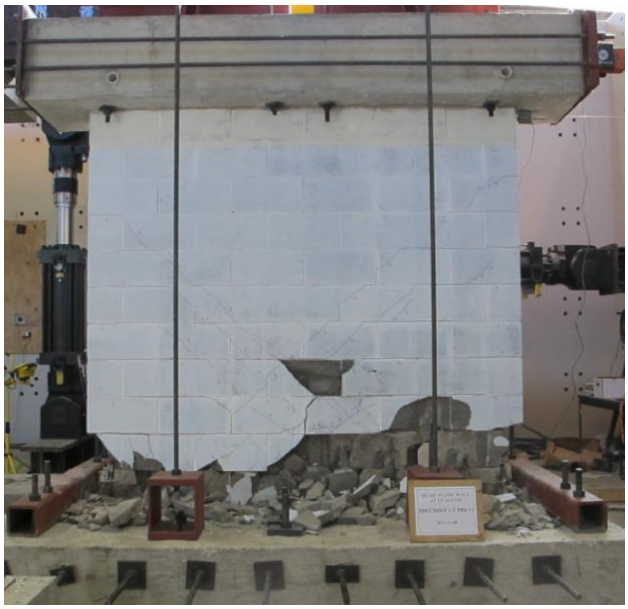

Figure 6-19 Specimen PBS-11 at end of test

(a) North end

(b) South end

Figure 6-20 Toes of Specimen PBS-11 at end of test

6.5.2. Load-Displacement Curve, Specimen PBS-11

The load-displacement curve (hysteretic curve) of Specimen PBS-11 is shown in Figure 6-21.

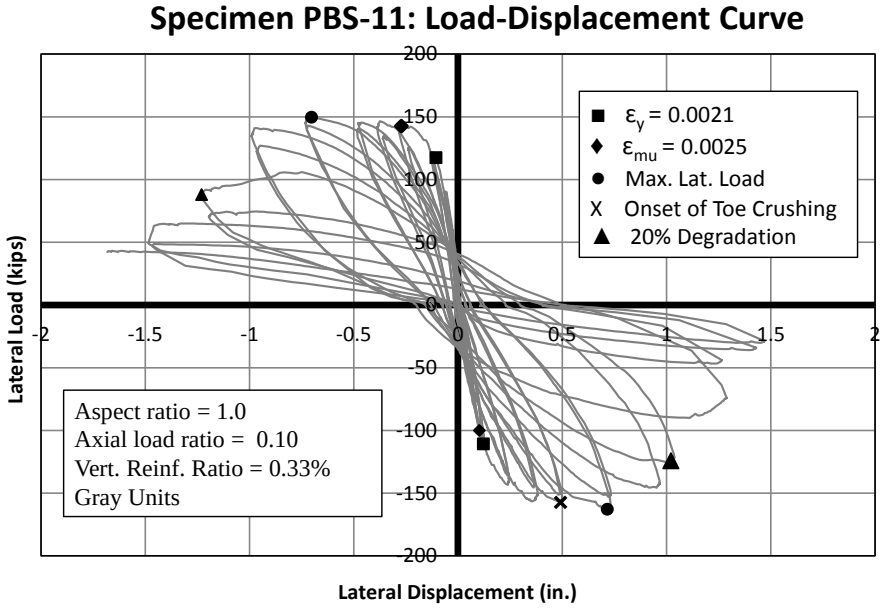

Figure 6-21 Load-displacement curve for Specimen PBS-11

The extreme vertical reinforcement at the south end yielded in the preliminary phase of the test while the one at the north end yielded at $1\Delta_y$ (0.125% drift ratio). The maximum useful strain in the masonry at the south toe occurred before $1\Delta_y$ (0.125% drift ratio); the maximum useful strain in the masonry at the north toe occurred at $2\Delta_y$ (0.25% drift ratio). Crushing was observed in the north toe at $2\Delta_y$ (0.25% drift ratio) and in the south toe at $4\Delta_y$ (0.50% drift ratio). The maximum lateral load in both directions occurred at $6\Delta_y$ (0.75% drift ratio): 142.46 kips in the north direction and 157.26 kips in the south direction. The 20% degradation of the maximum load took place at the first cycle in the south direction to $8\Delta_y$ (1.00% drift ratio) and at the second cycle in the north direction to $10\Delta_y$ (1.25% drift ratio).

6.6. SPECIMEN PBS-12

Specimen PBS-12 was 96-in. wide and 96-in. high (aspect ratio equal to 1.0) with #4 bars every 16 in. vertically and horizontally and axial load ratio, $P / (f_m' A_g)$, equal to 0.10. The dowels extended 16 in. (two courses) from the base of the wall segment. The expected moment capacity of Specimen PBS-12 was 858 ft-kips, equivalent to a lateral load of 98.06 kips as shown in Section 3.2. Specimen PBS-12 before the test is shown in Figure 6-22.

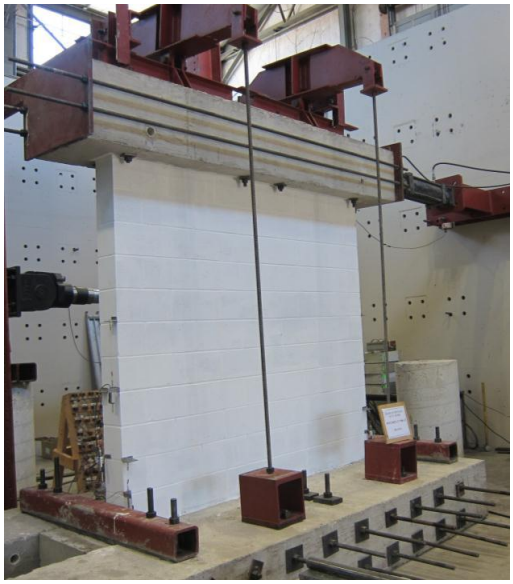

Figure 6-22 Specimen PBS-12 before testing

6.6.1. Test Observations, Specimen PBS-12

The value of Δ_y calculated in the preliminary phase of the test was 0.13 in., equivalent to a drift ratio of 0.14 %; no cracks were observed at this stage. Early in the test, 1Δy (0.14% drift ratio), a diagonal crack at the north toe (Figure 6-23a) and a major crack at the base in the south end (Figure 6-23b) were observed. Damage was concentrated at those points in the next cycles and flexural and shear cracking were slight elsewhere. Crushing was observed in the south toe at $4\Delta_y$ (0.54% drift ratio) and in the north toe at $6\Delta_y$ (0.81% drift ratio). At $8\Delta_y$ (1.08% drift ratio), spalling at the south toe suggested bar buckling; in addition, a wide crack at the north end indicated a possible sliding of the dowel. After this point, the degradation of the wall segment was based on crushing of the toes and sliding of the vertical bars, as shown in Figure 6-24. The test

was ended when the lateral capacity dropped to 20% at the first cycle to $20\Delta_y$ (2.71% drift ratio). The specimen at the end of the test is shown in Figure 6-25 and Figure 6-26.

(a) North end

(b) South end

Figure 6-23 Specimen PBS-12 at 1Δy

Figure 6-24 Specimen PBS-12 at 10Δy

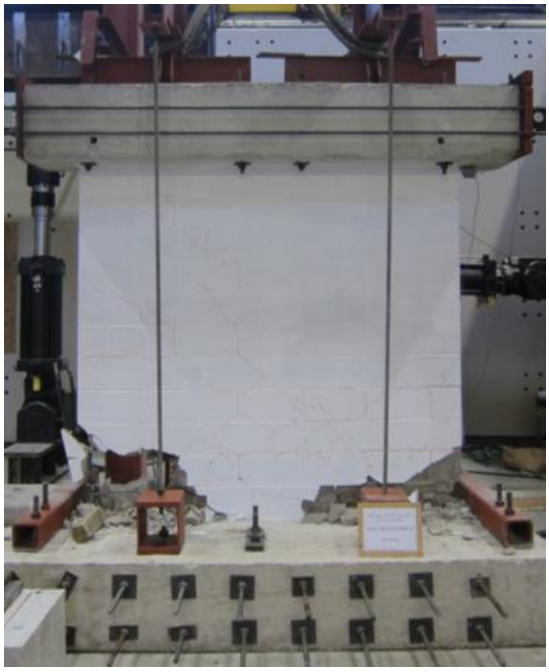

Figure 6-25 Specimen PBS-12 at end of test

(a) North end (b) South end

Figure 6-26 Toes of Specimen PBS-12 at end of test

6.6.2. Load-Displacement Curve, Specimen PBS-12

The load-displacement curve (hysteretic curve) of Specimen PBS-12 is shown in Figure 6-27.

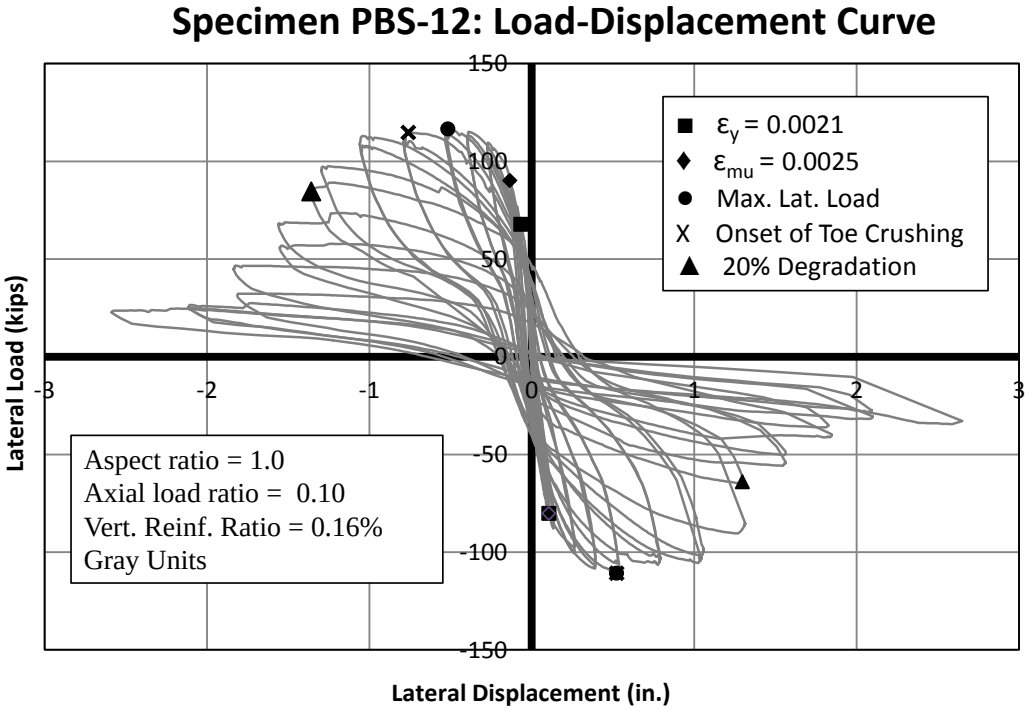

Figure 6-27 Load-displacement curve for Specimen PBS-12

In the preliminary phase of the test, the extreme vertical bars yielded at both ends at $1\Delta_y$ (0.14% drift ratio). The maximum useful strain in the masonry toe in both directions was found at $1\Delta_y$ (0.14% drift ratio); for loading to the south, yielding in extreme bars and maximum useful strain in masonry occurred simultaneously. The maximum lateral load occurred at $4\Delta_y$ (0.54% drift ratio) for both directions: 116.53 kips in the north direction and 110.85 kips in the south direction. Crushing was observed first in the south toe at $4\Delta_y$ (0.54% drift ratio), and then in the north toe at $6\Delta_y$ (0.81% drift

ratio). The 20% degradation of the maximum load took place at $12\Delta_y$ (1.63% drift ratio) in both directions.

6.7. SPECIMEN PBS-12G

Specimen PBS-12G was 96-in. wide and 96-in. high (aspect ratio equal to 1.0) with #4 bars every 16 in. vertically and horizontally and axial load ratio, $P / (f_m' A_g)$, equal to 0.10. The dowels were extended 16 in. (two courses) from the base of the wall segment. This specimen was built with "Green Blocks," which are hollow concrete masonry units containing recycled material. The expected moment capacity of Specimen PBS-12G was 858 ft-kips, equivalent to a lateral load of 98.06 kips as shown in Section 3.2. Specimen PBS-12G before the test is shown in Figure 6-28.

Figure 6-28 Specimen PBS-12G before testing

6.7.1. Test Observations, Specimen PBS-12G

The value of Δy calculated in the preliminary phase of the test was equal to 0.20 in., equivalent to a drift ratio of 0.21 %, and no cracks were observed. Within the test, rapid transition from flexural to shear cracks was observed at the first cycles, concentrated in the lowest four courses. The base joint cracked early in the test, at 1Δy (0.21% drift ratio), and the crack progressively widened in each cycle. Crushing of the north toe (Figure 6-29a) was identified at the second cycle to 3Δy (0.63% drift ratio), and in the south toe (Figure 6-29b) at the second cycle to 4Δy (0.83% drift ratio). The toes started to spall at 8Δy (1.67% drift ratio), accompanied by buckling of the extreme longitudinal bars. During this cycle, the degradation concentrated in the toes, producing more spalling, buckling in the longitudinal bars there, and slip of the dowels there, as shown in Figure 6-30. The test was ended when the specimen suddenly failed because of the lack of compression capacity at the toes. The specimen at the end of the test is shown in Figure 6-31.

(a) North end (b) South end

Figure 6-29 Toe crushing of Specimen PBS-12G at end of test

(a) North end

(b) South end

Figure 6-30 Specimen PBS-12G at 8∆y

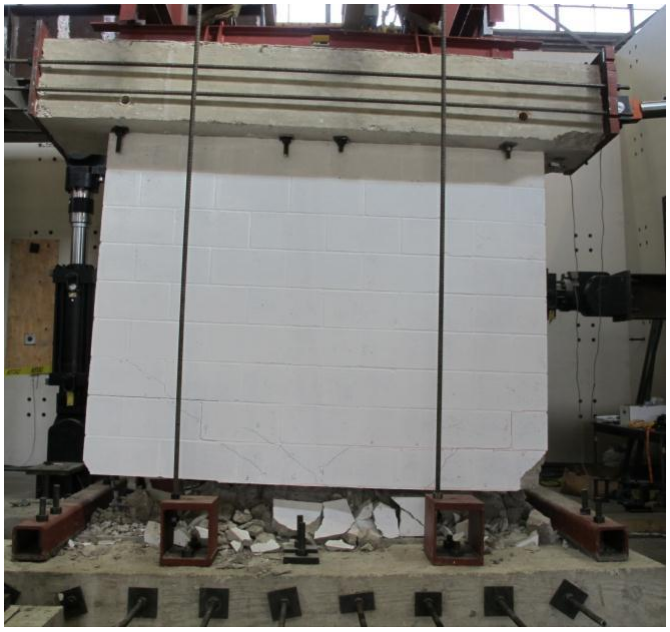

Figure 6-31 Specimen PBS-12G at end of test

6.7.2. Load-Displacement Curve, Specimen PBS-12G

The load-displacement curve (hysteretic curve) of Specimen PBS-12G is shown in Figure 6-32.

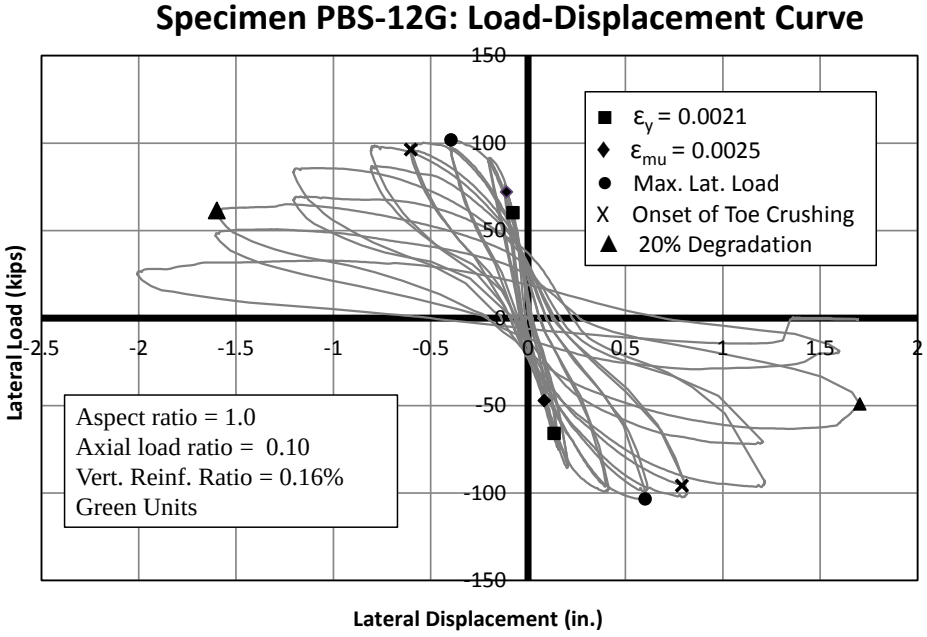

Figure 6-32 Load-displacement curve for Specimen PBS-12G

In the preliminary phase of the test, the extreme vertical bar yielded at the south end, and the maximum useful masonry strain was reached at both ends. The extreme bar at the north end yielded at $1\Delta_y$ (0.21 % drift ratio). Toes crushed in both directions after the maximum load. When loading to the north, the maximum load and the toe crushing appeared at $2\Delta_y$ and $3\Delta_y$ (0.42 and 0.63% drift ratio), respectively. When loading to the south, the maximum load and the toe crushing appeared at $3\Delta_y$ and $4\Delta_y$ (0.63 and 0.83% drift ratio), respectively. Degradation of 20% of the maximum load occurred in both directions at $8\Delta_y$ (1.67 % drift ratio).

Chapter 7 : Evaluation of Results

In this chapter, results from the testing of each wall are evaluated. To facilitate comparisons among wall segments tested at UT Austin and at Washington State University, results are evaluated here using the same parameters and calculation methods as have been used at Washington State.

7.1. WALL SEGMENT PBS-3

7.1.1. Displacement Components

The relative contribution of the average shear deformation to the lateral displacement of the wall segment is determined using the "X" configuration of string potentiometers (2 vertical and 2 diagonal) as explained in Massone and Wallace (2004). Pure flexural and pure shearing deformations are identified in Figure 7-1, whose geometry permits derivation of the formula for the average shear displacement, $\bar{U}_{s\_corrected}$.

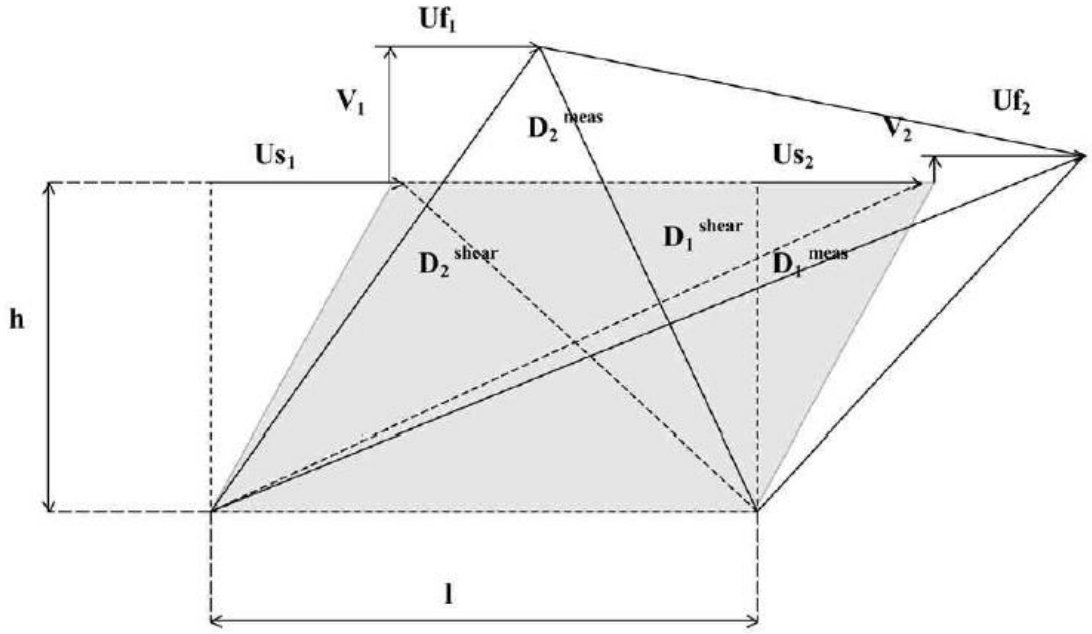

Figure 7-1 Flexural and shearing deformations (Massone and Wallace 2004)

$$\bar{U}_{s\_corrected} = \frac{\sqrt{D_1^{meas^2} - h^2} - \sqrt{D_2^{meas^2} - h^2}}{2} + \left(\frac{1}{2} - \alpha\right)\left(\frac{V_1 - V_2}{l}\right)h$$

Where

D_1^{meas} and D_2^{meas} = Diagonal length for the deformed X configuration as shown in Figure 7-1,

V_1 and V_2 = displacement values from the vertical sting potentiometers as shown in Figure 7-1,

h = height of the wall segment covered by the vertical string potentiometers,

α = distance from the top of the geometric model to the center of the centroid of the curvature distribution, equal to 0.67 as proposed by Massone and Wallace (2004), and

l = horizontal distance between vertical string potentiometers.

The sliding deformation at the top and base of the wall segment was calculated directly from linear potentiometers attached to the specimen. The remaining deformation was considered as flexural deformation. The relative contributions of flexural, shearing, and sliding deformation at maximum load and at 20% load degradation are summarized in Table 7-1.

Table 7-1 Relative flexural, shearing, and sliding deformation contributions for Specimen PBS-3

Direction	Maximum Load			20% Max Load Degradation		
	Flexure	Shear	Sliding	Flexure	Shear	Sliding
North-Push	68%	15%	17%	51%	19%	30%
South- Pull	59%	11%	30%	69%	9%	22%

7.1.2. Backbone and idealized elasto-plastic curve

The backbone curve for each direction (north-pushing and south-pulling) was calculated by connecting the points of maximum lateral force for each first cycle in the hysteresis curve. The approach for calculating the elasto-plastic curve is that proposed by Shedid *et al*. (2008) and used in the theses of Sherman (2011) and Kapoi (2012). This procedure considers the ultimate displacement, Δ_u, *as* the displacement at the 20%

degradation of the maximum load. The secant stiffness is calculated using the point corresponding to first yield of the extreme bar ($\varepsilon_y = 0.00212$) with the origin. Finally, the maximum load in the idealized elasto-plastic response (horizontal line), is calculated by iteration until the area under the elasto-plastic curve equaled the area under the backbone curve (Figure 7-2).

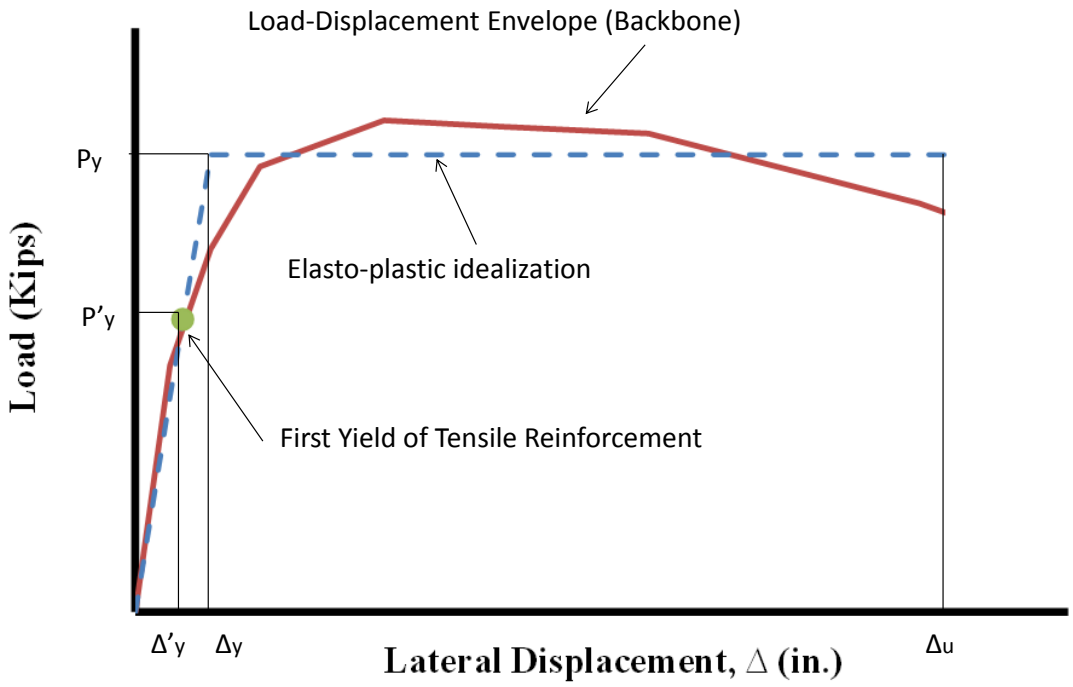

Figure 7-2 Backbone curve and elasto-plastic idealization (Sherman, 2011)

Figure 7-3 and Figure 7-4 show the backbone curve and elasto-plastic idealization for Specimen PBS-3 in both directions. Table 7-2 summarizes the principal elements of both graphs.

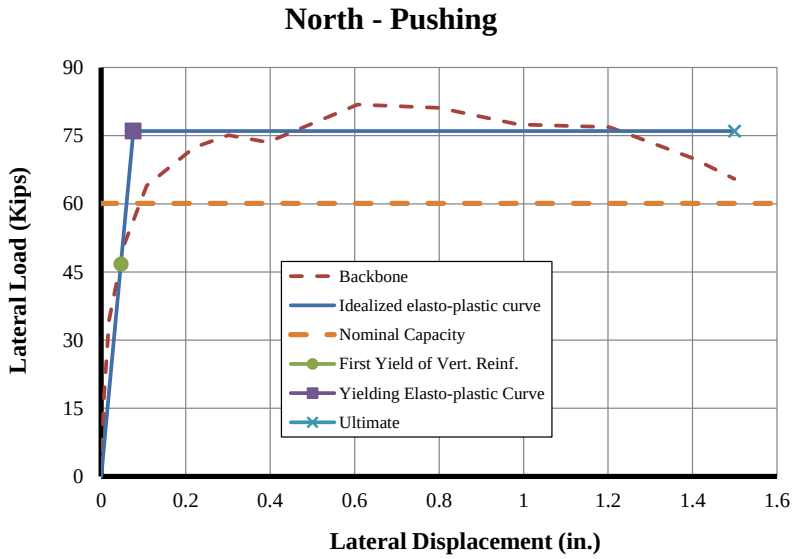

Figure 7-3 Backbone curve and elasto-plastic idealization for north-pushing direction for Specimen PBS-3

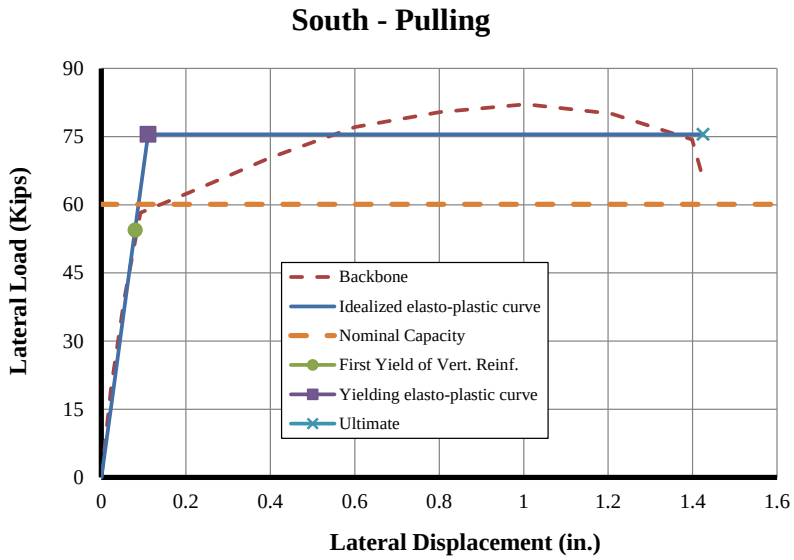

Figure 7-4 Backbone curve and elasto-plastic idealization for south-pulling direction for Specimen PBS-3

Table 7-2 Elasto-plastic and backbone curve main values for Specimen PBS-3

Direction	Elasto-plastic curve					Backbone	
	Δ'_y (in.)	P'_y (kips)	Δ_y (in.)	P_y (kips)	Δ_u (in.)	Δ_{Pmax} (in.)	P_{max} (kips)
North-Push	0.0468	46.76	0.0761	76.00	1.4992	0.6071	81.85
South- Pull	0.0798	54.43	0.1107	75.50	1.4248	1.0052	82.10

Where:

Δ'_y = displacement at the first yielding in vertical reinforcement (in.);

P'_y = lateral load at the first yielding in vertical reinforcement (kip);

Δ_y = yield displacement of idealized elasto-plastic curve (in.);

P_y = maximum lateral load of idealized elasto-plastic curve (kip);

Δ_u = displacement at 20% degradation of the maximum load (in.);

Δ_{Pmax} = displacement at maximum load of backbone curve (in); and

P_{max} = maximum lateral load of backbone curve (kip);

The values of the maximum lateral load of the elasto-plastic and backbone curve were higher than the nominal capacity for Specimen PBS-3 (60.11 kips) by 26% and 36%, respectively.

7.1.3. Displacement Ductility

The displacement ductility, μ_Δ, was calculated as the ratio of the ultimate displacement, Δ_u, to the equivalent yield displacement, Δ_y, obtained from the elasto-plastic idealization.

$$\mu_\Delta = \frac{\Delta_u}{\Delta_y}$$

Where:

μ_Δ = displacement ductility;

Δ_u = displacement at 20% degradation of the maximum load (in.); and

Δ_y = equivalent yield displacement of idealized elasto-plastic curve (in.)

Table 7-3 shows the values of ultimate and yield displacement, and the corresponding displacement ductility for Specimen PBS-3 in both directions.

Table 7-3 Displacement ductility for Specimen PBS-3

Direction	Δ_y (in.)	Δ_u (in.)	μ_Δ
North-Push	0.0761	1.4992	19.71
South- Pull	0.1107	1.4248	12.88
Average	**0.09336**	**1.4620**	**16.29**

7.1.4. Wall segment curvatures

The values of curvature at each first cycle were calculated using data from the linear potentiometers attached to both ends of the wall segment (LP-1 to LP-8). The displacements measured in the linear potentiometers were divided by the distance between the points that they connected to obtain the average strain at 4, 12, 24 and 40 in. from the base. Assuming plane sections, the curvature at each height was calculated as the sum of the average strains at both ends divided by the distance between their corresponding linear potentiometers. The curvature at the base was calculated by

extrapolating the curvature values from the linear potentiometers at 4 and 12 in. from the base. The curvatures of the last cycles of the test were not calculated because the instrumentation detached as a result of the block spalling. Figure 7-5 shows the curvature profile for Specimen PBS-3 at different cycles.

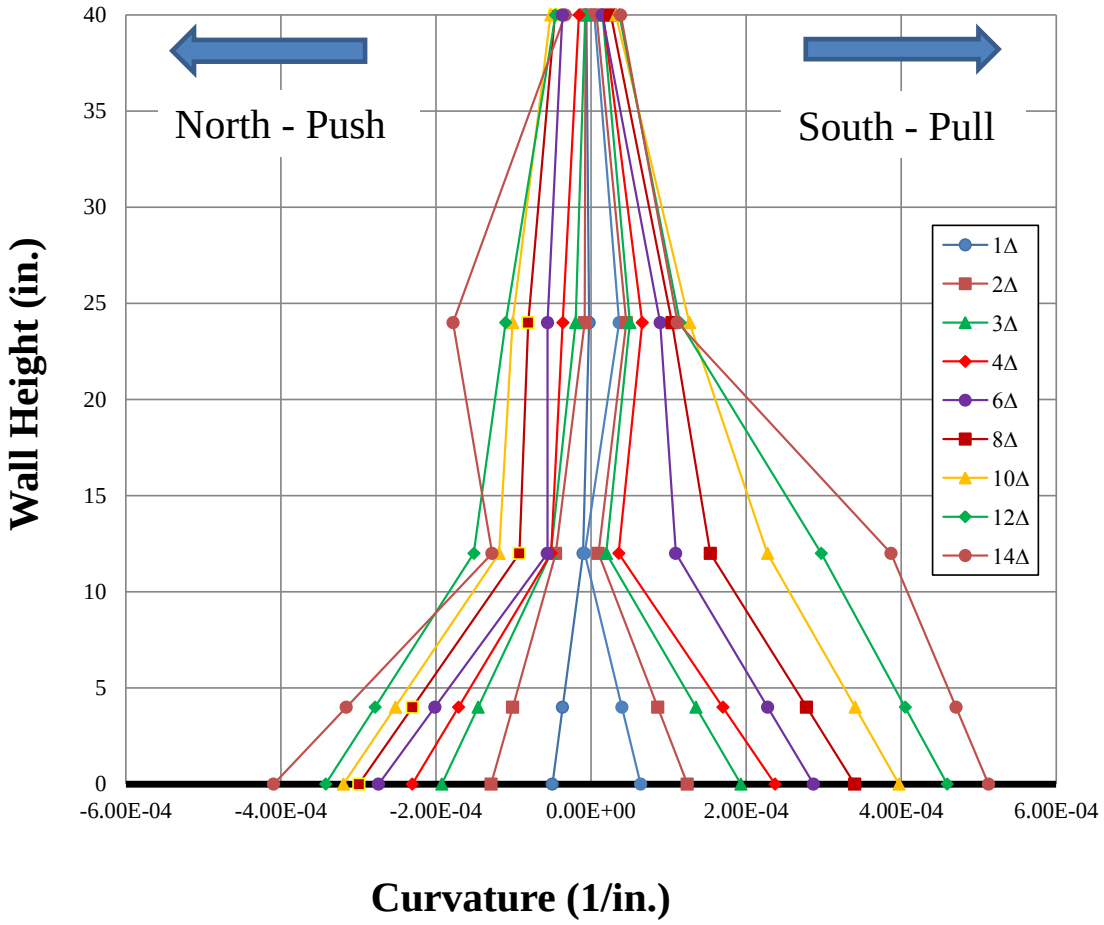

Figure 7-5 Curvature profile for Specimen PBS-3

7.1.5. Curvature Ductility

The curvature ductility, μ_ϕ, was calculated as the ratio of the ultimate curvature, ϕ_u, to the yield curvature, ϕ_y. The value of ultimate curvature was taken as the curvature at 20% degradation of the maximum load or the curvature at the last cycle where data were available.

$$\mu_\emptyset = \frac{\emptyset_u}{\emptyset_y}$$

Where:

μ_ϕ = curvature ductility;

ϕ_u = curvature at 20% degradation of the maximum load (in.$^{-1}$); and

ϕ_y = curvature at yielding of the elasto-plastic idealization (in. $^{-1}$)

Table 7-4 shows the values of ultimate and yield curvatures and the corresponding curvature ductility for Specimen PBS-3 in both directions.

Table 7-4 Curvature ductility for Specimen PBS-3

Direction	ϕ_y (x10^{-05} in.$^{-1}$)	ϕ_u (x10^{-05} in.$^{-1}$)	μ_ϕ
North-Push	4.92	40.95	8.33
South- Pull	6.19	51.27	8.29
Average	**5.55**	**46.11**	**8.31**

7.1.6. Height of Plasticity and Plastic Hinge Length

The height of plasticity, L_p, was considered as the height of the region, measured from the base of the wall segment, where curvatures are higher than the yield curvature. This value was calculated at ultimate curvature, at 20% degradation of maximum load or

using data from the last cycle available from the instrumentation. Table 7-5 shows the height of plasticity and its ratio with the total plan length of the wall segment for both directions of loading.

Table 7-5 Height of plasticity for Specimen PBS-3

Direction	L_p (in.)	L_p/L_w
North-Push	40.33	42%
South- Pull	38.63	40%
Average	**39.48**	**41%**

The plastic hinge length, l_p, was calculated by rearranging the formula for the idealized inelastic curvature distribution proposed by Paulay and Priestley (1992), as shown in Figure 7-6. The formula has two terms: the first considers elastic displacement, and the second, inelastic displacement.

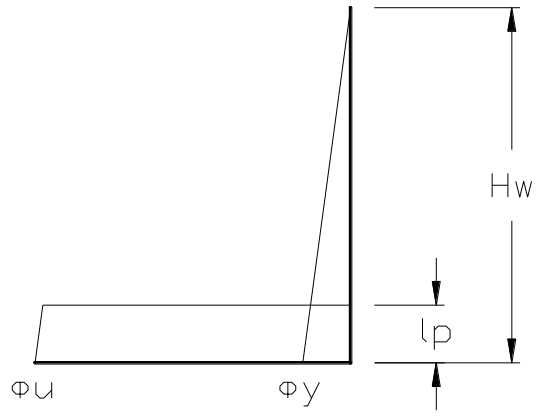

Figure 7-6 Idealized inelastic curvature distribution according to Park and Paulay (1975)

$$\Delta_u = \frac{\emptyset_y \, {H_w}^2}{3} + \left(\emptyset_u - \emptyset_y\right) l_p \left(H_w - \frac{l_p}{2}\right)$$

Where:

l_p = plastic hinge length (in.);

Δ_u = ultimate displacement, 20% degradation of the maximum load, (in.);

$\emptyset_u$ = ultimate curvature, 20% degradation of the maximum load, ($in.^{-1}$);

$\emptyset_y$ = yield curvature ($in.^{-1}$); and

H_w = wall segment height (in.)

Table 7-6 shows the plastic hinge length and its portion of the total plan length of the wall segment for Specimen PBS-3 in both directions of loading.

Table 7-6 Plastic hinge length for Specimen PBS-3

Direction	l_p (in.)	l_p/L_w
North-Push	48.22	50%
South- Pull	33.93	35%
Average	**41.07**	**43%**

7.1.7. Energy Dissipation and Equivalent Hysteretic Damping

Energy dissipation and equivalent hysteretic damping were calculated for the hysteretic loops whose drifts were close or equal to 0.6 and 1.5%. The energy dissipation, $E_{D\Delta t}$, was calculated as the area of the hysteretic loop using the trapezoidal rule. The equivalent hysteretic damping, ξ_{eq}, was determined as proposed by Clough and

Penzien (2003), where the nominal damping ratio, ξ_o , was taken as 0.05 as recommended by Priestley (2007).

$$\xi_{eq} = \frac{E_{D\Delta t}}{2\pi\, k_{eq}\, \Delta_t^2} + \xi_o$$

Figure 7-7 shows the hysteretic loops of 0.65% and 1.46% drift ratios for Specimen PBS-3, and Table 7-7 presents the value of energy dissipation and equivalent hysteretic damping for both curves.

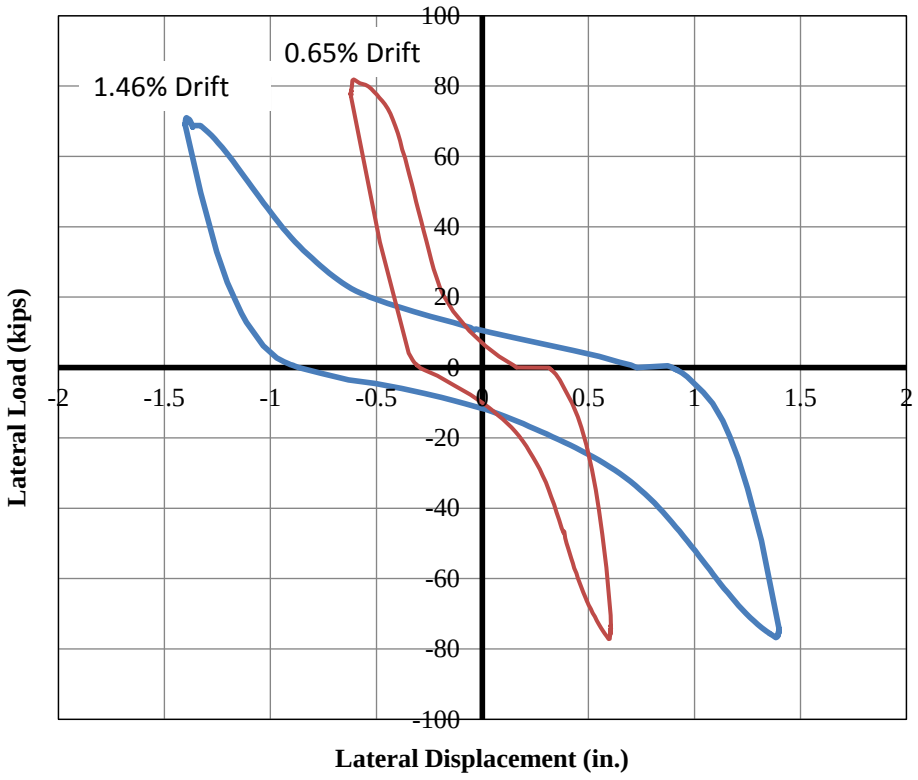

Figure 7-7 Hysteretic loops at 0.65% and 1.46% drift ratios for Specimen PBS-3

Table 7-7 Energy dissipation and equivalent hysteretic damping for Specimen PBS-3

Drift Level	Drift	$E_{D\Delta t}$ (kip-in)	ξ_{eq}
0.60%	0.65%	37.15	17.3%
1.50%	1.46%	84.44	18.9%

7.2. WALL SEGMENT PBS-4

7.2.1. Displacement Components

The relative contributions of flexural, shearing, and sliding deformation at maximum load and at 20% load degradation for Specimen PBS-4 are summarized in Table 7-8.

Table 7-8 Relative flexural, shearing, and sliding deformation contributions for Specimen PBS-4

Direction	Maximum Load			20% Max Load Degradation		
	Flexure	Shear	Sliding	Flexure	Shear	Sliding
North-Push	55%	15%	30%	68%	4%	28%
South- Pull	52%	6%	42%	63%	4%	33%

7.2.2. Backbone and idealized elasto-plastic curve

The backbone and elasto-plastic idealization for Specimen PBS-4 are plotted for each direction (north-pushing and south-pulling) as shown in Figure 7-8 and Figure 7-9. Table 7-9 summarizes the principal elements of both graphs.

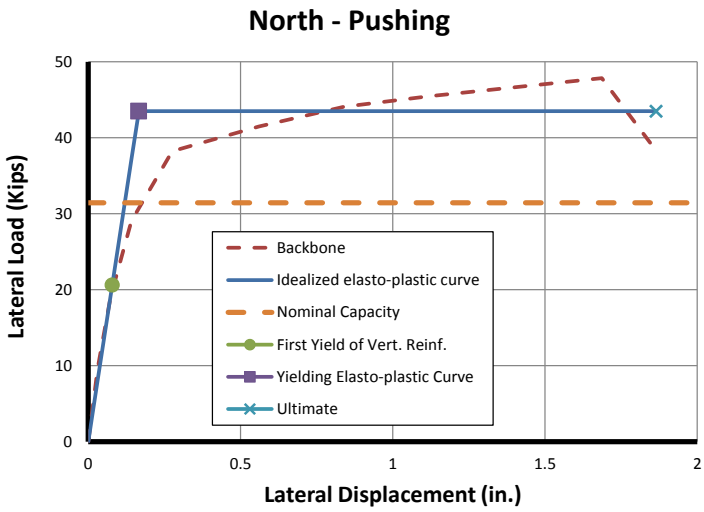

Figure 7-8 Backbone curve and elasto-plastic idealization for north-pushing direction for Specimen PBS-4

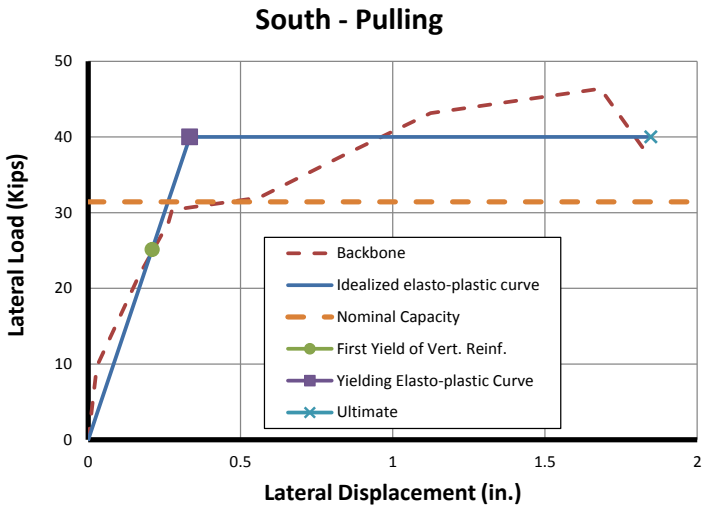

Figure 7-9 Backbone curve and elasto-plastic idealization for south-pulling direction for Specimen PBS-4

Table 7-9 Elasto-plastic and backbone curve for Specimen PBS-4

Direction	Elasto-plastic curve					Backbone	
	Δ'_y (in.)	P'_y (kips)	Δ_y (in.)	P_y (kips)	Δ_u (in.)	Δ_{Pmax} (in.)	P_{max} (kips)
North-Push	0.0787	20.62	0.1661	43.50	1.8651	1.6868	47.85
South- Pull	0.2098	25.14	0.3338	40.00	1.8474	1.6825	46.38

The values of the maximum lateral load of the elasto-plastic and backbone curve were higher than the nominal capacity for Specimen PBS-4 (31.43 kips) by 32% and 50%, respectively.

7.2.3. Displacement Ductility

The displacement ductility for Specimen PBS-4 was calculated from the elasto-plastic curve of each direction. Table 7-10 presents the values for both directions and their corresponding averages.

Table 7-10 Displacement ductility for Specimen PBS-4

Direction	Δ_y (in.)	Δ_u (in.)	μ_Δ
North-Push	0.1661	1.8651	11.23
South- Pull	0.3338	1.8474	5.53
Average	**0.24998**	**1.8563**	**8.38**

7.2.4. Wall segment curvatures

The curvatures along the height of the Specimen PBS-4 could not be calculated because of the problems in two linear potentiometers (LP-4 and LP-6). Several unsuccessful attempts were made to estimate what would have been the data from those

instruments. Because of the missing data, it was not possible to compute curvature ductility, height of plasticity, or plastic hinge length for this specimen.

7.2.5. Energy Dissipation and Equivalent Hysteretic Damping

Energy dissipation, $E_{D\Delta t}$, and equivalent hysteretic damping, ξ_{eq}, for Specimen PBS-4 were calculated for the hysteretic loops of 0.59% and 1.77% drift ratios, as shown in Figure 7-10. Table 7-11 presents the value of energy dissipation and equivalent hysteretic damping for both curves.

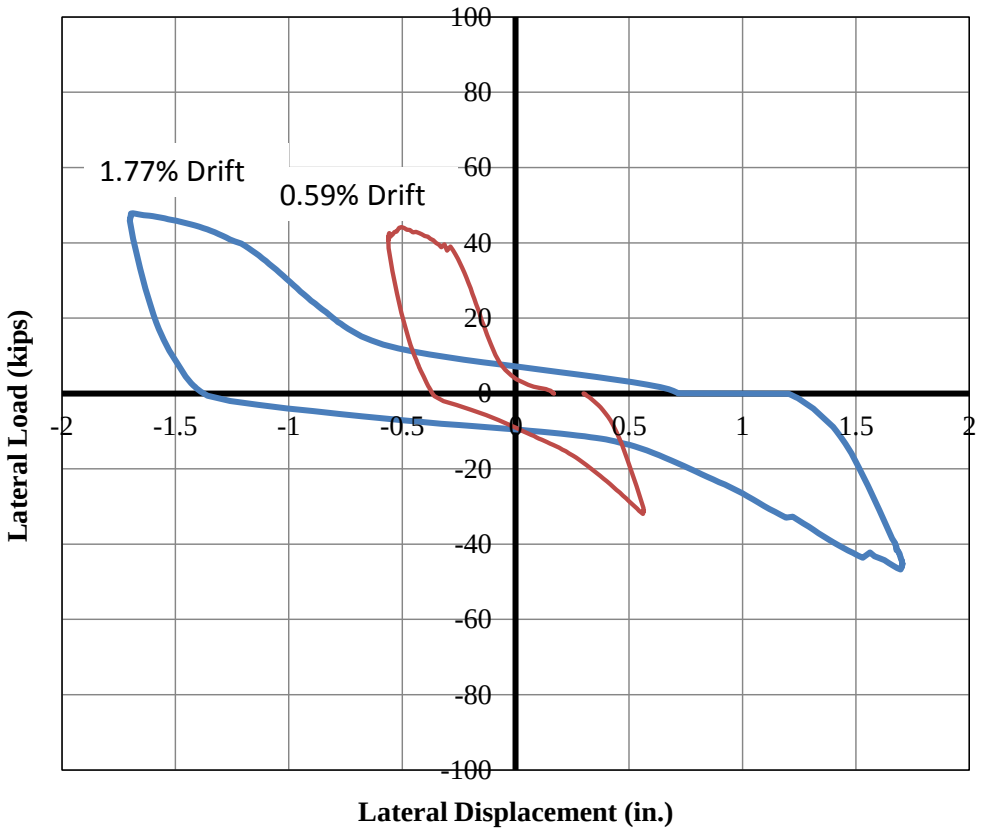

Figure 7-10 Hysteretic loops at 0.59% and 1.77% drift ratios for Specimen PBS-4

Table 7-11 Energy dissipation and equivalent hysteretic damping for Specimen PBS-4

Drift Level	Drift	$E_{D\Delta t}$ (kip-in)	ξ_{eq}
0.60%	**0.59%**	23.86	21.5%
1.50%	**1.77%**	82.40	21.8%

7.3. WALL SEGMENT PBS-4G

7.3.1. Displacement Components

The relative contributions of flexural, shearing, and sliding deformation at maximum load and at 20% load degradation for Specimen PBS-4G are summarized in Table 7-12. Values at 20% degradation of the maximum load could not be calculated for the north-pushing direction because of the above-mentioned problems with instrumentation at the last stages of the test.

Table 7-12 Relative flexural, shearing, and sliding deformation contributions for Specimen PBS-4G

Direction	Maximum Load			20% Max Load Degradation		
	Flexure	Shear	Sliding	Flexure	Shear	Sliding
North-Push	58%	22%	19%	-	-	-
South- Pull	50%	22%	27%	57%	20%	23%

7.3.2. Backbone and idealized elasto-plastic curve

The backbone and elasto-plastic idealization for Specimen PBS-4G are plotted for each direction (north-pushing and south-pulling) as shown in Figure 7-11 and Figure 7-12. Table 7-13 summarizes the principal elements of both graphs.

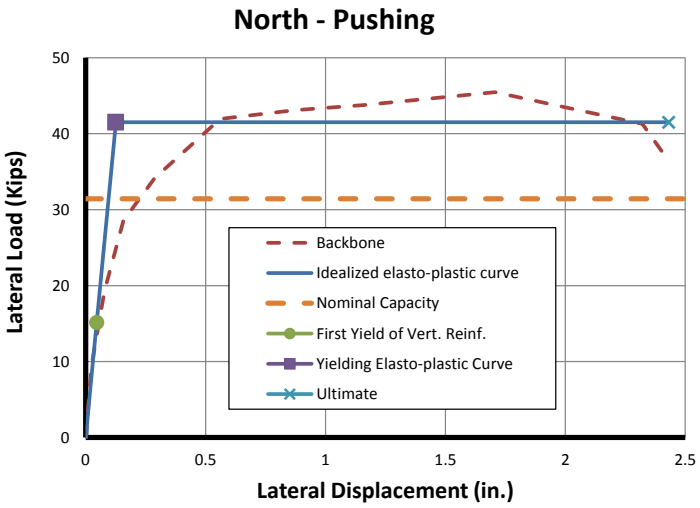

Figure 7-11 Backbone curve and elasto-plastic idealization for north-pushing direction for Specimen PBS-4G

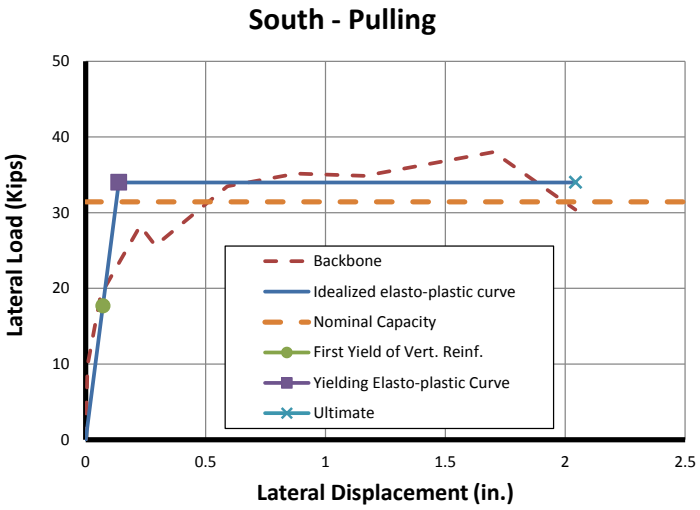

Figure 7-12 Backbone curve and elasto-plastic idealization for south-pulling direction for Specimen PBS-4G

Table 7-13 Elasto-plastic and backbone curve for Specimen PBS-4G

Direction	Elasto-plastic curve					Backbone	
	Δ'_y (in.)	P'_y (kips)	Δ_y (in.)	P_y (kips)	Δ_u (in.)	Δ_{Pmax} (in.)	P_{max} (kips)
North-Push	0.0460	15.15	0.1259	41.50	2.4311	1.7061	45.47
South- Pull	0.0720	17.68	0.1384	34.00	2.0425	1.7012	38.00

The average values of the maximum lateral load of the elasto-plastic and backbone curve were higher than the nominal capacity for Specimen PBS-4G (31.43 kips) by 20% and 33%, respectively.

7.3.3. Displacement Ductility

The displacement ductility for Specimen PBS-4G was calculated from the elasto-plastic curve of each direction. Table 7-14 presents the values for both directions and their average.

Table 7-14 Displacement ductility for Specimen PBS-4G

Direction	Δ_y (in.)	Δ_u (in.)	μ_Δ
North-Push	0.1259	2.4311	19.31
South- Pull	0.1384	2.0425	14.76
Average	**0.13214**	**2.2368**	**17.04**

7.3.4. Wall segment curvatures

The curvatures along the height of the Specimen PBS-4G were calculated for different cycles, as shown in

Figure 7-13. The curvatures after the first cycle to 8 Δy are not presented because the instrumentation detached as a consequence of masonry spalling.

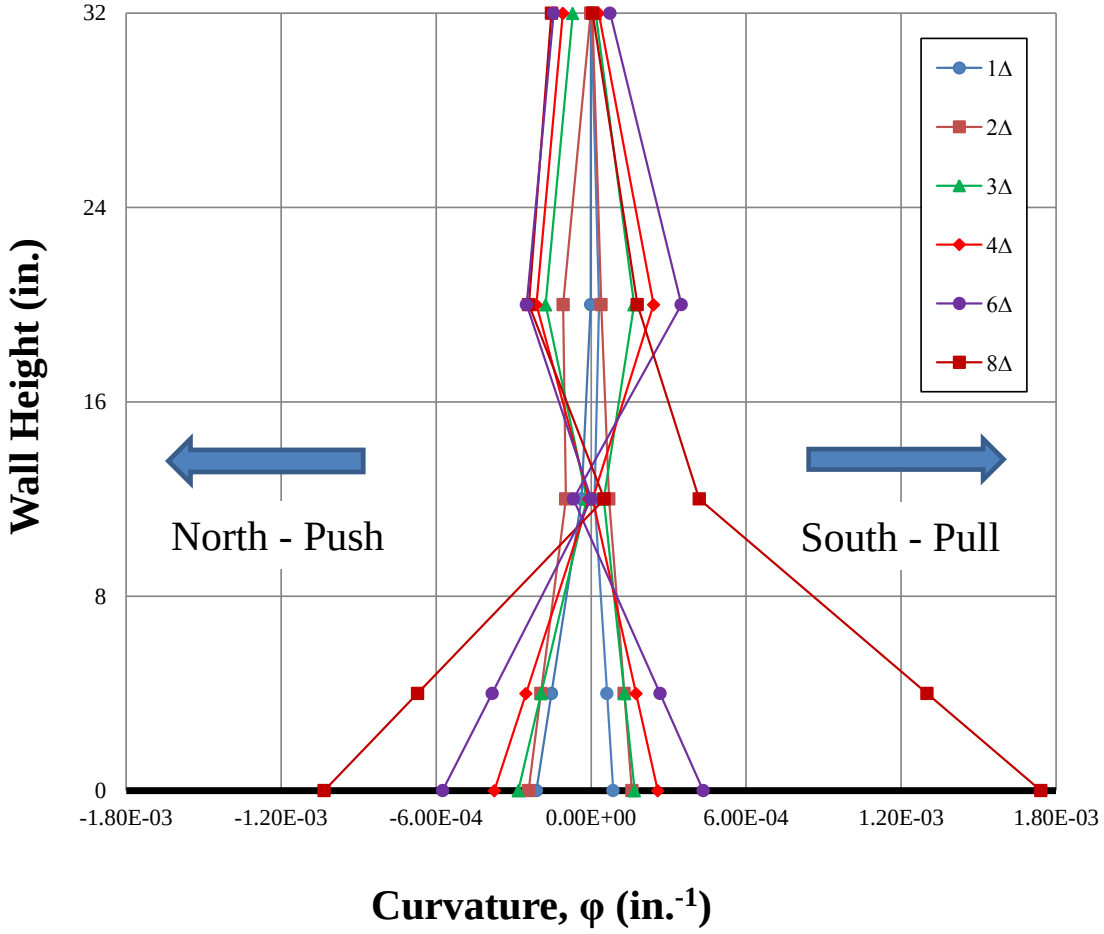

Figure 7-13 Curvature profile for Specimen PBS-4G

7.3.5. Curvature Ductility

Curvature ductility for Specimen PBS-4G was calculated as the ratio of ultimate curvature and yield curvature. Table 7-15 shows the value of yield curvature, ultimate curvature, and curvature ductility for both directions.

Table 7-15 Curvature ductility for Specimen PBS-4G

Direction	ϕ_y (x10^{-05} in.$^{-1}$)	ϕ_u (x10^{-05} in.$^{-1}$)	μ_ϕ
North-Push	8.77	103.34	11.78
South- Pull	6.92	174.08	25.15
Average	**7.85**	**138.71**	**18.47**

7.3.6. Height of Plasticity and Plastic Hinge Length

The height of plasticity, L_p, was calculated at ultimate curvature, at 20% degradation of maximum load or using data from the last cycle available from the instrumentation. Table 7-16 shows the height of plasticity and its portion of the total plan length of the wall segment for both directions of loading.

Table 7-16 Height of plasticity for Specimen PBS-4G

Direction	L_p (in.)	L_p/L_w
North-Push	48.55	51%
South- Pull	29.94	31%
Average	**39.25**	**41%**

Table 7-17 shows the plastic hinge length and its portion of the total plan length of the wall segment for both directions of loading.

Table 7-17 Plastic hinge length for Specimen PBS-4G

Direction	l_p (in.)	l_p/L_w
North-Push	26.24	27%
South- Pull	14.81	15%
Average	**20.52**	**21%**

7.3.7. Energy Dissipation and Equivalent Hysteretic Damping

Energy dissipation, $E_{D\Delta t}$, and equivalent hysteretic damping, ξ_{eq} , of Specimen PBS-4G were calculated for the hysteretic loops of 0.59% and 1.81% drift ratios, as shown in Figure 7-14 and Table 7-18 presents the value of energy dissipation and equivalent hysteretic damping for both curves.

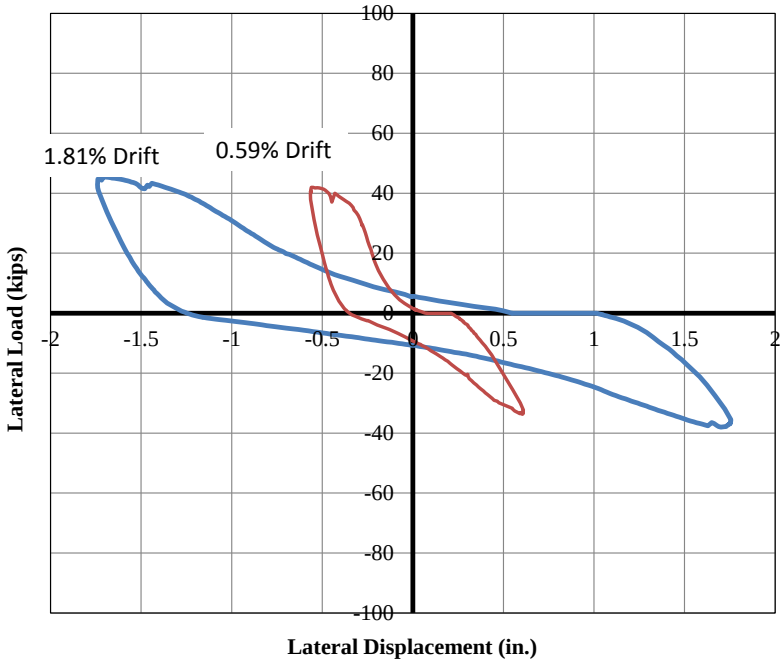

Figure 7-14 Hysteretic loops at 0.59% and 1.81% drift ratios for Specimen PBS-4G

Table 7-18 Energy dissipation and equivalent hysteretic damping for Specimen PBS-4G

Drift Level	Drift	$E_{D\Delta t}$ (kip-in)	ξ_{eq}
0.60%	0.59%	20.68	19.6%
1.50%	1.81%	78.71	21.8%

7.4. WALL SEGMENT PBS-11

7.4.1. Displacement Components

The relative contributions of flexural, shearing, and sliding deformation at maximum load and at 20% load degradation for Specimen PBS-11 were not included because the data of the string potentiometers showed inconsistencies.

7.4.2. Backbone and idealized elasto-plastic curve

The backbone and elasto-plastic curve for Specimen PBS-11 are plotted for each direction (north-pushing and south-pulling) as shown in Figure 7-15 and Figure 7-16. Table 7-19 summarizes the principal elements of both graphs.

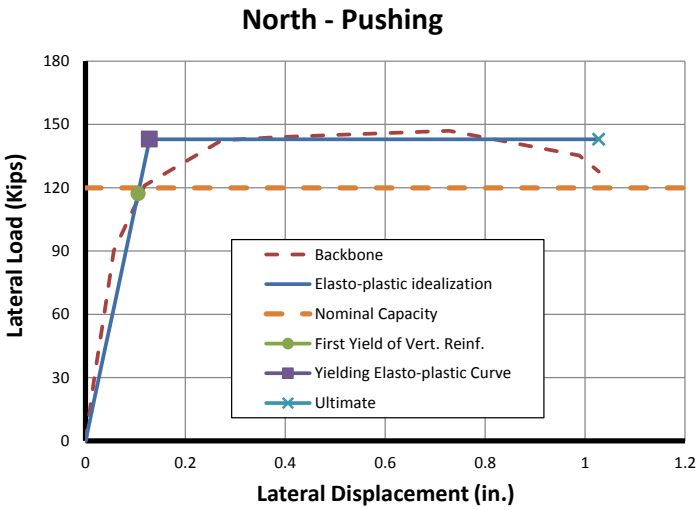

Figure 7-15 Backbone curve and elasto-plastic idealization for north-pushing direction for Specimen PBS-11

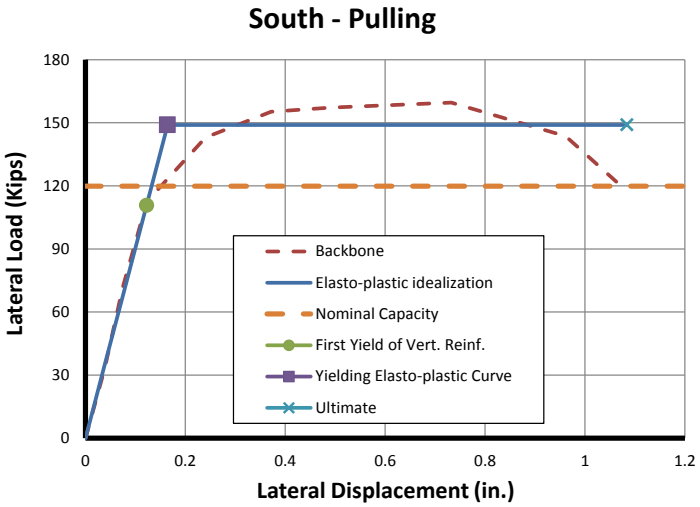

Figure 7-16 Backbone curve and elasto-plastic idealization for south-pulling direction for Specimen PBS-11

Table 7-19 Elasto-plastic and backbone curve for Specimen PBS-11

Direction	Elasto-plastic curve					Backbone	
	Δ'_y (in.)	P'_y (kips)	Δ_y (in.)	P_y (kips)	Δ_u (in.)	Δ_{Pmax} (in.)	P_{max} (kips)
North-Push	0.1052	117.30	0.1283	143.00	1.0272	0.7280	146.95
South- Pull	0.1222	110.82	0.1643	149.00	1.0836	0.7324	159.60

The values of the maximum lateral load of the elasto-plastic and backbone curve were higher than the nominal capacity for Specimen PBS-11 (119.89 kips) by 21% and 28%, respectively.

7.4.3. Displacement Ductility

The displacement ductility for Specimen PBS-11 was calculated from the elasto-plastic curve of each direction. Table 7-20 presents the values for both directions and their average.

Table 7-20 Displacement ductility for Specimen PBS-11

Direction	Δ_y **(in.)**	Δ_u **(in.)**	μ_Δ
North-Push	0.1283	1.0272	8.01
South- Pull	0.1643	1.0836	6.59
Average	**0.1463**	**1.0554**	**7.30**

7.4.4. Wall segment curvatures

The curvatures along the height of the Specimen PBS-11 were calculated for different cycles, as shown in Figure 7-17. The curvatures after the first cycle to 8 Δy are not presented because the instrumentation detached as a consequence of masonry spalling.

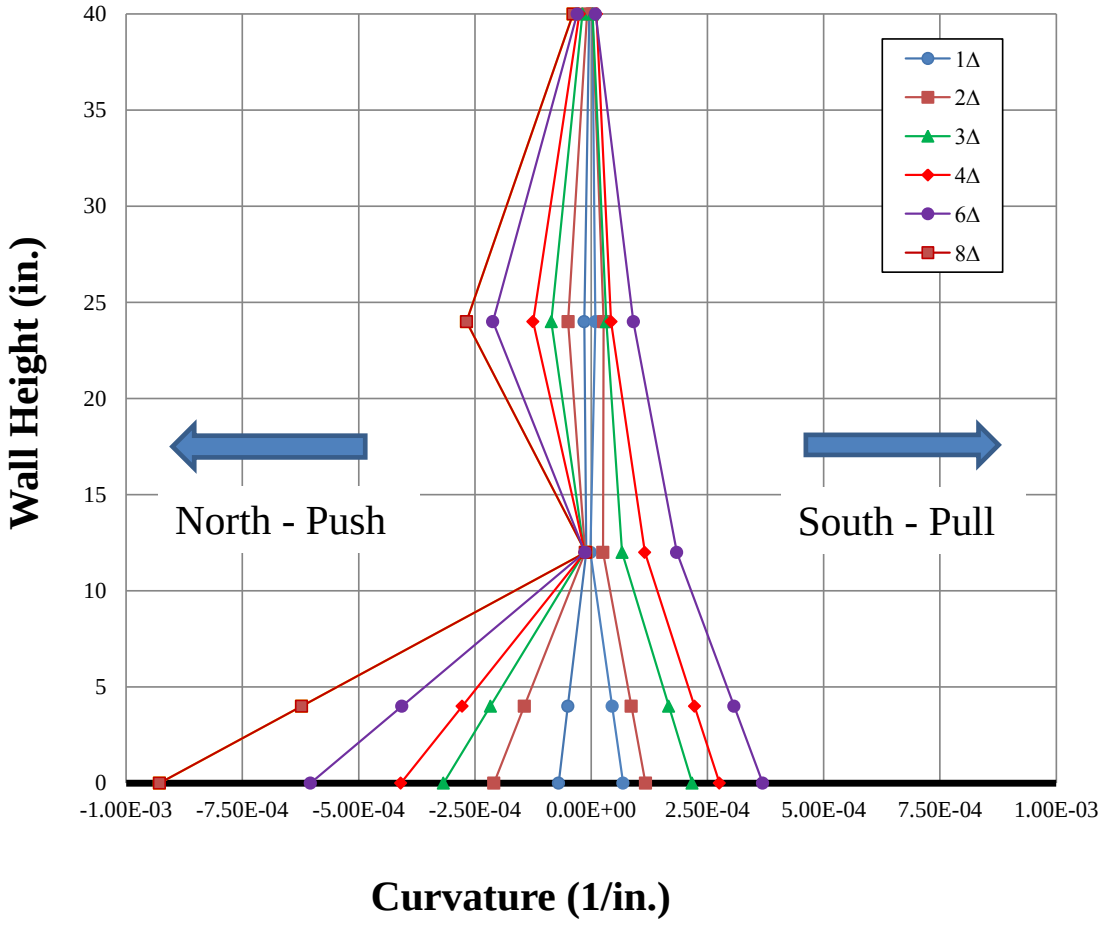

Figure 7-17 Curvature profile for Specimen PBS-11

7.4.5. Curvature Ductility

Curvature ductility for Specimen PBS-11 was calculated as the ratio of ultimate curvature and yield curvature. Table 7-21 shows the value of yield curvature, ultimate curvature, and curvature ductility for both directions.

Table 7-21 Curvature ductility for Specimen PBS-11

Direction	ϕ_y (x10^{-05} in.$^{-1}$)	ϕ_u (x10^{-05} in.$^{-1}$)	μ_ϕ
North-Push	7.36	36.87	5.01
South- Pull	9.61	92.80	9.66
Average	**8.48**	**64.84**	**7.33**

7.4.6. Height of Plasticity and Plastic Hinge Length

The height of plasticity, L_p, was calculated at ultimate curvature, 20% degradation of maximum load or using data from the last cycle available from the instrumentation. Table 7-22 shows the height of plasticity and its portion of the total plan length of the wall segment for both directions of loading.

Table 7-22 Height of plasticity for Specimen PBS-11

Direction	L_p (in.)	L_p/L_w
North-Push	29.96	31%
South- Pull	37.72	39%
Average	**33.84**	**35%**

Table 7-23 shows the plastic hinge length and its portion of the total plan length of the wall segment for both directions of loading.

Table 7-23 Plastic hinge length for Specimen PBS-11

Direction	l_p (in.)	l_p/L_w
North-Push	32.35	34%
South- Pull	5.64	6%
Average	**19.00**	**20%**

7.4.7. Energy Dissipation and Equivalent Hysteretic Damping

Energy dissipation, $E_{D\Delta t}$, and equivalent hysteretic damping, ξ_{eq}, for Specimen PBS-11 were calculated for the hysteretic loop of 0.73% and 1.73% drift ratios, as shown in Figure 7-18. Table 7-24 presents the value of energy dissipation and equivalent hysteretic damping for both curves. It can be seen that the energy dissipated at 1.73% drift was smaller than the one at 0.73%, which resulted in a lower equivalent hysteretic damping at the end of the test.

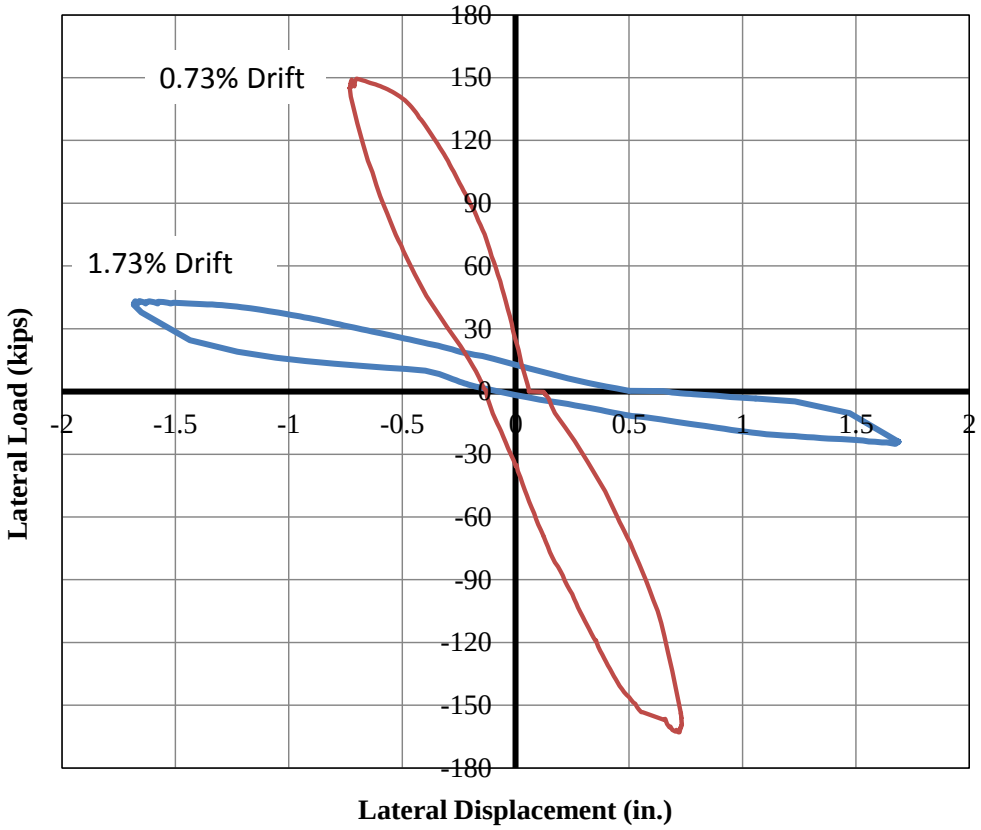

Figure 7-18 Hysteretic loops at 0.73% and 1.73% drift ratios for Specimen PBS-11

Table 7-24 Energy dissipation and equivalent hysteretic damping for Specimen PBS-11

Drift Level	Drift	$E_{D\Delta t}$ (kip-in)	ξ_{eq}
0.60%	**0.76%**	95.50	19.4%
1.50%	**1.75%**	50.14	16.4%

7.5. WALL SEGMENT PBS-12

7.5.1. Displacement Components

The relative contributions of flexural, shearing, and sliding deformation at maximum load and at 20% load degradation for Specimen PBS-12 are summarized in Table 7-25. Values at 20% degradation of the maximum load were not possible to calculate for the south-pulling direction because of problems in instrumentation at the last stages of the test.

Table 7-25 Relative flexural, shearing, and sliding deformation contributions for Specimen PBS-12

Direction	Maximum Load			20% Max Load Degradation		
	Flexure	Shear	Sliding	Flexure	Shear	Sliding
North-Push	73%	15%	12%	77%	13%	10%
South- Pull	89%	10%	2%	-	-	-

7.5.2. Backbone and idealized elasto-plastic curve

The backbone and elasto-plastic curve for Specimen PBS-12 are plotted for each direction (north-pushing and south-pulling) as shown in Figure 7-19 and Figure 7-20. Table 7-26 summarizes the principal elements of both graphs.

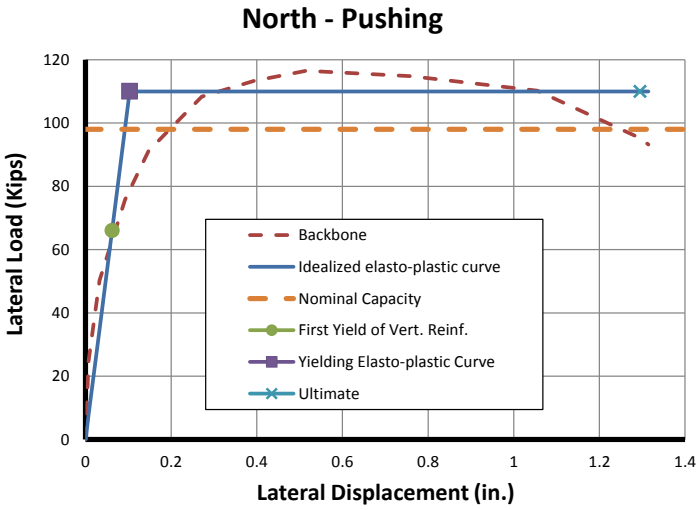

Figure 7-19 Backbone curve and elasto-plastic idealization for north-pushing direction for Specimen PBS-12

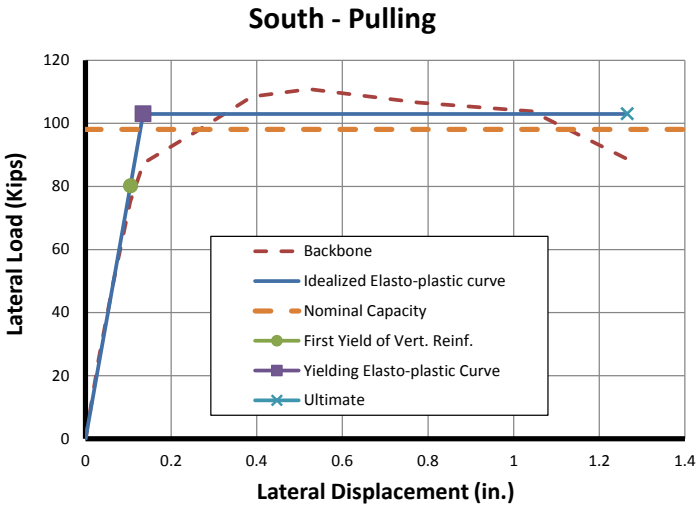

Figure 7-20 Backbone curve and elasto-plastic idealization for south-pulling direction for Specimen PBS-12

Table 7-26 Elasto-plastic and backbone curve for Specimen PBS-12

Direction	Elasto-plastic curve					Backbone	
	Δ'_y (in.)	P'_y (kips)	Δ_y (in.)	P_y (kips)	Δ_u (in.)	Δ_{Pmax} (in.)	P_{max} (kips)
North-Push	0.0620	66.10	0.1031	110.00	1.3143	0.5152	116.53
South- Pull	0.1050	80.24	0.1348	103.00	1.2655	0.5226	110.85

The values of the maximum lateral load of the elasto-plastic and backbone curve were higher than the nominal capacity for Specimen PBS-12 (98.06 kips) by 9% and 16%, respectively.

7.5.3. Displacement Ductility

The displacement ductility for Specimen PBS-12 was calculated from the elasto-plastic curve of each direction. Table 7-27 presents the values for both directions and their average.

Table 7-27 Displacement ductility for Specimen PBS-12

Direction	Δ_y (in.)	Δ_u (in.)	μ_Δ
North-Push	0.1031	1.3143	12.75
South- Pull	0.1348	1.2655	9.39
Average	**0.11896**	**1.2899**	**11.07**

7.5.4. Wall segment curvatures

The curvatures along the height of the Specimen PBS-12 were calculated for different cycles, as shown in Figure 7-21. The curvatures after the cycle of 8 Δy are not presented because the instrumentation detached as a consequence of masonry spalling.

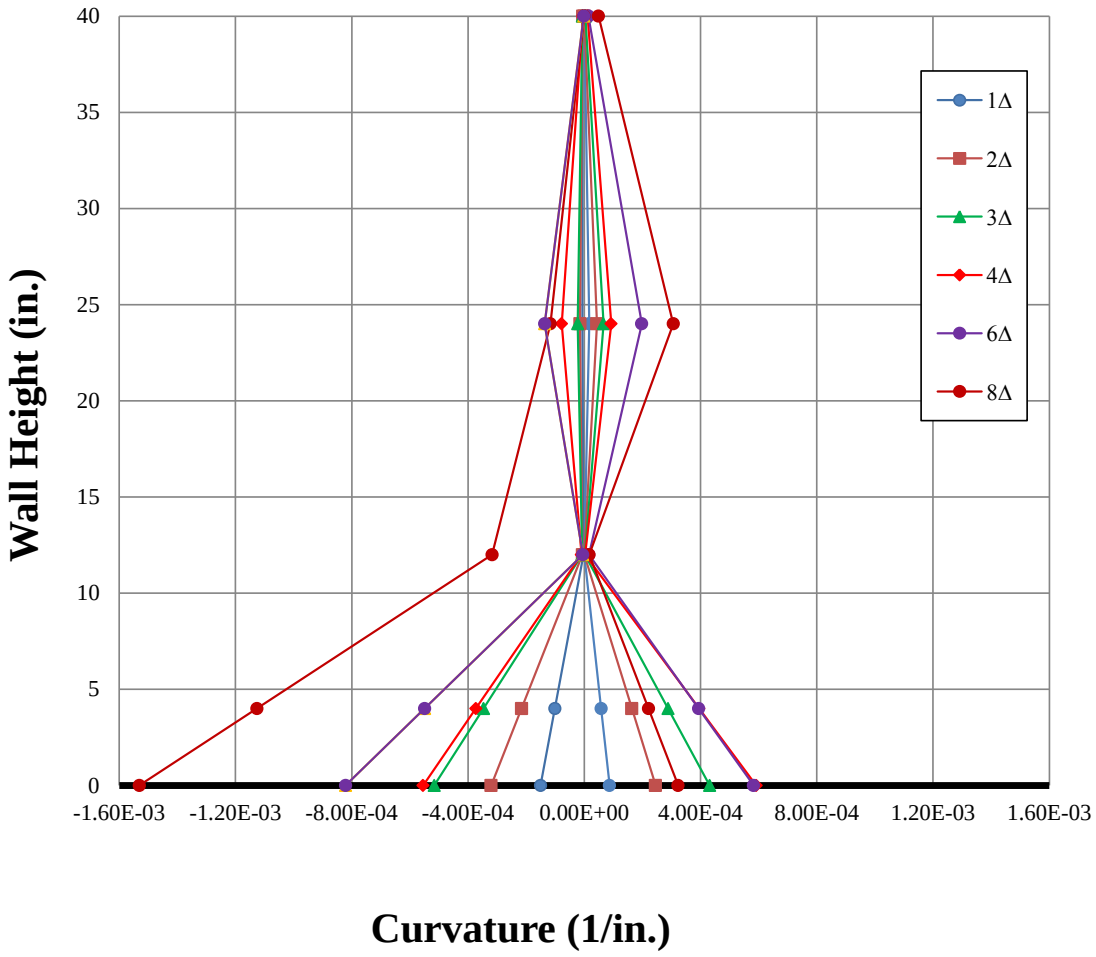

Figure 7-21 Curvature profile for Specimen PBS-12

7.5.5. Curvature Ductility

Curvature ductility for Specimen PBS-12 was calculated as the ratio of ultimate curvature and yield curvature. Table 7-28 shows the value of yield curvature, ultimate curvature, and curvature ductility for both directions.

Table 7-28 Curvature ductility for Specimen PBS-12

Direction	ϕ_y (x10^{-05} in.$^{-1}$)	ϕ_u (x10^{-05} in.$^{-1}$)	μ_ϕ
North-Push	8.56	153.10	17.89
South- Pull	6.45	32.28	5.00
Average	**7.50**	**92.69**	**11.45**

7.5.6. Height of Plasticity and Plastic Hinge Length

The height of plasticity, L_p, was calculated at ultimate curvature, 20% degradation of maximum load or using data from the last cycle available from the instrumentation. Table 7-29 shows the height of plasticity and its portion of the total plan length of the wall segment for both directions of loading.

Table 7-29 Height of plasticity for Specimen PBS-12

Direction	L_p (in.)	L_p/L_w
North-Push	45.75	48%
South- Pull	47.00	49%
Average	**46.38**	**48%**

Table 7-30 shows the plastic hinge length and its portion of the total plan length of the wall segment for both directions of loading.

Table 7-30 Plastic hinge length for Specimen PBS-12

Direction	l_p (in.)	l_p/L_w
North-Push	5.89	6%
South- Pull	44.24	46%
Average	**25.06**	**26%**

7.5.7. Energy Dissipation and Equivalent Hysteretic Damping

Energy dissipation, $E_{D\Delta t}$, and equivalent hysteretic damping, ξ_{eq} , were calculated for the hysteretic loops whose drifts were close or equal to 0.6 and 1.5%. Figure 7-22 shows the hysteretic loops of 0.55% and 1.63% drift ratios for Specimen PBS-12, and Table 7-31 presents the value of energy dissipation and equivalent hysteretic damping for both curves.

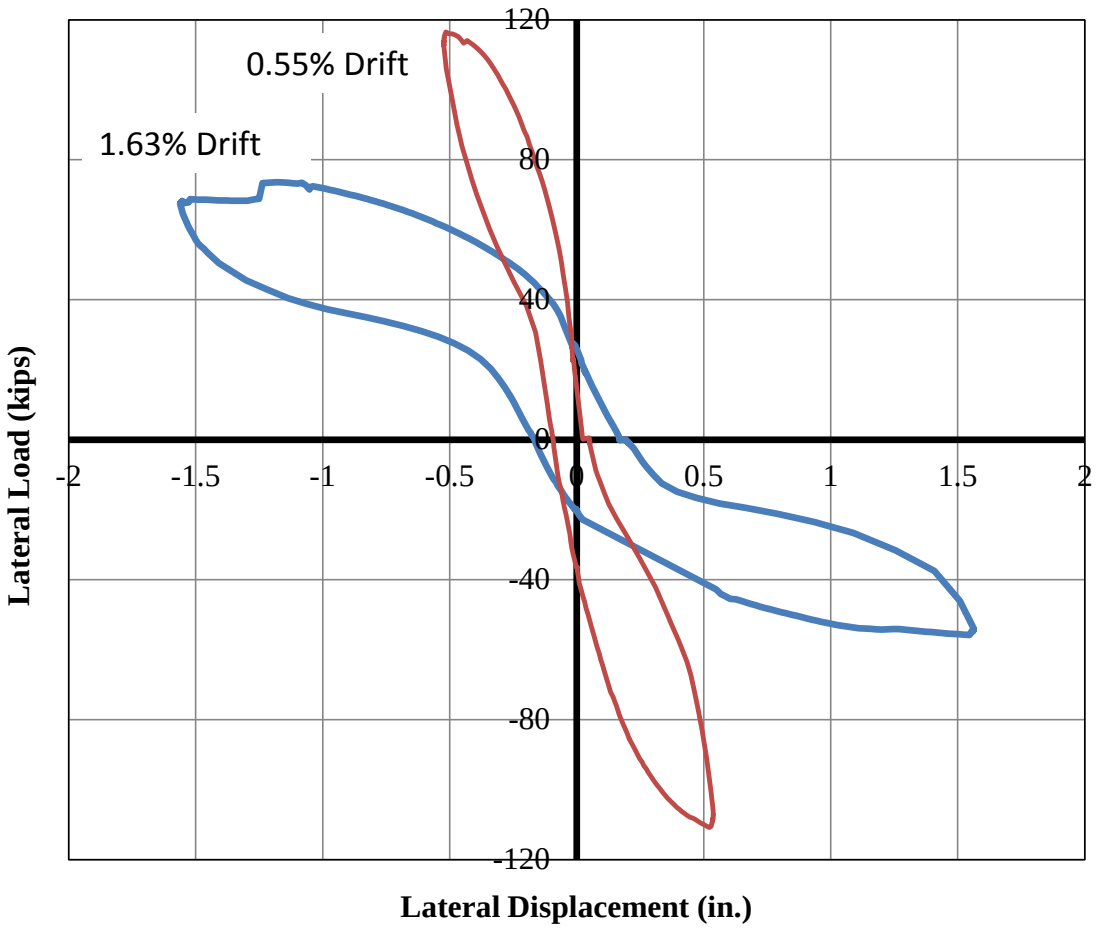

Figure 7-22 Hysteretic loops at 0.55% and 1.63% drift ratios for Specimen PBS-12

Table 7-31 Energy dissipation and equivalent hysteretic damping for Specimen PBS-12

Drift Level	Drift	$E_{D\Delta t}$ (kip-in)	ξ_{eq}
0.60%	**0.55%**	49.96	18.4%
1.50%	**1.63%**	89.12	18.5%

7.6. WALL SEGMENT PBS-12G

7.6.1. Displacement Components

The relative contributions of flexural, shearing, and sliding deformation at maximum load and at 20% load degradation for Specimen PBS-12G are summarized in Table 7-32. Values at the 20% degradation of the maximum load were not possible to calculate for the north-pushing direction because of problems in instrumentation at the last stages of the test.

Table 7-32 Relative flexural, shearing, and sliding deformation contributions for Specimen PBS-12G

Direction	Maximum Load			20% Max Load Degradation		
	Flexure	Shear	Sliding	Flexure	Shear	Sliding
North-Push	82%	11%	6%	-	-	-
South- Pull	79%	15%	6%	93%	5%	2%

7.6.2. Backbone and idealized elasto-plastic curve

The backbone and elasto-plastic curve for Specimen PBS-12G are plotted for each direction (north-pushing and south-pulling) as shown in Figure 7-23 and Figure 7-24. Table 7-33 summarizes the principal elements of both graphs.

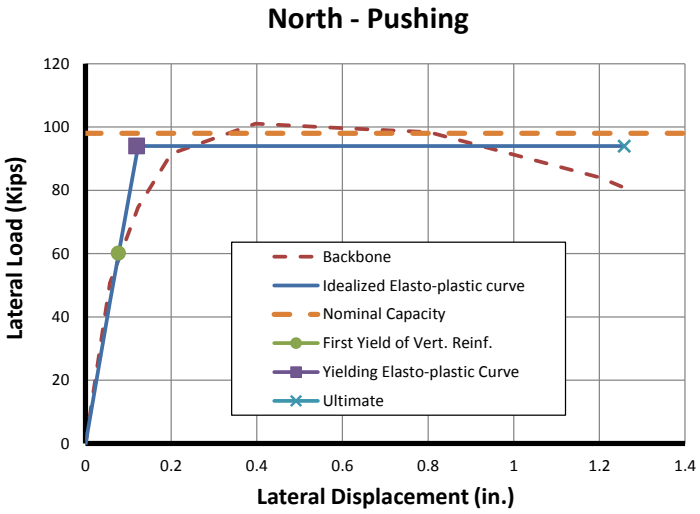

Figure 7-23 Backbone curve and elasto-plastic idealization for north-pushing direction for Specimen PBS-12G

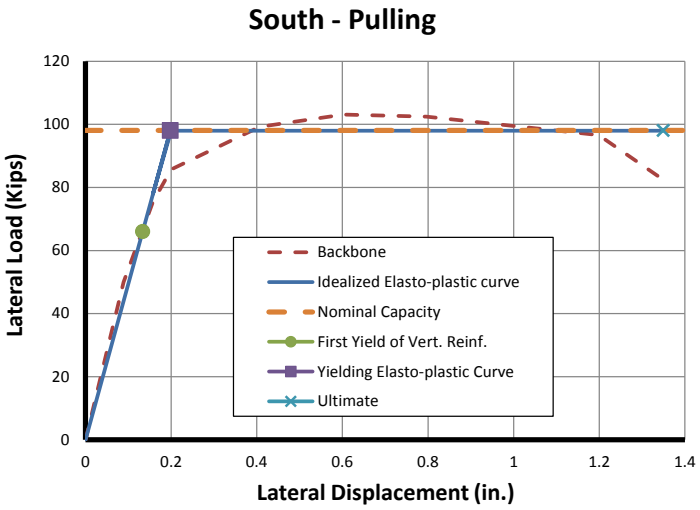

Figure 7-24 Backbone curve and elasto-plastic idealization for south-pulling direction for Specimen PBS-12G

Table 7-33 Elasto-plastic and backbone curve for Specimen PBS-12G

Direction	Elasto-plastic curve					Backbone	
	Δ'_y (in.)	P'_y (kips)	Δ_y (in.)	P_y (kips)	Δ_u (in.)	Δ_{Pmax} (in.)	P_{max} (kips)
North-Push	0.0766	60.20	0.1196	94.00	1.2578	0.3972	101.07
South- Pull	0.1335	66.03	0.1982	98.00	1.3490	0.6026	103.14

The values of the maximum lateral load of the elasto-plastic and backbone curve were 3% less and 4% higher, respectively, than the nominal capacity for Specimen PBS-12G (98.06 kips).

7.6.3. Displacement Ductility

The displacement ductility for Specimen PBS-12G was calculated from the elasto-plastic curve of each direction. Table 7-34 presents the values for both directions and their average.

Table 7-34 Displacement ductility for Specimen PBS-12G

Direction	Δ_y (in.)	Δ_u (in.)	μ_Δ
North-Push	0.1196	1.2578	10.52
South- Pull	0.1982	1.3490	6.81
Average	**0.15887**	**1.3034**	**8.66**

7.6.4. Wall segment curvatures

The curvatures along the height of the Specimen PBS-12G were calculated for different cycles, as shown in Figure 7-25. The curvatures after the first cycle to 4 Δy are not presented because the instrumentation detached as a consequence of masonry spalling.

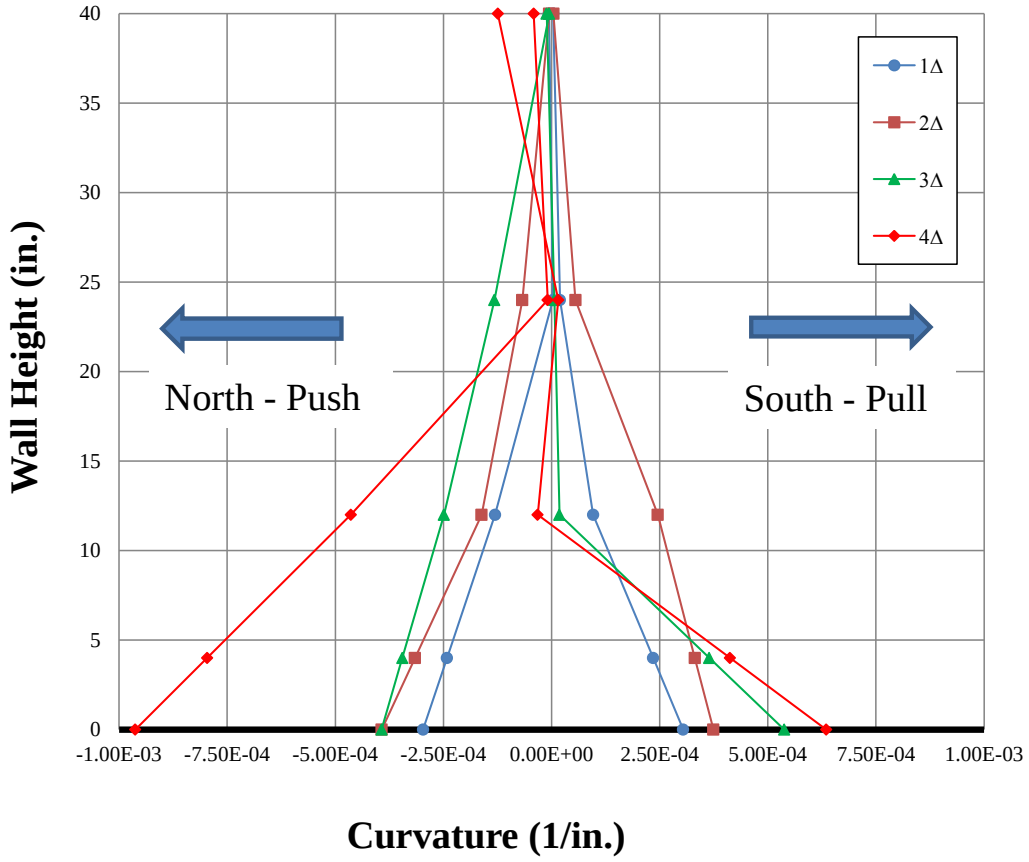

Figure 7-25 Curvature profile for Specimen PBS-12G

7.6.5. Curvature Ductility

Curvature ductility for Specimen PBS-12G was calculated as the ratio of ultimate curvature and yield curvature. Table 7-35 shows the value of yield curvature, ultimate curvature, and curvature ductility for both directions.

Table 7-35 Curvature ductility for Specimen PBS-12G

Direction	ϕ_y (x10^{-05} in.$^{-1}$)	ϕ_u (x10^{-05} in.$^{-1}$)	μ_ϕ
North-Push	11.27	96.23	8.54
South- Pull	6.39	63.49	9.93
Average	**8.83**	**79.86**	**9.23**

7.6.6. Height of Plasticity and Plastic Hinge Length

The height of plasticity, L_p, was calculated at ultimate curvature, 20% degradation of maximum load or using data from the last cycle available from the instrumentation. Table 7-36 shows the height of plasticity and its portion of the total plan length of the wall segment for both directions of loading.

Table 7-36 Height of plasticity for Specimen PBS-12G

Direction	L_p (in.)	L_p/L_w
North-Push	55.41	58%
South- Pull	20.84	22%
Average	**38.12**	**40%**

Table 7-37 shows the plastic hinge length and its portion of the total plan length of the wall segment for both directions of loading.

Table 7-37 Plastic hinge length for Specimen PBS-12G

Direction	l_p (in.)	l_p/L_w
North-Push	11.15	12%
South- Pull	20.46	21%
Average	**15.81**	**16%**

7.6.7. Energy Dissipation and Equivalent Hysteretic Damping

Energy dissipation, $E_{D\Delta t}$, and equivalent hysteretic damping, ξ_{eq} , were calculated for the hysteretic loops whose drifts were close or equal to 0.6 and 1.5%. Figure 7-26 shows the hysteretic loops of 0.62% and 1.67% drift ratios for Specimen PBS-12G, and Table 7-38 presents the value of energy dissipation and equivalent hysteretic damping for both curves.

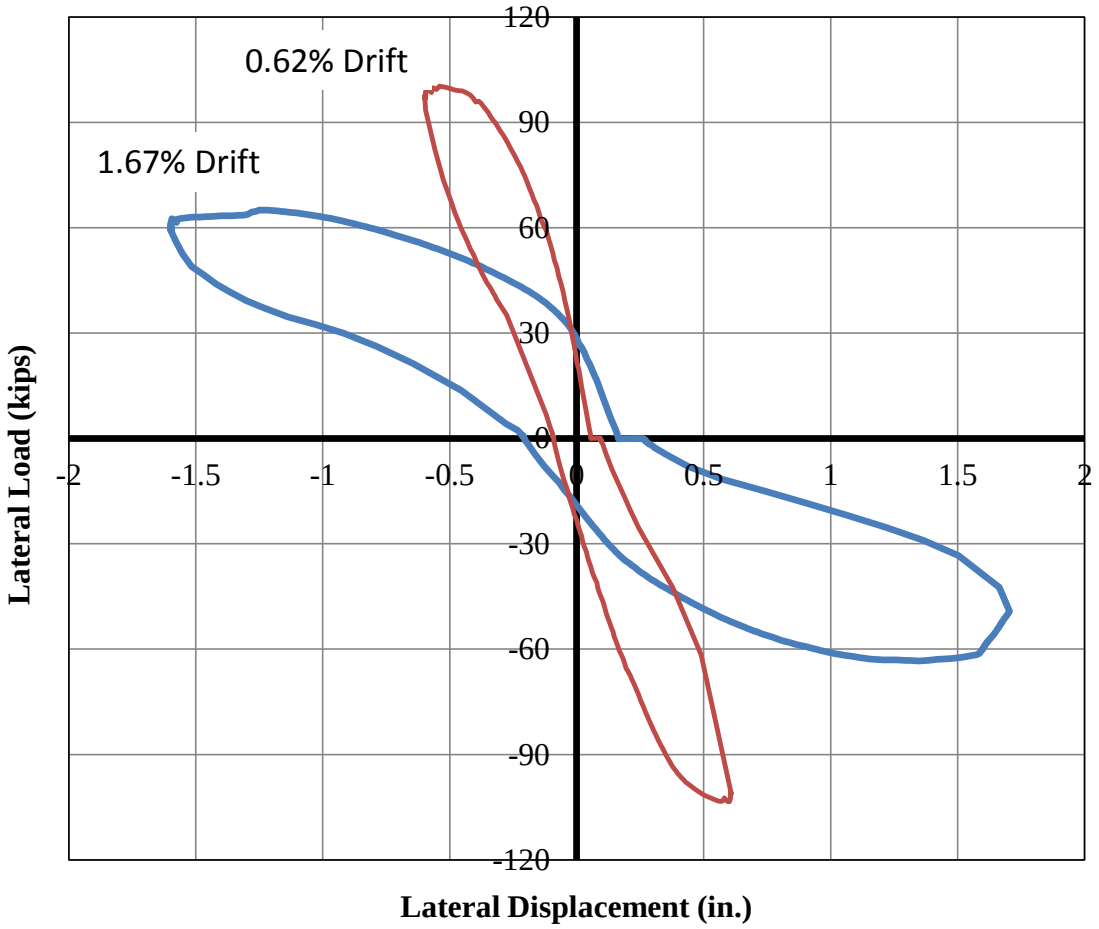

Figure 7-26 Hysteretic loops at 0.62% and 1.67% drift ratios for Specimen PBS-12G

Table 7-38 Energy dissipation and equivalent hysteretic damping for Specimen PBS-12G

Drift Level	Drift	$E_{D\Delta t}$ (kip-in)	ξ_{eq}
0.60%	**0.62%**	51.24	19.1%
1.50%	**1.67%**	113.57	23.8%

7.7. SUMMARY OF EVALUATION OF RESULTS

In this section, the test results for all six specimens are summarized and evaluated. Computed capacity is compared with experimental capacity. Values of relative deformation contribution, drift ratios, load-displacement curve, displacement ductility, height of plasticity, plastic hinge length, energy dissipation, and equivalent hysteretic damping are summarized and correlated with the level of axial load and vertical reinforcement ratio of each specimen. Finally, the effects of the use of "green" units on the performance of the wall segments are evaluated.

7.7.1. Observed versus Computed flexural capacities

The expected flexural capacity of each wall segment was calculated before testing as explained in Section 3.2. The computed values and those obtained during testing are summarized in Table 7-39. Maximum loads in the test ranged from 3% to 52% higher than the predicted capacities. Specimen PBS-12G, which had problems with slip in vertical reinforcement early during testing, provided the closest results to the predicted. Excluding Specimen PBS-12G, test results ranged from 13% to 52% higher than the predicted capacities.

Table 7-39 Nominal and observed flexural capacities for all specimens

Specimen	Aspect Ratio	Vertical Reinforcement (percentage)	Axial Load Ratio $P/(A_g f'_m)$	Direction	Max. Load (kips)	Computed Capacity (kips)
PBS-3	1.0	#4 @ 8 in. 0.33	0	**North-Push**	81.85	60.11
				South- Pull	82.10	
PBS-4	1.0	#4 @ 16 in. 0.16	0	**North-Push**	47.85	31.43
				South- Pull	46.38	
PBS-4G	1.0	#4 @ 16 in. 0.16	0	**North-Push**	45.47	
				South- Pull	38.00	
PBS-11	1.0	#4 @ 8 in. 0.33	0.10	**North-Push**	146.95	119.89
				South- Pull	159.60	
PBS-12	1.0	#4 @ 16 in. 0.16	0.10	**North-Push**	116.53	98.06
				South- Pull	110.85	
PBS-12G	1.0	#4 @ 16 in. 0.16	0.10	**North-Push**	101.07	
				South- Pull	103.14	

7.7.2. Relative contributions from flexural, shearing, and sliding deformations

Relative contributions from flexural, shearing, and sliding deformation for all specimens are summarized in Table 7-40. Relative deformations for Specimen PBS-11 could not be computed due to problems in the instrumentation. Flexural deformation dominated in all specimens at maximum load and at ultimate load (20% maximum load degradation). Shearing deformations contributed more at maximum load than at ultimate loads. Sliding deformation was more important for walls with zero axial load. The vertical reinforcement ratio did not affect the relative contributions to overall deformation.

Table 7-40 Relative contributions from flexural, shearing, and sliding deformation for all specimens

Specimen	Direction	Maximum Load			20% Max Load Degradation		
		Flexure	Shear	Sliding	Flexure	Shear	Sliding
PBS-3	North-Push	68%	15%	17%	51%	19%	30%
	South- Pull	59%	11%	30%	69%	9%	22%
PBS-4	North-Push	55%	15%	30%	68%	4%	28%
	South- Pull	52%	6%	42%	63%	4%	33%
PBS-4G	North-Push	58%	22%	19%	-	-	-
	South- Pull	50%	22%	27%	57%	20%	23%
PBS-11*	North-Push	-	-	-	-	-	-
	South- Pull	-	-	-	-	-	-
PBS-12	North-Push	73%	15%	12%	77%	13%	10%
	South- Pull	89%	10%	2%	-	-	-
PBS-12G	North-Push	82%	11%	6%	-	-	-
	South- Pull	79%	15%	6%	93%	5%	2%

* Instrumentation failed

7.7.3. Drift ratios

Drift ratios at the maximum and ultimate load for all the specimens are summarized in Table 7-41. Results showed higher drift capacity for specimens with zero axial load; this can be also attributed to the contribution of sliding in the lateral displacement, especially at ultimate loads. Vertical reinforcement did not affect the drift ratios. Note that the 2011 MSJC Code requires that special reinforced masonry shear walls be tension-controlled.

Table 7-41 Drift ratios for maximum and ultimate load

Specimen	Aspect Ratio	Vertical Reinforcement (percentage)	Axial Load Ratio $P/(A_g f'_m)$	Direction	Drift Ratio	
					Max. Load	Ultimate
PBS-3	1.0	#4 @ 8 in. 0.33	0	**North-Push**	0.63%	1.66%
				South- Pull	1.05%	1.66%
PBS-4	1.0	#4 @ 16 in. 0.16	0	**North-Push**	1.76%	2.50%
				South- Pull	1.75%	2.53%
PBS-4G	1.0	#4 @ 16 in. 0.16	0	**North-Push**	1.78%	3.03%
				South- Pull	1.77%	2.50%
PBS-11	1.0	#4 @ 8 in. 0.33	0.10	**North-Push**	0.76%	1.28%
				South- Pull	0.76%	1.34%
PBS-12	1.0	#4 @ 16 in. 0.16	0.10	**North-Push**	0.54%	1.35%
				South- Pull	0.54%	1.37%
PBS-12G	1.0	#4 @ 16 in. 0.16	0.10	**North-Push**	0.41%	1.66%
				South- Pull	0.63%	1.78%

7.7.4. Load-displacement curve (backbone)

The load-displacement curves (backbone) for all specimens are plotted in Figure 5-5. The following observations are made:

- Displacement ductility is varies inversely with flexural capacity. Because ductility is not sensitive to the flexural reinforcement ratio (all specimens are designed with the same critical strain gradient for maximum longitudinal reinforcement), flexural capacity increases with increasing axial load. Increasing axial load is associated with lower ductility.

- For specimens with equal vertical reinforcement ratios, flexural capacity (lateral load capacity) increases with increasing axial load. This is obviously consistent

with the expected shape of the moment-axial force interaction diagram below the balance point.

- For specimens with equal axial load ratios, flexural capacity (lateral load capacity) increases with increasing vertical reinforcement. This is obviously consistent with the expected shape of the moment-axial force interaction diagram.

- Stiffness increases with increasing vertical reinforcement ratio. This is obviously consistent with the expected flexural stiffness of the cracked, transformed section.

- Stiffness increase with increasing axial load ratio. This is obviously consistent with the expected flexural stiffness of the cracked, transformed section.

- Specimens made of "green blocks" (PBS-4G and PBS-12G) performed similarly to otherwise identical specimen made of "gray blocks" (PBS-4 and PBS-12). This point is discussed further in a subsequent section of this chapter.

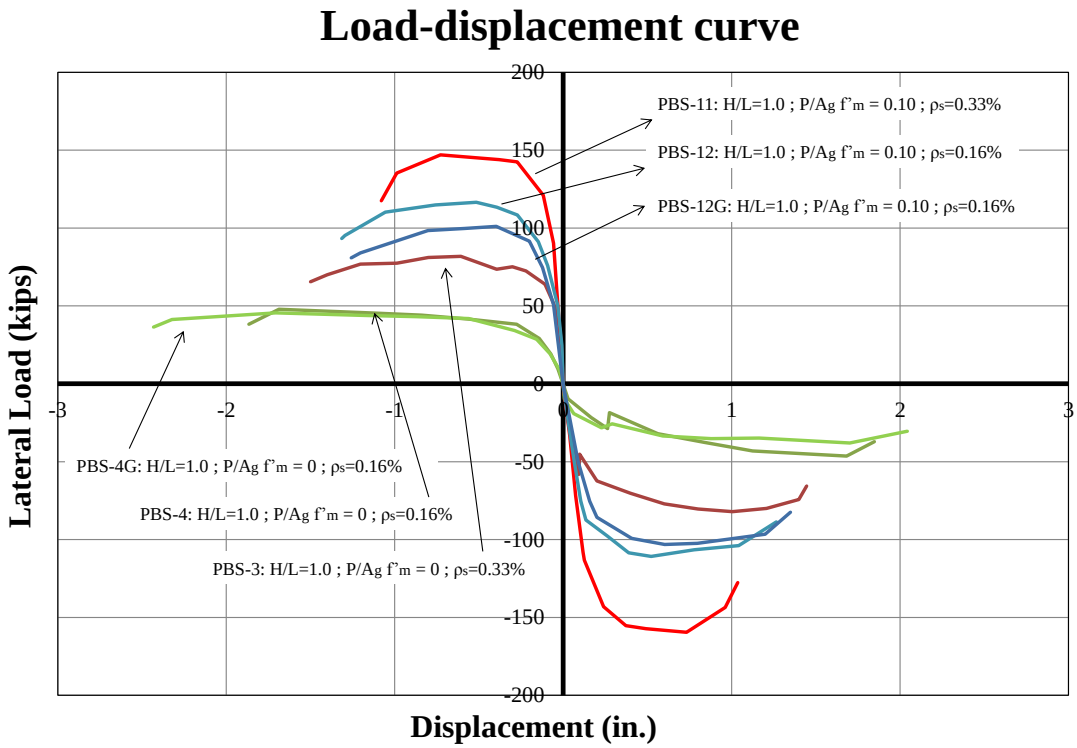

Figure 7-27 Load-displacement curves for all specimens

Large ultimate displacement for specimens with zero axial load are evident in Figure 7-27. This was the result of the sliding component of deformation in the lateral displacement. To assess the effects of sliding, the envelope curves were also calculated removing sliding deformations. Results are shown in Figure 7-28.

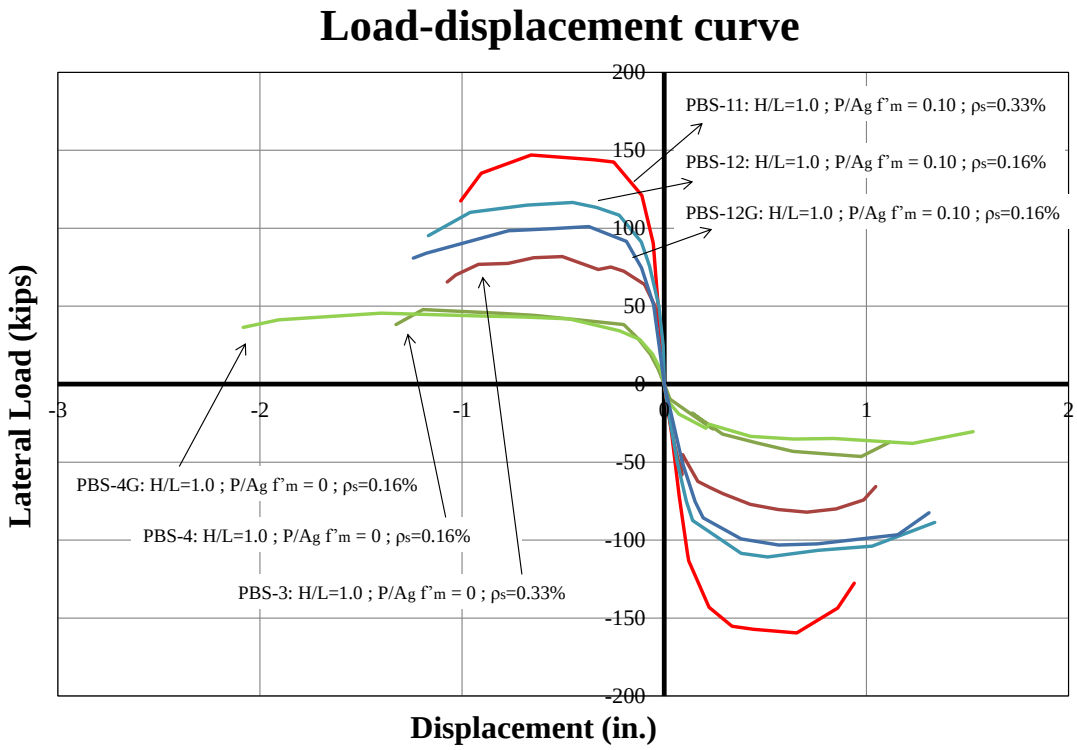

Figure 7-28 Load-displacement curves for all specimens, sliding deformations removed

As anticipated, removing the sliding component in the lateral displacement reduced considerably the ultimate displacement for specimens with zero axial load; moreover, the trends explained before are still valid.

7.7.5. Displacement ductility

Displacement ductility in both directions and their averages are shown in Table 7-42 for all the specimens. Excluding PBS-4 which had slip in lap splices, higher displacement ductilities were found for specimens with zero axial load. For specimens with same level of axial load, no clear influence in the displacement ductility was

observed due higher vertical reinforcement ratios. The displacement ductility for the first direction of loading (north) was always higher that for the south direction.

In general, the displacement ductilities obtained in the tests were higher than the expected; part of this was due the inclusion of the sliding deformation in the total response of the specimens. Table 7-42 presents corrected displacement ductilities (ignoring sliding) in both directions of loading and their average for all specimens. Corrected displacement ductility for specimens PBS-3 and PBS-4 decreased to 80% and 66% of the original values, respectively; however, displacement ductility for other specimens remained approximately the same.

Table 7-42 Displacement ductility for all specimens

Specimen	Aspect Ratio	Vertical Reinforcement	Axial Load Ratio	Displacement Ductility		
		(percentage)	P/ (Ag f'm)	North	South	Average
PBS-3	1.0	#4 @ 8 in. (0.33)	0	19.71	12.88	**16.29**
				(15.71)	(10.08)	**(12.90)**
PBS-4	1.0	#4 @ 16 in. (0.16)	0	11.23	5.53	**8.38**
				(7.71)	(3.39)	**(5.55)**
PBS-4G	1.0	#4 @ 16 in. (0.16)	0	19.31	14.76	**17.04**
				(22.93)	(10.48)	**(16.71)**
PBS-11	1.0	#4 @ 8 in. (0.33)	0.10	8.01	6.59	**7.30**
				(8.35)	(5.84)	**(7.10)**
PBS-12	1.0	#4 @ 16 in. (0.16)	0.10	12.75	9.39	**11.07**
				(13.87)	(9.11)	**(11.49)**
PBS-12G	1.0	#4 @ 16 in. (0.16)	0.10	10.52	6.81	**8.66**
				(11.17)	(6.72)	**(8.94)**

( ) Sliding deformation removed

Calculated displacement ductilities in this thesis were generally higher than displacement ductilities reported in parallel work at Washington State University (Sherman 2011; Kapoi 2012) as shown in Table 7-43. An extensive study of the differences in the displacement ductility of the specimens studied in this thesis and those studied by Sherman and Kapoi was conducted as explained below:

Table 7-43 Displacement ductility for Washington State and UT Austin specimens

Specimen	Direction	Elasto-plastic curve							
		1st Yield		Yield Disp.		Ultimate Disp.		Disp. Ductility	
		Disp. (in.)	Drift Ratio (%)	Disp. (in.)	Drift Ratio (%)	Disp. (in.)	Drift Ratio (%)		Average
UT Austin Specimens									
PBS-3	**North**	0.04	0.04%	0.07	0.07%	1.07	1.12%	15.7	12.90
	South	0.07	0.08%	0.10	0.11%	1.05	1.09%	10.1	
PBS-4	**North**	0.07	0.08%	0.15	0.16%	1.73	1.80%	11.2	8.05
	South	0.19	0.20%	0.33	0.34%	1.62	1.69%	4.9	
PBS-4G	**North**	0.03	0.03%	0.09	0.09%	2.08	2.17%	22.9	16.71
	South	0.07	0.08%	0.15	0.15%	1.53	1.59%	10.5	
PBS-11	**North**	0.10	0.10%	0.12	0.13%	1.01	1.05%	8.3	7.10
	South	0.12	0.12%	0.16	0.17%	0.94	0.98%	5.8	
PBS-12	**North**	0.05	0.05%	0.08	0.09%	1.17	1.22%	13.9	11.49
	South	0.11	0.12%	0.15	0.15%	1.34	1.39%	9.1	
PBS-12G	**North**	0.07	0.07%	0.11	0.12%	1.24	1.29%	11.2	8.94
	South	0.13	0.14%	0.19	0.20%	1.31	1.36%	6.7	
Washington State University Specimens									
Sherman Spec. 3	**North**	0.11	0.15%	0.17	0.24%	0.74	1.03%	4.4	5.06
	South	0.09	0.13%	0.13	0.18%	0.75	1.04%	5.8	
Sherman Spec. 4	**North**	0.10	0.14%	0.14	0.19%	0.64	0.89%	4.6	4.79
	South	0.09	0.13%	0.13	0.18%	0.65	0.90%	5.0	
Kapoi Spec. C5	**North**	0.21	0.29%	0.26	0.36%	1.04	1.44%	4.0	2.79
	South	0.54	0.75%	0.68	0.94%	1.07	1.49%	1.6	

Differences in the design parameters of the specimens

Table 7-44 shows the design parameters (aspect ratio, vertical reinforcement ratio, and axial load ratio) for the specimens tested in this work and the specimens with aspect ratio equal to 1.0 tested at WSU. Sherman's Specimen 3 has the same design parameters of Specimen PBS-3, and Specimen 4 (axial load ratio equal to 0.0625) is an intermediate

case between Specimens PBS-3 and PBS-11. Displacement ductilities among those specimens are expected to be the same at UT Austin and at Washington State.

Table 7-44 UT and WSU specimens with aspect ratio equal to 1.0

Specimen	Hw (in.)	Lw (in.)	Aspect Ratio	Vertical Reinforcement (percentage)	Axial Load Ratio $P/(A_g f'_m)$
UT Specimens					
PBS-3	96	96	1.0	#4 @ 8 in. (0.33)	0
PBS-4	96	96	1.0	#4 @ 16 in. (0.16)	0
PBS-4G	96	96	1.0	#4 @ 16 in. (0.16)	0
PBS-11	96	96	1.0	#4 @ 8 in. (0.33)	0.10
PBS-12	96	96	1.0	#4 @ 16 in. (0.16)	0.10
PBS-12G	96	96	1.0	#4 @ 16 in. (0.16)	0.10
WSU Specimens					
Kapoi - Specimen C5	72	72	1.0	#7 @ 16 in. (0.55)	0.0625
Sherman - Specimen 3	72	72	1.0	#4 @ 8 in. (0.33)	0
Sherman - Specimen 4	72	72	1.0	#4 @ 8 in. (0.33)	0.0625

Differences in the load-displacement curves (backbone)

Contrary to this expectation, the specimens from UT Austin and Washington State behaved differently. The backbone load-displacement curves for specimens with the same design parameters, Sherman's Specimen 3 and PBS-3, are compared in Figure 7-29 and Figure 7-30.

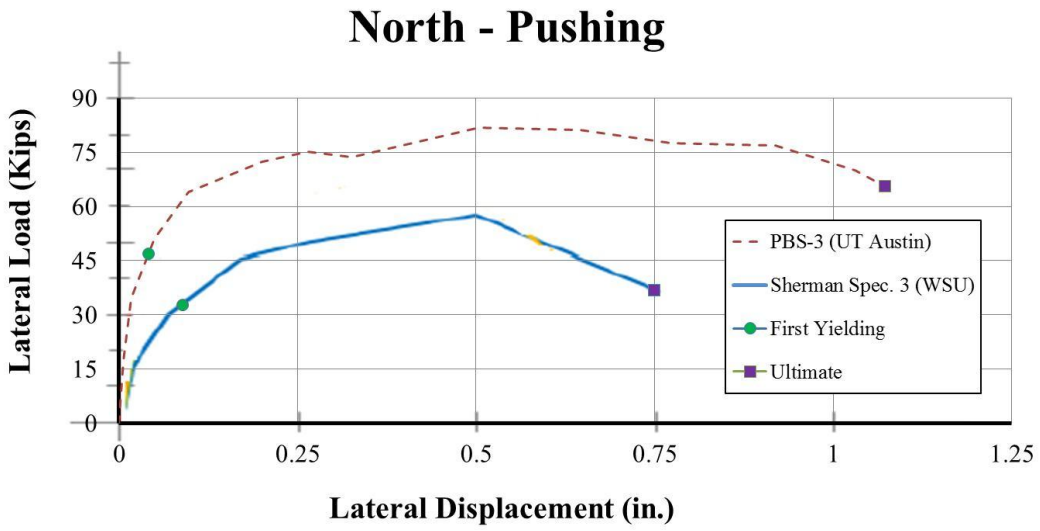

Figure 7-29 Load-displacement curves (backbone) for Specimen 3 (Sherman 2011) and PBS-3 in the north direction

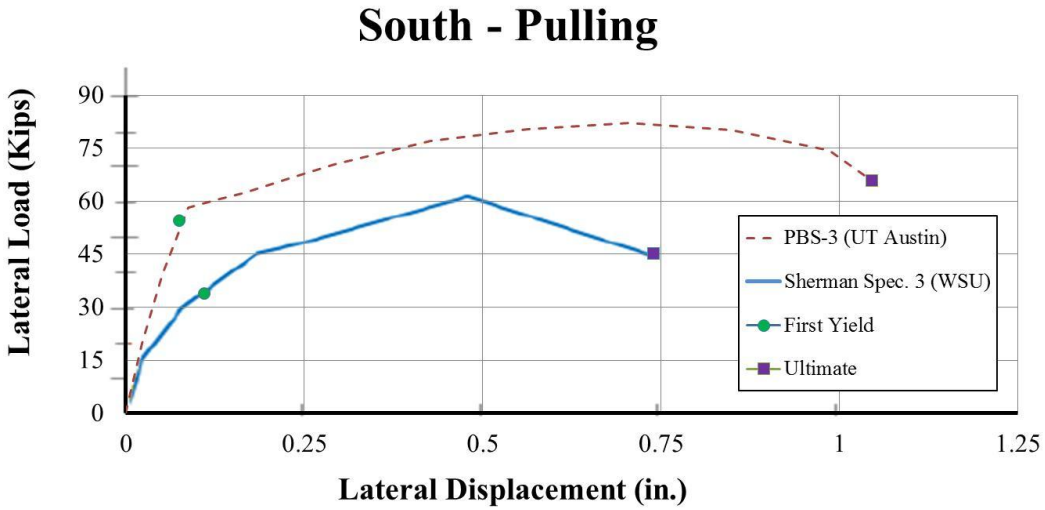

Figure 7-30 Load-displacement curves (backbone) for Specimen 3 (Sherman 2011) and PBS-3 in the south direction

The lower values of stiffness and capacity for Sherman's Specimen 3 are a consequence of the smaller dimensions of Washington State specimens. Drift ratios at ultimate displacement for Specimen PBS-3 were 50% higher than for Sherman's Specimen 3. Those differences are consistent with the observed behavior of each specimen during testing. Figure 7-31 shows Sherman's Specimen 3 and Specimen PBS-3 at the end of the test. In contrast to Specimen 3, Specimen PBS-3 shows wider flexural cracking and the start of damage to the south compression toe.

Specimen 3 (Sherman 2011)

PBS-3

Figure 7-31 Comparison Specimen 3 (Sherman 2011) and Specimen PBS-3 at end of test

Sherman (2011) reports shear cracking along the height of the Specimen 3 but no crushing or spalling was observed at the toe regions. In contrast, flexural and shear cracking, toe crushing, and fracture was observed in PBS-3. Also, in applying the loading protocol, the assumed yield displacement used to control the lateral displacement at each

cycle was 2.5 times higher for Sherman's Specimen 3 than for PBS-3, which resulted in a considerably lower number of cycles to reach the failure of the Specimen 3. This lower number of cycles precluded progressive degradation of WSU Specimen 3, and resulted in a lower ultimate drift ratio.

Differences in the determination of the first yield point

Procedures to identify the first yield in the extreme vertical reinforcement were the same for both universities. The first yield point was obtained from the reading of the strain gauge at the base of the extreme-fiber dowels. The strains in the dowels were verified using the average strains measured by the linear potentiometers at each end of the specimens, resulting in good agreement. However, the comparison of the drift ratio at the first yield displacement for specimens with the same design parameters showed lower drift ratios at yield for PBS-3 than for Sherman's Specimen 3 (Table 7-43, Figure 7-29, and Figure 7-30). This difference can be attributed to the position of the extreme vertical reinforcement compared with the plan length of the specimen (Shedid 2008).

Differences in the determination of the elasto-plastic idealization

The procedure used to determine the elasto-plastic idealization, explained in Section 7.1.2., was the same for both universities. The values obtained in the elasto-plastic idealization for these specimens showed that data were internally consistent, and also consistent with the performance of the walls. However, the method to calculate the elasto-plastic idealization was quite sensitive to the initial secant stiffness of the specimen and the ultimate displacement. As explained above, those parameters could differ even for specimens with the same design parameters. This resulted on differences between

calculated displacement ductilities in specimens tested at Washington State and at UT Austin.

Other studies such as Shedid (2008) and Vaughan (2010) address the variability of displacement ductility among specimens, and report maximum displacement ductilities of 7 and 12 respectively. Those values are consistent with values obtained at UT Austin.

7.7.6. Height of plasticity

The ratio of the height of plasticity to the plan length of the specimen is summarized in Table 7-45 for all the wall segments. Average values ranged from 35 to 48%. The height of plasticity was not influenced by vertical reinforcement ratio or axial load.

Table 7-45 Height of plasticity

Specimen	Aspect Ratio	Vertical Reinforcement (percentage)	Axial Load Ratio $P/(A_g f'_m)$	Height of plasticity (%Lw)		
				North	South	Average
PBS-3	1.0	#4 @ 8 in. (0.33)	0	42%	40%	**41%**
PBS-4	1.0	#4 @ 16 in. (0.16)	0	-	-	-
PBS-4G	1.0	#4 @ 16 in. (0.16)	0	51%	31%	**41%**
PBS-11	1.0	#4 @ 8 in. (0.33)	0.10	31%	39%	**35%**
PBS-12	1.0	#4 @ 16 in. (0.16)	0.10	48%	49%	**48%**
PBS-12G	1.0	#4 @ 16 in. (0.16)	0.10	58%	22%	**40%**

7.7.7. Plastic hinge length

The ratio of plastic hinge length to the plan length of the specimen is summarized

in Table 7-46 for all the wall segments. Values for Specimen PBS-4G could not be computed due to problems in the instrumentation. Axial load ratio and vertical reinforcement ratio had no evident effects in the plastic hinge length.

Table 7-46 Plastic hinge length

Specimen	Aspect Ratio	Vertical Reinforcement (percentage)	Axial Load Ratio $P/(A_g f'_m)$	Plastic Hinge Length (%Lw)		
				North	South	Average
PBS-3	1.0	#4 @ 8 in. (0.33)	0	50%	35%	**43%**
PBS-4	1.0	#4 @ 16 in. (0.16)	0	-	-	-
PBS-4G	1.0	#4 @ 16 in. (0.16)	0	27%	15%	**21%**
PBS-11	1.0	#4 @ 8 in. (0.33)	0.10	34%	6%	**20%**
PBS-12	1.0	#4 @ 16 in. (0.16)	0.10	6%	46%	**26%**
PBS-12G	1.0	#4 @ 16 in. (0.16)	0.10	12%	21%	**16%**

7.7.8. Energy dissipation

Energy dissipation, $E_{D\Delta t}$, for hysteretic loops with maximum lateral displacement equivalent to 0.6% and 1.5% drift ratios is summarized in Table 7-47. All specimens but PBS-11 dissipated more energy at 1.5% drift than at 0.6%. Specimen PBS-11 had the lowest ultimate displacement capacity; as a result, degradation was more severe at 1.5% drift level, and was probably controlled by shear friction without large dissipation of energy. Specimens with higher axial load ratio dissipated more energy than their similar with zero axial load. Specimens with higher vertical reinforcement ratio dissipated more energy at 0.6% drift level; however, no trend was found for 1.5% drift level. No difference in energy dissipation was noticed for specimens made of "green" units.

Table 7-47 Energy dissipation

				≈ 0.6% Drift ratio	≈ 1.5% Drift ratio
Specimen	**Aspect Ratio**	**Vertical Reinforcement (percentage)**	**Axial Load Ratio $P/(A_g f'_m)$**	**Energy Dissipation (kip-in)**	**Energy Dissipation (kip-in)**
PBS-3	1.0	#4 @ 8 in. (0.33)	0	37.15	84.44
PBS-4	1.0	#4 @ 16 in. (0.16)	0	23.86	82.40
PBS-4G	1.0	#4 @ 16 in. (0.16)	0	20.68	78.71
PBS-11	1.0	#4 @ 8 in. (0.33)	0.10	95.50	50.14
PBS-12	1.0	#4 @ 16 in. (0.16)	0.10	49.96	89.12
PBS-12G	1.0	#4 @ 16 in. (0.16)	0.10	51.24	113.57

7.7.9. Equivalent hysteretic damping

Equivalent hysteretic damping, ξ_{eq} , for drift ratios approximately equal to 0.6% and 1.5% is summarized in Table 7-48. As with energy dissipation, an anomaly occurred for Specimen PBS-11 where the equivalent hysteretic damping for a drift ratio of 0.6% was higher than for a drift ratio of 1.5%. This can be explained by the severe degradation at 1.5% drift ratio. Slightly lower values were found for specimens with high vertical reinforcement percentages (PBS-3 and PBS-11), but in general no major trends were identified.

Table 7-48 Equivalent hysteretic damping

				≈ 0.6% Drift ratio	≈ 1.5% Drift ratio
Specimen	**Aspect Ratio**	**Vertical Reinforcement (percentage)**	**Axial Load Ratio $P/(A_g f'_m)$**	**Equivalent Hysteretic Damping (%)**	**Equivalent Hysteretic Damping (%)**
PBS-3	1.0	#4 @ 8 in. (0.33)	0	17%	19%
PBS-4	1.0	#4 @ 16 in. (0.16)	0	22%	22%
PBS-4G	1.0	#4 @ 16 in. (0.16)	0	20%	22%
PBS-11	1.0	#4 @ 8 in. (0.33)	0.10	19%	16%
PBS-12	1.0	#4 @ 16 in. (0.16)	0.10	18%	18%
PBS-12G	1.0	#4 @ 16 in. (0.16)	0.10	19%	24%

7.7.10. "Gray" units versus "Green" units

Load-displacement curves (backbone curves) were used to compare the performance of the specimens constructed with "green" units (PBS-4G and PBS-12G) and their similar constructed with "gray" units (PBS-4 and PBS-12). Load-displacement curves for specimens PBS-4 and PBS-4G are shown in Figure 7-32 and for specimens PBS-12 and PBS-12G in Figure 7-33.

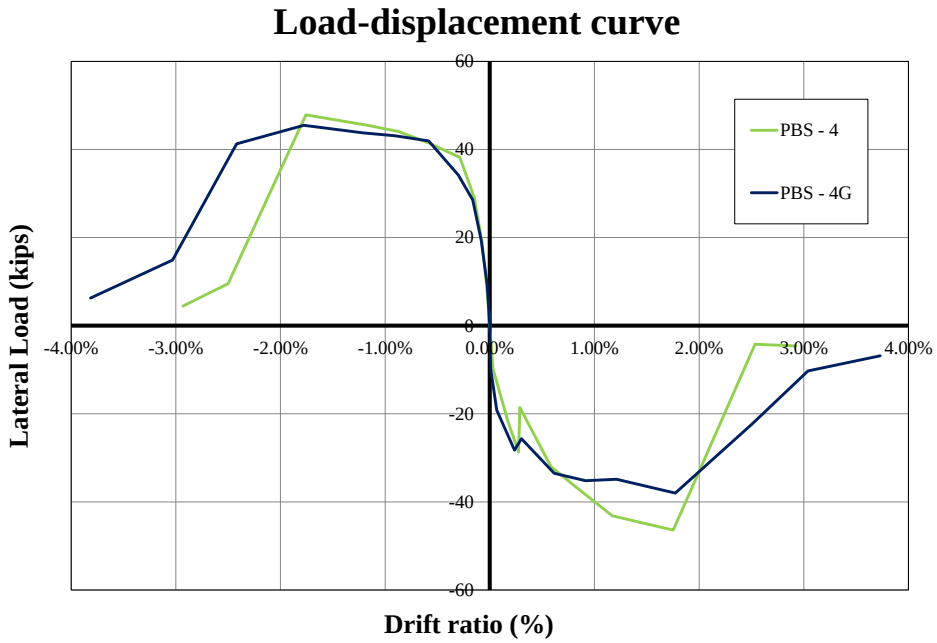

Figure 7-32 Load-displacement curves for Specimens PBS-4 and PBS-4G

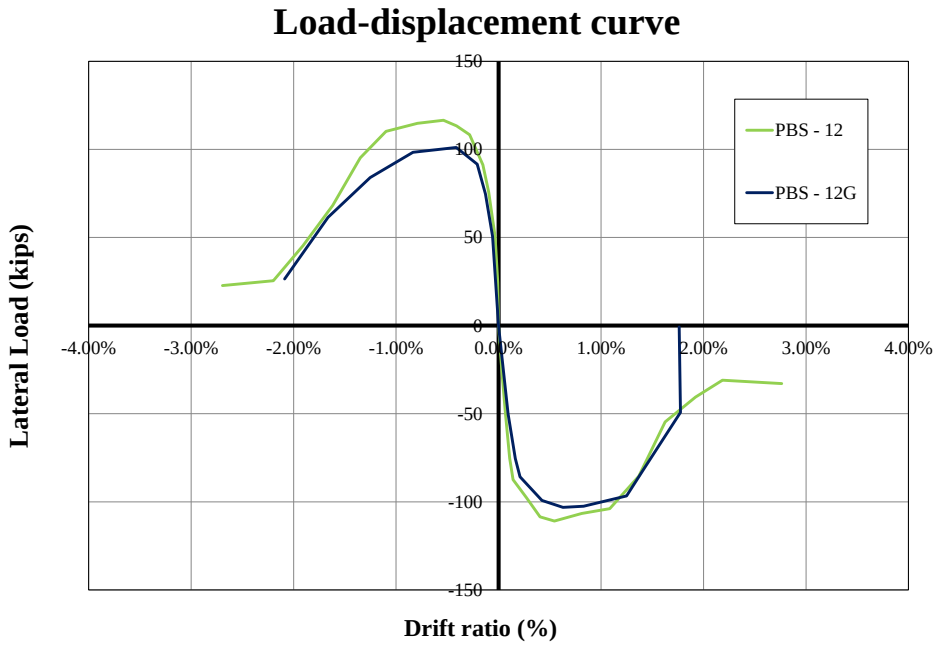

Figure 7-33 Load-displacement curves for Specimens PBS-12 and PBS-12G

Although material testing for both types of concrete masonry units (CMU) provided similar results (Table 7-49), differences in the performance of the specimens constructed with "green" units and "gray" units were identified. Reasons for these differences are explained below.

Table 7-49 Average compressive strengths of material test for "gray" and "green" units

Specimen Test	"Gray" Units Average Compressive Strength (psi)	"Green" Units Average Compressive Strength (psi)
CMU	3480	2850
Mortar	2103	1821
Grout	4513	4670
CMU prisms	4206	3522

Specimens PBS-4 and PBS-4G

Differences in the performance of the specimens PBS-4 and PBS-4G were particularly evident after maximum capacity. Differences in crack patterns in Specimens PBS-4 and PBS-4G are compared in Figure 7-34.

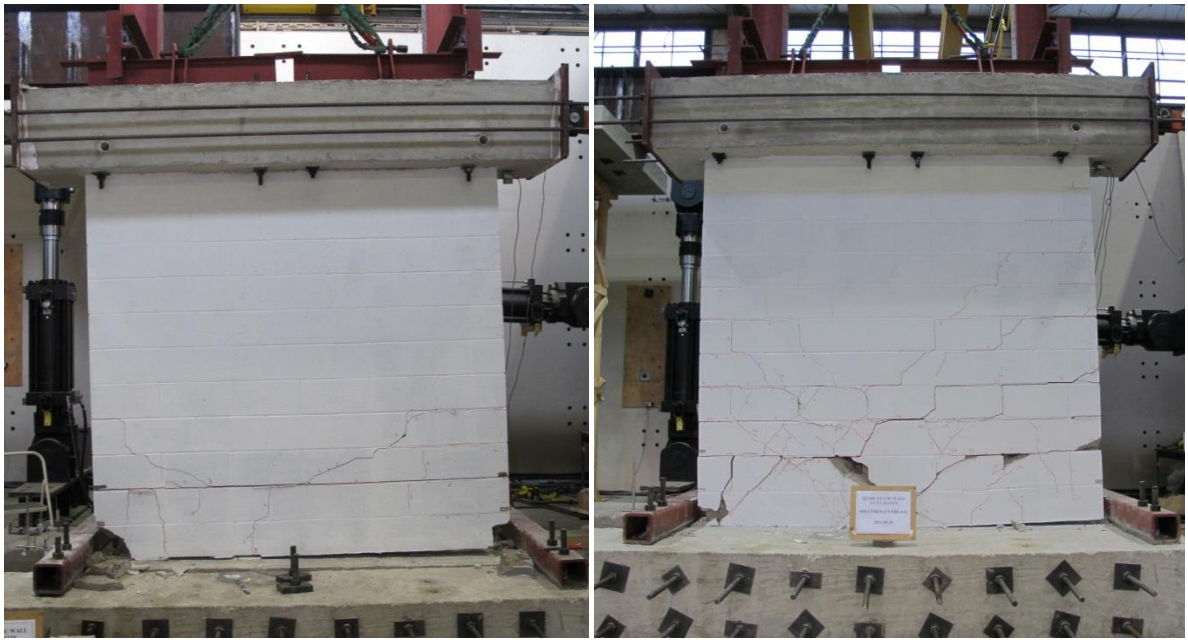

PBS-4 PBS-4G

Figure 7-34 Specimen PBS-4 and PBS-4G at 3% drift ratio

An asymmetrical cracking pattern was observed in Specimen PBS-4. Damage was concentrated in the lowest four courses; it included major flexural cracks at the base and second bed joint, and one shear-flexural crack at each end of the wall. In contrast, Specimen PBS-4G showed distributed damage over its height; flexural cracks developed in the lowest nine courses, and severe shear degradation were observed.

It was hypothesized that differences between the performance of the Specimens PBS-4 and PBS-4G, and the asymmetrical degradation of Specimen PBS-4, could be attributed to slip of one or more lap splices at the south end. To evaluate this hypothesis, the strain gradient at the base of the Specimen PBS-4 for +0.03% and -0.03% drift are plotted in Figure 7-36 and Figure 7-37. This graph presents the strains measured by the strain gauges on the dowels at the base of wall, as shown in Figure 7-35. Tensile strains

are upward (positive). The strain gauge on the dowel D2 was found to be broken from the beginning of the test.

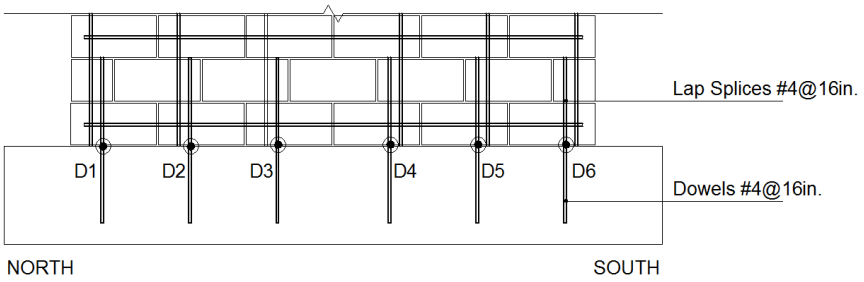

Figure 7-35 Locations and identifiers of strain gauges on dowels of Specimen PBS-4

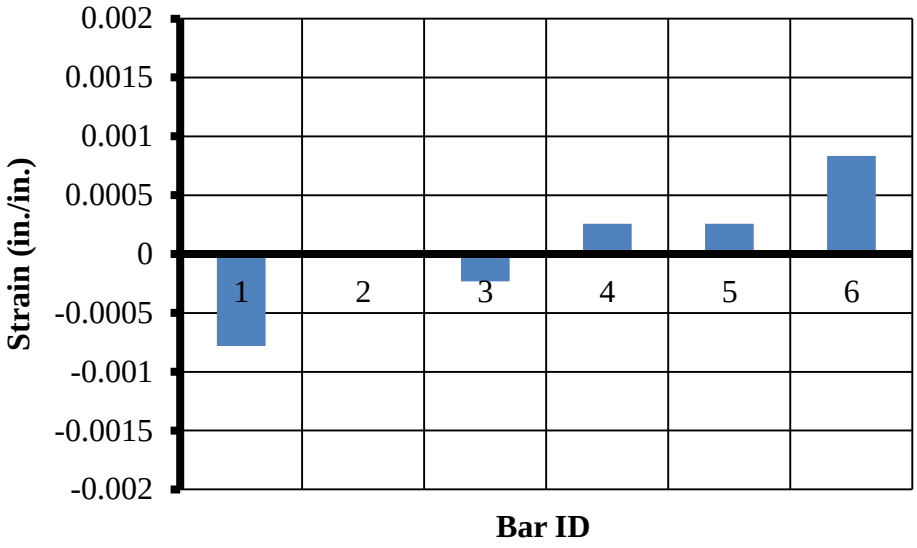

Figure 7-36 Strain gradient at +0.03% drift ratio for Specimen PBS-4

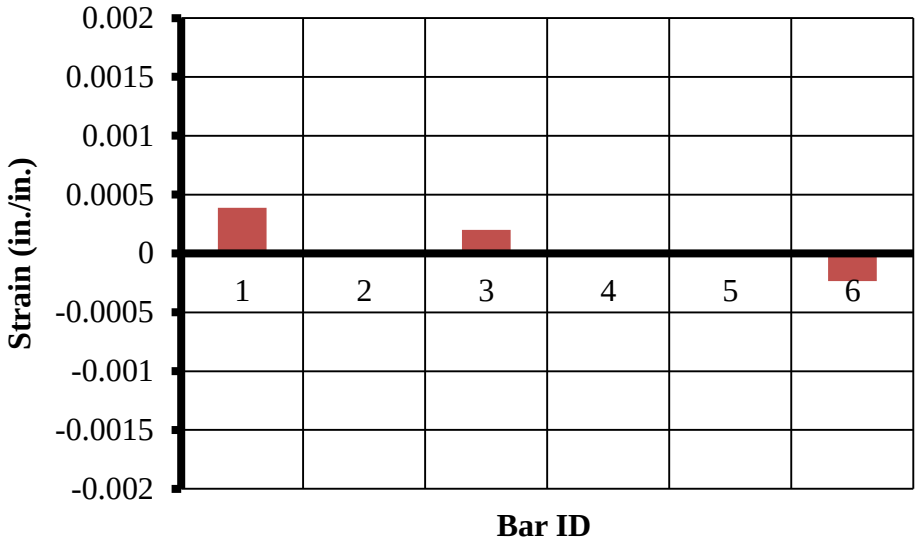

Figure 7-37 Strain gradient at -0.03% drift ratio for Specimen PBS-4

Strain gradients at the base of the Specimen PBS-4 showed low strains in dowels D4 and D5 for both directions, which is in complete agreement with the hypothesis of slip in the lap splices.

Due to this slip in the splices at the south end, tensile strains at the south end of Specimen PBS-4 were not controlled by the vertical reinforcement, deteriorating the masonry at that toe. Furthermore, this mode of failure, controlled by flexure, acted as a fuse which concentrated all the damage at the base not letting the specimen develop more flexural and shear cracking.

The deterioration of the masonry would be especially detrimental after reaching the maximum capacity of the specimen; it would permit buckling of the vertical reinforcement which would produce an abrupt decrease in capacity. Those characteristics

were observed for Specimen PBS-4, and provide further corroboration of the hypothesis of slip in the lap splices at the south end of Specimen PBS-4. Slip in the lap splices could have been caused by a low value of grout slump. The slump of the grout was not measured in the construction process.

Specimens PBS-12 and PBS-12G

Specimens PBS-12 and PBS-12G showed differences in initial stiffness, maximum load capacity, and ultimate displacement. Degradation patterns for each specimen are compared in Figure 7-38 through Figure 7-42.

PBS-12 (0.54% drift ratio)

PBS-12G (0.61% drift ratio)

Figure 7-38 North toe at approximately 0.60% drift ratio

PBS-12 (0.79%)

PBS-12G (0.83%)

Figure 7-39 South toe at approximately 0.80% drift ratio

PBS-12 (1.62%)

PBS-12G (1.66%)

Figure 7-40 North toe at approximately 1.65% drift ratio

PBS-12 (1.63%)

PBS-12G (1.78%)

Figure 7-41 South toe at approximately 1.70% drift ratio

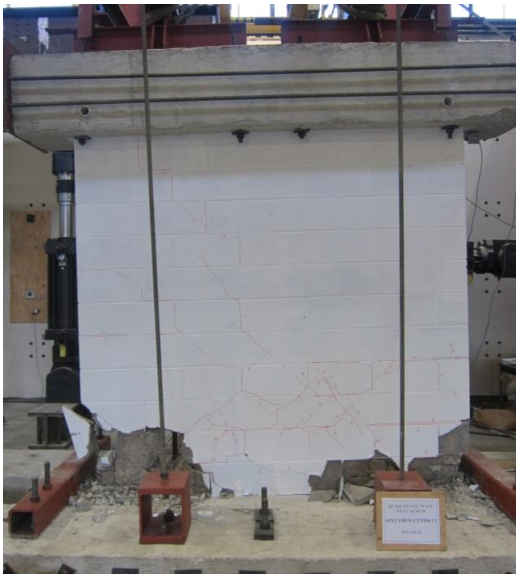

PBS-12 (2.20%)

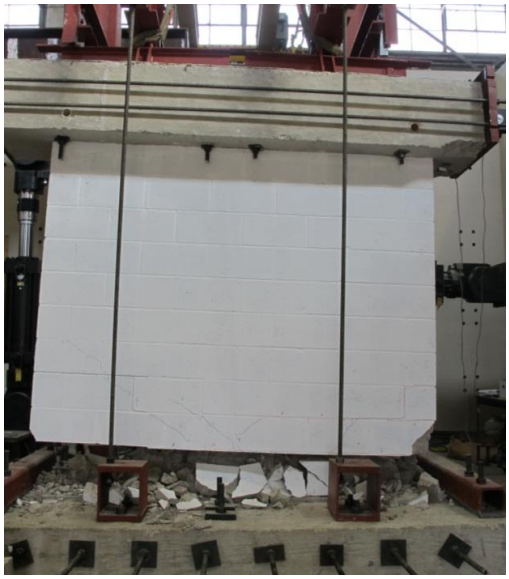

PBS-12G (2.09%)

Figure 7-42 Wall degradation at 2.10% drift ratio

Although deterioration of Specimens PBS-12 and PBS-12G seemed to be similar at equivalent drift ratios (Figure 7-38 to Figure 7-41), damage in Specimen PBS-12G concentrated at the base of the wall, while Specimen PBS-12 developed cracking in higher courses (Figure 7-42).

A lower stiffness for Specimen PBS-12, at the first cycles of the test, resulted in a lower expected yield displacement, Δ_y , and a higher number of reversed cycles to reach certain drift level. This was because the loading protocol was based on the expected yield displacement. The shear cracks in Specimen PBS-12 (Figure 7-42) were probably caused by the large number of reversed cycles to which it was subjected.

At the last cycles of the test, loss of significant cells and face shells were observed for Specimen PBS-12G. This is especially detrimental for specimens with high axial load. In contrast, intact face shells in Specimen PBS-12 permitted it to resist the axial load up to the end of the test.

The loss in stiffness, reduced capacity, and concentrated degradation at the base could be produced by the slip of one or more of the lap splices at the south end of Specimen PBS-12G. To evaluate this hypothesis, the strain gradient at the base of the Specimen PBS-12G for +0.21% and -0.21% drift are plotted in Figure 7-44 and Figure 7-45. This graph presents the strains measured by the strain gauges on the dowels at the base of wall, as shown in Figure 7-43. Tensile strains are upward (positive).

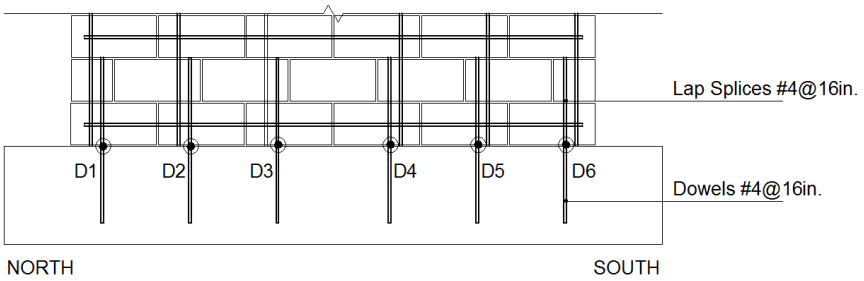

Figure 7-43 Locations and identifiers of strain gauges on dowels of Specimen PBS-12G

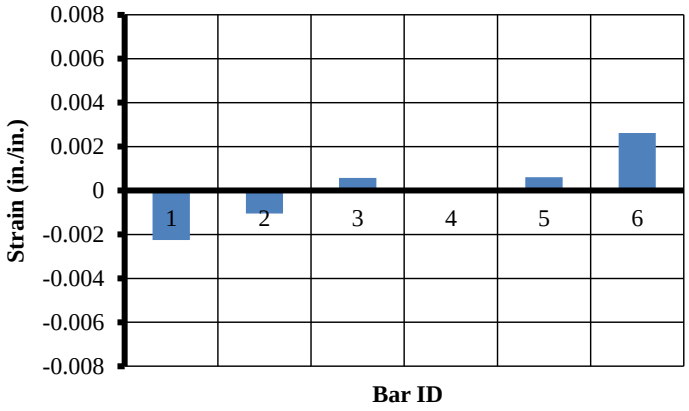

Figure 7-44 Strain gradient at +0.21% drift ratio for Specimen PBS-12G

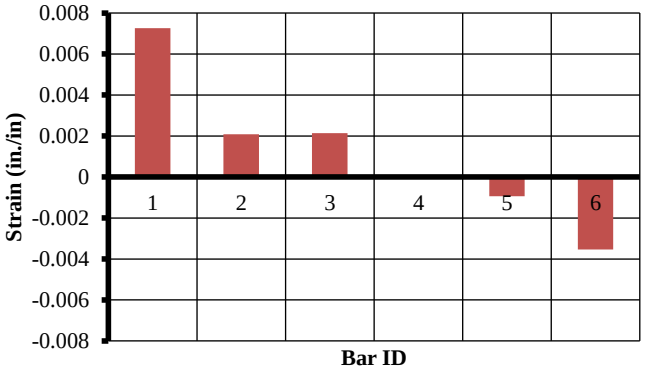

Figure 7-45 Strain gradient at -0.21% drift ratio for Specimen PBS-12G

Strain gradients at the base of the Specimen PBS-12G showed low strains in dowels D4 and D5 for both directions, which is in complete agreement with the hypothesis of the slip in the lap splices. From the results analyzed above, differences in performance of specimens PBS-12 and PBS-12G could be attributed to slip in the lap splices. A possible cause of the slip in the lap splices could have been a low slump in the grout. The slump was not checked during construction.

UT researchers concluded that wall specimens constructed with "Green" units behaved similarly to otherwise identical specimens constructed with "Gray" units, indicating equivalence of those two types of units.

Chapter 8 : Summary, Conclusions and Recommendations

8.1. SUMMARY

This thesis describes work done as part of a project on "Performance-Based Seismic Design Methods and Tools for Reinforced Masonry Shear-Wall Structures," sponsored by the National Institute for Standards and Technology (NIST), and carried out jointly by researchers from the University of Texas at Austin (UT Austin), the University of California at San Diego (UCSD), and Washington State University (WSU). The overall objectives of the project are to produce much-needed experimental data to better understand the seismic performance of reinforced masonry shear-wall structures, and to develop improved design methodologies, detailing requirements, and analytical methods for the design and performance assessment of these structures.

The primary objective of this thesis was to study how the behavior of flexure-dominated masonry shear-wall segments is affected by changes in the normalized axial load and the percentage of vertical reinforcement. The secondary objective was to see if there would be any significant differences between the behavior of shear-wall segments constructed with conventional concrete masonry units ("gray units"), and otherwise identical shear-wall segments constructed with concrete masonry units containing a required minimum percentage of recycled material ("green units").

Six reinforced masonry shear-wall segment were constructed and tested at the Ferguson Structural Engineering Laboratory of the University of Texas at Austin. Specimens were 96-in. wide and 96-in. high (aspect ratio equal to 1.0) and were tested with different combinations of axial load ratio (zero and 0.10) and vertical reinforcement

ratios (0.33% and 0.16%). Specimens met 2011 MSJC Code requirements for special reinforced masonry shear walls, and were tested under quasi-static in-plane reversed cyclic loads.

The loading system consisted of a lateral loading system, a gravity loading system, and an out-of-plane bracing system. Instrumentation was composed of linear potentiometers, string potentiometers, strain gages, and load cells which measured lateral displacement, strains in reinforcing bars, strain in the concrete extreme fiber, base sliding, and applied lateral load. Specimens were tested following the testing protocol established for all specimens as part of the overall project. Load-displacement curves (hysteretic curves) were obtained during testing and the modes of failure were reported. Analytical work for each wall included the computation of relative displacement contributions, drift ratio, backbone curve, elasto-plastic idealization, displacement and curvature ductility, height of plasticity, plastic hinge length, energy dissipation, and equivalent hysteretic damping. Results were related to the level of axial load and the vertical reinforcement ratio of the specimens. Finally, the effects of the use of "green" units on the performance of the wall segments were assessed.

8.2. CONCLUSIONS

1. Specimens referred to in this thesis (aspect ratio equal to 1.0) exhibited predominantly flexural behavior, as expected. Specimens exhibited flexural cracking, yielding of vertical reinforcement, degradation of the compression toe, inelastic buckling of vertical reinforcement near the base, spalling of the

toe regions, and in some cases fracture of the vertical reinforcement. Specimens exhibited high displacement ductility (5.6 to 16.7), as expected for flexure-dominated specimens.

2. Specimen behavior was in good agreement with that reported in previous research work. The provisions of the 2011 MSJC *Code* (MSJC 2011a,b) gave conservative (low) predictions of flexural capacity. As expected, flexural capacity and initial stiffness increased with increasing axial load and vertical reinforcement ratio. Displacement ductility decreased with increasing axial load.

3. Sliding deformation, ultimate displacement, and displacement ductility decreased with increasing axial load. Energy dissipation, in contrast, increased with increasing axial load (well below the balance point).

4. No consistent trend was found for the effects of axial load and vertical reinforcement ratio on the height of plasticity, plastic hinge length, or equivalent hysteretic damping.

5. Specimens constructed with "green" units behaved essentially like otherwise identical specimens constructed with conventional ("gray") units. Some differences were observed, and careful evaluation of data showed that those differences were due to slip of a few lap splices in Specimen PBS-4 ("gray units") and Specimen PBS-12G ("green units"). The differences were not due to the type of units used ("gray" versus "green").

8.3. RECOMMENDATIONS FOR IMPLEMENTATION

1. Specimen behavior was consistent with the expectations inherent in the design provisions of the 2011 MSJC *Code* (MSJC 2011a)for special reinforced masonry shear walls. Those provisions should be maintained.

2. Research in this study showed that "green" units resulted in behavior essentially identical to that of "gray" units. The use of units conforming to ASTM C90 and also meeting requirements for minimum recycled content should be encouraged.

3. Two wall specimens showed slip in lap splices. It is believed that this slip occurred because the splice was not sufficiently surrounded by grout. This insufficient surround occurred because the grout did not have a sufficiently high slump during construction. This observation underscores the importance of adherence to MSJC *Specification* (MSJC 2011b) requirements for grouting.

References

ACI 318-11 (2011): "Building Code Requirements for Structural Concrete (ACI 318-11) and Commentary (ACI 318R-11)," American Concrete Institute, Farmington Hills, Michigan.

ASCE 7-10 (2010): "Minimum Design Loads for Buildings and Other Structures (ASCE 7-10) (with Supplement)," American Society of Civil Engineers, Reston, Virginia.

ASTM A476-10 (2010): "Standard Specification for Grout for Masonry," American Society for Testing and Materials, West Conshohocken, PA.

ASTM C90-11a (2011): "Standard Specification for Loadbearing Concrete Masonry Units," American Society for Testing and Materials, West Conshohocken, PA.

ASTM C140-99b (1999): "Standard Test Methods for Sampling and Testing Concrete Masonry Units and Related Units," American Society for Testing and Materials, West Conshohocken, PA.

ASTM C1314-11a (2011): "Standard Test Method for Compressive Strength of Masonry Prisms," American Society for Testing and Materials, West Conshohocken, PA.

ASTM C780-11 (2011): "Standard Test Method for Preconstruction and Construction Evaluation of Mortars for Plain and Reinforced Unit Masonry," American Society for Testing and Materials, West Conshohocken, PA.

ASTM C1019-11 (2011): "Standard Test Method for Sampling and Testing Grout," American Society for Testing and Materials, West Conshohocken, PA.

ASTM C270-12 (2012): "Standard Specification for Mortar for Unit Masonry," American Society for Testing and Materials, West Conshohocken, PA.

Clough, R. W., and Penzien, J. (2003): *Dynamics of Structures*, 3rd Ed., Computers and Structures, Inc., Berkeley, California.

Davis, C. L. (2008): "Evaluation of Design Provisions for In-Plane Shear in Masonry Walls," Master's thesis, Washington State University, Pullman, Washington.

Eikanas, I. K. (2003): "Behavior of Concrete Masonry Shear Walls with Varying Aspect Ratio and Flexural Reinforcement," Master's thesis, Washington State University, Pullman, Washington.

Kapoi, C. M. (2011): "Experimental Performance of Concrete Masonry Shear Walls Under In-Plane Loading," Master's thesis, Washington State University, Pullman, Washington.

MSJC 2008a (2008): "Building Code Requirements for Masonry Structures (TMS 402-08 / ACI 530-08 / ASCE 5-08)," The Masonry Society, Boulder, Colorado, the American Concrete Institute, Farmington Hills, Michigan, and the American Society of Civil Engineers, Reston, Virginia.

MSJC 2008b (2008): "Specification for Masonry Structures (TMS 602-08 / ACI 530.1-08 / ASCE 6-08)," The Masonry Society, Boulder, Colorado, the American Concrete Institute, Farmington Hills, Michigan, and the American Society of Civil Engineers, Reston, Virginia.

MSJC 2011a (2011): "Building Code Requirements for Masonry Structures (TMS 402-11 / ACI 530-11 / ASCE 5-11)," The Masonry Society, Boulder, Colorado, the American Concrete Institute, Farmington Hills, Michigan, and the American Society of Civil Engineers, Reston, Virginia.

MSJC 2011b (2011): "Specification for Masonry Structures (TMS 602-11 / ACI 530.1-11 / ASCE 6-11)," The Masonry Society, Boulder, Colorado, the American Concrete Institute, Farmington Hills, Michigan, and the American Society of Civil Engineers, Reston, Virginia.

Massone, L. M., and Wallace, J. W. (2004): "Load-Deformation Responses of Slender Reinforced Concrete Walls," *ACI Structural Journal*, Vol.101, No. 1, 103-113.

Paulay, T., and Priestley, M. J. N. (1992): *Seismic Design of Reinforced Concrete and Masonry Buildings*, John Wiley & Sons, Inc., New York.

Priestley, M. J. N. (1986): "Seismic Design of Concrete Masonry Shearwalls," *ACI Structural Journal*, Vol. 83, No. 1, 58-68.

Shedid, M. T., Drysdale, R. G., and El-Dakhakhni, W. W. (2008): "Behavior of Fully Grouted Reinforced Concrete Masonry Shear Walls Failing in Flexure: Experimental Results," *Journal of Structural Engineering*, ASCE, Vol. 134, No. 11, 1754-1767.

Shedid, M. T., Drysdale, R. G., and El-Dakhakhni, W. W. (2010): "Seismic Performance Parameters for Reinforced Concrete-Block Shear Wall

Construction," *Journal of Performance of Constructed Facilities*, Vol. 24, No. 1, 4-18.

Sherman, J. D. (2011): "Effects of Key Parameters on the Performance of Concrete Masonry Shear Walls Under In-Plane Loading," Master's thesis, Whashington State University, Pullman, Washington.

Shing, P. B., Noland, J. L., Klamerus, E., and Spaeh, H. (1989): "Inelastic Behavior of Concrete Masonry Shear Walls," *Journal of Structural Engineering*, ASCE, Vol. 115, No. 9, 2204-2225.

Shing, P. B., Schuller, M., and Hoskere, V. S. (1990): "In-Plane Resistance of Reinforced Masonry Shear Walls," *Journal of Structural Engineering*, ASCE, Vol. 116, No. 3, 619-640.

Shing, P. B., Schuller, M., Hoskere, V. S., and Carter, E. (1990): "Flexural and Shear Response of Reinforced Masonry Walls," *ACI Structural Journal*, Vol. 87, No. 6, 646-656.

Vaughan, T. P. (2010): "Evaluation of Masonry Wall Performance Under Cyclic Loading," Master's thesis, Washington State University, Pullman, Washington.

Voon, K. C., and Ingham, J. M. (2006): "Experimental In-Plane Shear Strength Investigation of Reinforced Concrete Masonry Walls," *Journal of Structural Engineering*, ASCE, Vol. 132, No. 3, 400-408.